FINAL REPORT

Demonstration and Validation of a Portable Raman Sensor for *In-Situ* Detection and Monitoring of Perchlorate (ClO_4-)

ESTCP Project ER-201327

MARCH 2017

Dr. Baohua Gu
Dr. Aaron Jubb
Dr. Gyula Eres
Oak Ridge National Laboratory

Dr. Paul B. Hatzinger
CB&I Federal Services

Page Intentionally Left Blank

This report was prepared under contract to the Department of Defense, Environmental Security Technology Certification Program (ESTCP). The publication of this report does not indicate endorsement by the U.S. Department of Defense, nor should the contents be construed as reflecting the official policy or position of the Department of Defense. Reference herein to any specific commercial product, process, or service by trade name, trademark, manufacturer, or otherwise, does not necessarily constitute or imply its endorsement, recommendation, or favoring by the Department of Defense.

Page Intentionally Left Blank

REPORT DOCUMENTATION PAGE

Form Approved
OMB No. 0704-0188

1. REPORT DATE *(DD-MM-YYYY)*	**2. REPORT TYPE**	**3. DATES COVERED** *(From - To)*
03-31-2017	Final	January 2013 – March 2017

4. TITLE AND SUBTITLE
Demonstration and Validation of a Portable Raman Sensor for In-Situ Detection and Monitoring of Perchlorate (ClO_4^-)

5a. CONTRACT NUMBER
W74RDV60915508

5b. GRANT NUMBER
N/A

5c. PROGRAM ELEMENT NUMBER
N/A

6. AUTHOR(S)
Gu, Baohua (ORNL); Jubb, Aaron (ORNL); Eres, Gyula (ORNL)
Hatzinger, Paul B. (CB&I)

5d. PROJECT NUMBER
ER-201327

5e. TASK NUMBER
N/A

5f. WORK UNIT NUMBER
N/A

7. PERFORMING ORGANIZATION NAME(S) AND ADDRESS(ES)
Environmental Sciences Division
Oak Ridge National Laboratory
1 Bethel Valley Road, 1505-218
Oak Ridge, TN 37831

8. PERFORMING ORGANIZATION REPORT NUMBER
N/A

9. SPONSORING / MONITORING AGENCY NAME(S) AND ADDRESS(ES)
Environmental Security Technology Certification Program (ESTCP)
4800 Mark Center Drive, Suite 17D03
Alexandria, VA 22350-3605

10. SPONSOR/MONITOR'S ACRONYM(S)
ESTCP

11. SPONSOR/MONITOR'S REPORT NUMBER(S)
N/A

12. DISTRIBUTION / AVAILABILITY STATEMENT
Approved for public release; Distribution is unlimited

13. SUPPLEMENTARY NOTES
None

14. ABSTRACT

15. SUBJECT TERMS
Perchlorate, Raman, SERS,

16. SECURITY CLASSIFICATION OF:			**17. LIMITATION OF ABSTRACT**	**18. NUMBER OF PAGES**	**19a. NAME OF RESPONSIBLE PERSON**
a. REPORT	**b. ABSTRACT**	**c. THIS PAGE**			Baohua Gu
U	U	U	UU	106	**19b. TELEPHONE NUMBER** *(include area code)* (865)-574-7286

Standard Form 298 (Rev. 8-98)
Prescribed by ANSI Std. Z39.18

Page Intentionally Left Blank

FINAL REPORT
Project: ER-201327

TABLE OF CONTENTS

Page

TABLE OF CONTENTS (Continued)

Page

LIST OF FIGURES

Page

LIST OF FIGURES

Page

LIST OF FIGURES

Page

LIST OF TABLES

Page

ACRONYMS AND ABBREVIATIONS

Ag	silver
Au	gold
Br^-	bromide
CCD	center-to-center distance
Cl^-	chloride
ClO_3^-	chlorate
ClO_4^-	perchlorate
cm	centimeter
cm^{-1}	wavenumber
Cr	chromium
Cu	copper
DMAET	2-(dimethylamino) ethane-thiol
DoD	Department of Defense
E	electric field
EBL	electron beam lithography
EF	enhancement factor
ESI	electrospray ionization
ESTCP	Environmental Security Technology Certification Program
FDTD	finite difference time domain
F^-	fluoride
Fe^{2+}	ferrous iron
$FeSO_4$	ferrous sulfate
FTIR	Fourier transform infrared
g	gram
HCO_3^-	bicarbonate
HPLC	high-performance liquid chromatography
$H_2PO_4^-$	dihydrogen phosphate
HPO_4^{2-}	hydrogen phosphate
IC	ion chromatography
L	liter
LC	liquid chromatography
LSP	localized surface plasmon
M	molar
MCT	mercury cadmium telluride

min	minute
mg	milligram
mM	millimolar
mW	milliwatt
MΩ	megaohms
N_2	nitrogen
NaCl	sodium chloride
$NaClO_4$	sodium perchlorate
$NaNO_3$	sodium nitrate
Na_2SO_4	sodium sulfate
NIL	Nanoimprint lithography
nm	nanometer
NO_2^-	nitrite
NO_3^-	nitrate
ORNL	Oak Ridge National Laboratory
pg	picogram
*p*MA	*p*-mercaptoaniline
PO_4^{3-}	phosphate
ppb	parts per billion
ppm	parts per million
RIE	reactive ion etching
RRD	row-to-row distance
s	second
SEM	scanning electron microscope
SERDP	Strategic Environmental Research and Development Program
SERS	surface enhanced Raman scattering
Si	silicon
SO_4^{2-}	sulfate
TDS	total dissolved solids
TNT	2,4,6-trinitrotoluene
µg	microgram
µL	microliter
µm	micrometer
µM	micromolar

ACKNOWLEDGEMENTS

We wish to thank Ms. Xiangping Yin and Dr. Scott T. Retterer at Oak Ridge National Laboratory (ORNL) for technical assistance, Dr. Andrew Ritts and Dr. Xin Sun at Nanova Inc. for assistance in nanoimprint SERS substrate fabrication and evaluation, Dr. Randi Rothmel and Mr. Paul Hedman from CB&I for sampling and analytical assistance, and Dr. Andrea Leeson of the Environmental Security Technology Certification Program (ESTCP) for her support and oversight during this project. We also wish to acknowledge personnel at both the Indian Head Division, Naval Surface Warfare Center and Redstone Arsenal for providing site access and supporting this research effort. The project was funded by the ESTCP Program (Project ER-201327) to ORNL, which is managed by UT-Battelle LLC for U.S. Department of Energy (DOE) under contract DE-AC05-00OR22725. The fabrication of elevated Au ellipse dimers by electron beam lithography was conducted at the Center for Nanophase Materials Sciences (CNMS) of ORNL, which is sponsored by DOE Scientific User Facilities Division.

Page Intentionally Left Blank

EXECUTIVE SUMMARY

Costs for environmental analysis and monitoring are increasing at a rapid rate and represent a significant percentage of the total and future remedial expenses at many U.S. Department of Defense (DoD) contaminated sites. It has been reported that about 30 to 40% of the remediation budget is usually spent on long-term monitoring (LTM), of which a large percentage represents laboratory analytical costs. Energetics such as perchlorate (ClO_4^-) are among the most frequently detected contaminants in groundwater and surface water at or near military installations due to their persistence and mobility. Currently, the standard protocol entails collecting samples in the field, packaging them, and shipping them overnight to a designated laboratory for analysis. This process requires significant sample preparation and handling, and analytical results may not be available for several days to weeks. In this project, we developed and demonstrated a portable Raman sensor based on surface enhanced Raman scattering (SERS) technology to detect ClO_4^- in contaminated water. We summarize major accomplishments as follows:

- A SERS sensor based on elevated gold (Au) nano-ellipse dimer architectures was designed and developed for ClO_4^- with a detection limit of ~10^{-6} M (or 100 μg/L); The performance of these sensors was evaluated and optimized through variation of their geometric characteristics (i.e., dimer aspect ratio, dimer separation, etc.).
- Large-scale commercial production of SERS substrate sensors via nanoimprinting by Nanova Inc. and Nanoimprint lithography (NIL) technology was successfully demonstrated. This is a substantial step forward toward the commercialization of the SERS sensors and may potentially lead to significantly reduced fabrication costs of SERS substrates.
- Commercially produced SERS sensors were demonstrated to detect ClO_4^- at levels above 10^{-6} M using a portable Raman analyzer. The performance of the commercial SERS sensors for ClO_4^- detection in the presence and absence of interferences was determined for a series of standard solutions. Sulfate (SO_4^{2-}) was found to exhibit the greatest interference for the anions tested, which included Cl^-, NO_3^-, and SO_4^{2-}.
- Field demonstration of the portable Raman sensor with commercially produced SERS substrates was completed at two Department of Defense (DoD) sites; twice at the Indian Head Naval Surface Warfare Center, Indian Head, MD, and once at Redstone Arsenal, Huntsville, AL. Multiple wells were sampled at both DoD sites, where a standard addition method was employed using the sensor to determine the ClO_4^- for each groundwater sample. Groundwater samples were also collected for method intercomparison with the standard ion chromatography (IC) approach. Results were generally comparable, although significant variations were observed due to the presence of interference ions and/or co-contaminants in the groundwater in some samples.

To our knowledge, this is the first demonstration of a field portable SERS/Raman sensor that combines a portable Raman analyzer with novel elevated gold ellipse nanostructural arrays. The technology shows the potential to provide a tool for rapid, in-situ screening and analysis of ClO_4^- and possibly other energetics that are both important for environmental monitoring and of interest for national security. However, we point out that SERS technology is also prone to interferences due to its sensitivity and responses to other ionic species, such as NO_3^-, SO_4^{2-}, and dissolved organics or co-contaminants present in the groundwater, which could potentially mask the SERS signal of the target analyte (i.e., ClO_4^-). As such, SERS analysis was

subject to significant variations (e.g., ±20% or more), and its detection limit for ClO_4^- from field studies (10^{-6} M) was higher than our performance objectives (3×10^{-8} M) and was substantially higher than what we anticipated from laboratory studies. However, despite these complications, the portable Raman sensor developed in this project could be used as a rapid screening tool for ClO_4^- at concentrations above 10^{-6} M. Future studies are warranted to further develop the technology and to optimize its performance, and eventually to bring the technology to the market. With additional development and demonstration, the sensor has the potential to reduce analytical costs by eliminating shipping and typical costs associated with laboratory analysis. A cost savings of 30–45% may be realized during a typical sampling event and, more importantly, the technology could allow rapid turn-around of information to decision makers for site characterization and remediation.

1.0 INTRODUCTION

1.1 BACKGROUND

Costs for environmental analysis and monitoring represent a significant percentage of the total and future remedial expenses at many of the U.S. Department of Defense (DoD) contaminated sites. It has been reported that about 30 to 40% of the remediation budget is usually spent on long-term monitoring (LTM), of which a large percentage represents laboratory analytical costs. Perchlorate (ClO_4^-) is one of the prevalent contaminants in groundwater and surface water at DoD military testing and training ranges such as the Naval Surface Warfare Centers (NSWC) at Indian Head, Maryland and Dahlgren, Virginia, and Redstone Arsenal in Alabama, USA (Clausen et al., 2009; Gu and Coates, 2006; Sass, 2004; Suidan et al., 2008). Perchlorate in these contaminated sites ranges from sub-ppb (µg/L) up to hundreds or thousands of ppm (mg/L) concentrations (e.g., at Indian Head NSWC; IHDIV) and often occurs with many other common ionic species in groundwater such as nitrate (NO_3^-), chloride (Cl^-), and sulfate ($SO_4^{=}$) with wide variations in total dissolved solids (TDS). ClO_4^- is a key component of explosives and solid rocket fuels, although it is also present in a number of commercial products such as fireworks, road flares and Chilean nitrate fertilizers (Sass 2004; Gu and Coates 2006). Currently, the established detection and analysis methods for ClO_4^- in water are ion chromatography (IC) (EPA Method 314) and IC with electrospray ionization and mass spectrometry (IC/ESI/MS; EPA Method 6860). Each of these analytical techniques requires sample collection and shipping in addition to the use of expensive analytical equipment and significant time for sample preparation and analysis. Furthermore, typical turnaround times for these analyses by commercial laboratories are generally two weeks.

Therefore, rapid, cost-effective field detection and screening technologies are highly desirable for site assessments and both short- and long-term monitoring. In this work, we demonstrate a portable Raman sensor based on surface-enhanced Raman scattering (SERS) technology, allowing real-time analysis of ClO_4^- in contaminated groundwater or surface water. A field-ready portable instrument with the capability of multiple species detection would thus be of significant benefit for site assessment at many DoD training and testing ranges and may significantly reduce the costs associated with long term monitoring at these sites.

1.2 PROJECT OBJECTIVES

The overall goal of the project was to field-demonstrate, validate, and optimize the performance and sensitivity of a portable Raman sensor for rapid detection and analysis of the energetic compound, ClO_4^-, in groundwater.

Our specific objectives were to:

1) Construct and validate the performance of a portable Raman sensor for the detection of ClO_4^- as a target analyte in groundwater with varying geochemical characteristics;
2) Optimize the performance and sensitivity of the sensor through nano-fabrication of surface-enhanced Raman scattering (SERS) substrates and the fiber-optic sensor probe;
3) Optimize field-testing methodologies and establish testing protocols;

4) Partner with a commercial vendor for large-scale production of SERS substrates via nanoimprinting; and

5) Evaluate and document the cost effectiveness of the new sensing technology by comparing with conventional laboratory-based analytical protocols.

1.3 REGULATORY DRIVERS

There is currently no federal drinking water standard (maximum contaminant level [MCL]) for ClO_4^-. However, the U.S. Environmental Protection Agency (USEPA) has previously listed ClO_4^- on the Draft Drinking Water Candidate Contaminant List (http://water.epa.gov/scitech/drinkingwater/dws/ccl/ccl3.cfm) and the Unregulated Contaminant Monitoring Regulation List (http://water.epa.gov/lawsregs/rulesregs/sdwa/ucmr/factsheet.cfm) and has previously announced their intention to establish a Federal MCL for ClO_4^- under the Safe Drinking Water Act (http://water.epa.gov/drink/contaminants/unregulated/upload/FactSheet_PerchlorateDetermination.pdf). The states of Massachusetts and California currently have drinking water MCL values for ClO_4^- of 1 µg/L and 6 µg/L, respectively. Although there is no Federal MCL, many DoD sites are actively involved in the sampling and analysis of ClO_4^-. The objective of this project is to demonstrate a field-based method for rapid ClO_4^- analysis.

2.0 TECHNOLOGY

2.1 TECHNOLOGY DESCRIPTION

Raman spectroscopy is a spectroscopic technique that gives information about the vibrational frequency shifts or modes of chemical bonds in certain molecules such as ClO_4^- (Gu et al., 2009; Hatab et al., 2010b; Kneipp et al., 1997; Nie and Emory, 1997; Ruan et al., 2007b; Ruan et al., 2006b). The Cl–O bond in ClO_4^- gives a characteristic Raman frequency shift at ~ 935 cm^{-1} (or the strongest Raman band for ClO_4^-). Since each molecule (or chemical bond) has its own vibrational frequency, the technique is specific and can in principle provide unique fingerprinting for various organic and inorganic compounds that are Raman active. However, one of the major limitations of conventional Raman spectroscopy is its relatively weak signal when compared with other optical techniques such as fluorescence spectroscopy. Until recently this shortcoming has greatly limited the use of conventional Raman spectroscopy as an analytical tool in environmental analysis.

SERS overcomes above limitations by providing orders of magnitude higher (10^4–10^{12}) enhanced Raman signal from Raman-active molecules that are either adsorbed onto or at the close proximity of specially prepared noble metal surfaces (Gu et al., 2009; Hatab et al., 2010b; Kneipp et al., 1997; Nie and Emory, 1997; Ruan et al., 2007b; Ruan et al., 2006b). Such surfaces are usually made with nanostructured gold (Au) or silver (Ag) arrays with nanometer gap sizes, as detailed in Section 2.2. First demonstrated in 1974 (Kneipp et al., 1997; Nie and Emory, 1997), SERS has developed into an ultra-sensitive technique for detecting and analyzing a variety of chemical and biological agents. Target analyte molecules near or adsorbed at nanostructured Au or Ag surfaces give rise to a million-fold or greater enhancement of the Raman signals due to interactions between target molecules and the SERS-active surface. As a result, the SERS technique allows the detection of analyte molecules at ultra-trace to single molecular concentration levels (Hatab et al., 2010b; Ruan et al., 2007b). Thus, in comparison with fluorescence and optical absorption spectroscopic techniques, SERS is much more sensitive with greater molecular selectivity due to the molecular vibrational information provided by the Raman methodology. This is a significant advantage of SERS since the surface selectivity and sensitivity extends the utility of Raman spectroscopy to a wide variety of applications previously impossible to achieve with conventional Raman techniques. Furthermore, SERS is nondestructive and can be performed under ambient conditions in water, thereby allowing direct analysis of environmental samples such as groundwater and surface water.

2.2 TECHNOLOGY DEVELOPMENT

The key to successful application of SERS for chemical and environmental analyses is the fabrication of noble metallic nanostructured arrays (or substrates) with small gap sizes that are highly reproducible, sensitive and selective to target analyte molecules. SERS relies on the activation of plasmon effects existing at the noble metal surface where analyte molecules of interest are located. The localized surface plasmon (LSP) effect, existing in the proximity of sharp metallic sub wavelength features, is one of the most commonly utilized plasmon effects to enhance the Raman signal. LSP based SERS substrates containing random structures such as metallic nanopores, cubes and triangles, colloidal nanoparticles, nanoshells, and nanowires have been demonstrated to enable high detection sensitivity and, in a few cases, single molecule detection (Gu et al., 2009; Kneipp et al., 1997; Nie and Emory, 1997; Ruan et al., 2007a).

In contrast to most random-structure based SERS substrates that are typically fabricated through wet-chemical methods, highly reproducible nanofabrication techniques have also been used to produce SERS substrates. These nanofabricated substrates possess large SERS enhancement factors at spatially-defined locations which obviates the need to search for active or hot spots as is the case for random structure based SERS substrates. Previously demonstrated examples of this approach include lithography defined nanoparticles with various shapes, deposition assisted nanogaps, chemical template directed nanoparticle deposition, ink-jet directed deposition, and sub-wavelength gratings (D'Andrea et al., 2013; De Jesus et al., 2005; Hatab et al., 2010b; Hatab et al., 2011a; Wells et al., 2009). Because these nanofabricated SERS templates offer well defined features with long range order they provide greater reproducibility than is typically observed for SERS substrates produced via chemical methods. Most importantly, plasmon effects can be precisely controlled and optimized in these nanofabricated structures, and therefore these structures provide an engineering method for the tenability of SERS substrates (D'Andrea et al., 2013).

Over the last 10+ years, we have been developing novel SERS substrate materials for the detection and characterization of a range of chemical, biological agents and environmental pollutants such as perchlorate, nitrate, 2,4,6-trinitrotoluene (TNT), and radioactive uranium and technetium (Dai et al., 1996; Gu et al., 2009; Gu et al., 2004; Hatab et al., 2010a; Hatab et al., 2010b; Hatab et al., 2011b; Ruan et al., 2007b; Ruan et al., 2006b;2007c; Wang and Gu, 2005). Several technological advances in the fabrication of Au- or Ag-based SERS substrates have been realized in our laboratory. We also developed techniques for functionalizing SERS substrates to resolve issues related to selectivity and sensitivity using Au or Ag nanomaterials.

For example, we showed the detection of ClO_4^- at 0.1 μg/L (or 10^{-9} M) concentrations in a laboratory simulated solution with a TDS of ~ 100 mg/L (consisting various competing anions such as Cl^-, $SO_4^=$ and NO_3^-) (Gu et al., 2009), and at ~10^{-5} M in contaminated groundwater (Hatab et al., 2011a; Jubb et al., 2017). A clear Raman band at ~ 935 cm^{-1} was observed for ClO_4^-. The band intensity increased with an increase of ClO_4^- concentration so that the technique can be used for quantitative or semi-quantitative analysis. Molecular recognition functional groups such as dimethylamino-ethanethiol and dimethylamine can also be grafted onto the surface of Au nanoparticles resulting in an enhanced selectivity for ClO_4^- detection because of the interactions between negatively-charged ClO_4^- and positively-charged amine functional groups. These observations indicate the capability of using SERS for the detection and analysis of various energetic pollutants at environmentally relevant concentrations.

We also developed and demonstrated a new type of ordered and elevated gold bowtie arrays with nanoparticle gap sizes of < 8 nm (Fig. 2.1) (Hatab et al., 2010b). This small gap size between two opposing nano-triangular prisms is necessary to achieve maximal SERS enhancement due to strong electromagnetic field enhancement within the gap region of the bowtie arrays (Fig. 2.1d). Both theoretical calculations and experiments have shown that the SERS enhancement factor increases exponentially with decreasing gap size at the nano-scale (Fig. 2.1e) (Hatab et al., 2010b; Jain et al., 2007b; Zuloaga et al., 2009). These bowtie arrays were fabricated by combining electron beam lithography (EBL), reactive ion etching, metal deposition and lift-off techniques as detailed in Hatab et al. (Hatab et al., 2010b). EBL is the ideal tool for fabricating SERS substrates with precisely defined shape and systematically variable nanogap sizes necessary for achieving SERS enhancement and for gaining insight into the underlying enhancement mechanisms.

A controlled deposition of 40 nm gold on top of 100 nm to 200 nm tall silicon (Si) posts was used to close the 20-nm gap size defined by conventional EBL technique. This new approach allowed the fabrication of clean and reproducible overhanging bowtie arrays with a small gap (Fig. 2.1) (Hatab et al., 2010b). These ordered gold array substrates have shown superior reproducibility and high sensitivity with an enhancement factor on the order of 10^{11}. We also demonstrated their applicability for the detection of ClO_4^- and other contaminants in both laboratory prepared aqueous solutions and contaminated groundwater, as described in Sections 6.2 and 6.5.

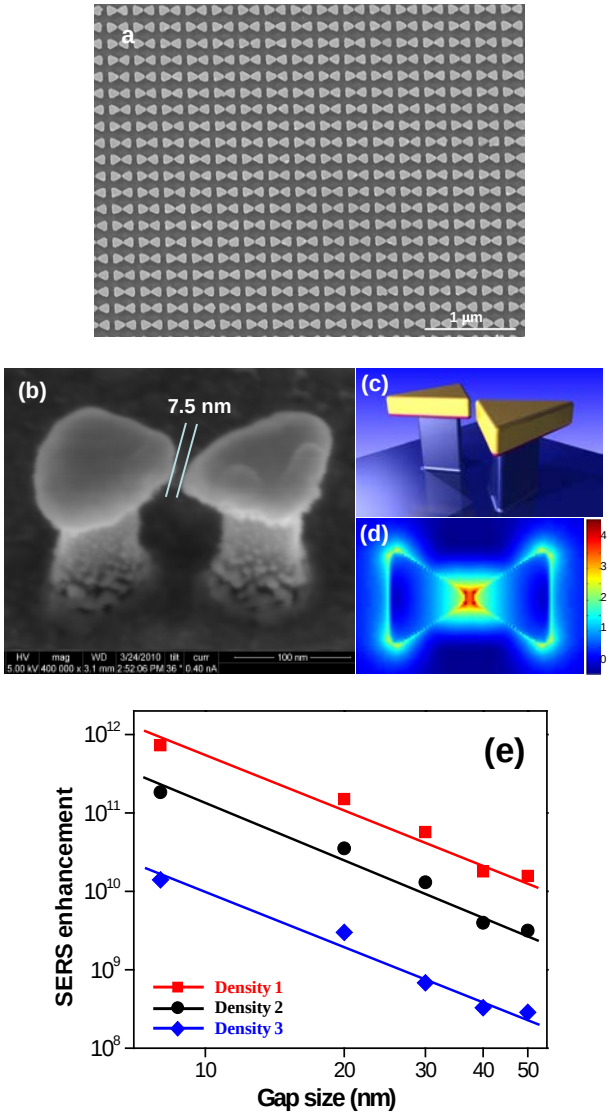

Figure 2.1. (a) Top View SEM Image of a nano-fabricated Gold Bowtie Array Substrate by EBL; (b) Enlarged, Tilted View of a Three-dimensional Gold Bowtie from (a) with a Gap Size of 8±1 nm; (c) Artistic Drawing of a Gold Bowtie on Top of Silicon Posts; (d) Model Calculations of the Electromagnetic Field Enhancement Within the Gap Region of a Bowtie; (e) Model (lines) and Experiments (symbols) Showing that the SERS Enhancement Increases Exponentially with Decreasing Gap Sizes at Varying Bowtie Densities (Hatab et al., 2010b).

2.3 ADVANTAGES AND LIMITATIONS OF THE TECHNOLOGY

The new SERS technology is designed to provide rapid detection and screening of ClO_4^- in environmental samples such as contaminated groundwater and surface water. It is useful for field sensing applications that require rapid identification outside the typical laboratory environment. The technology also has the potential to detect other energetic compounds or pollutants such as TNT in groundwater although additional development and optimization are needed since SERS substrate design is affected by specific contaminant molecules. As stated earlier, in comparison with fluorescence and optical absorption spectroscopic techniques, SERS is more sensitive with greater molecular selectivity (or fingerprinting) due to the molecular vibrational information provided by the Raman methodology. This is a significant advantage by using SERS since the surface selectivity and sensitivity extends Raman spectroscopy utility to a wide variety of applications previously impossible to achieve with conventional Raman techniques. Furthermore, SERS is nondestructive and can be performed under ambient conditions in water, thereby allowing direct analysis of environmental samples such as groundwater and surface water.

Similar to other techniques, however, analysis of realistic environmental samples by SERS presents a challenge because of the complex geochemistry and mixed contaminants resulting in interference with the analysis or false positive responses. This is also complicated by the fact that concentrations of the analytes of interest (ClO_4^- in this case) are usually orders of magnitude lower than organic and inorganic interfering ions such as total organic carbon (TOC), nitrate and sulfate, which also give strong Raman signals and can thus mask the detection of the analyte itself or cause significant variations in analysis. The standard addition method (described in Section 5.3.1) is sometimes used to minimize potential matrix interferences due to unknown background organic or inorganic materials in the groundwater. As part of this ESTCP demonstration, we further clarify the factors that cause interference issues with the Raman technique, better define the lower limits of instrument accuracy, and confirm the overall utility of the instrument for site assessment applications and potentially long-term monitoring.

3.0 PERFORMANCE OBJECTIVES

Table 3.1 provides a list of performance objectives, data requirements, and success criteria for the project with additional details provided in Sections 3.1 to 3.4. Since the overall objective of the project was to develop, demonstrate and validate a new instrument (field-ready Raman sensor) for ClO_4^- detection and analysis in groundwater, the main performance objectives are to determine the selectivity and sensitivity of the instrument to quantify ClO_4^- in groundwater under differing conditions (such as differing natural anion concentrations, pH, ORP, and co-contaminants, such as TCE) and varying ClO_4^- concentration ranges at multiple DoD sites. We compare results between SERS measurements and EPA approved IC methodologies to determine if the two methods are comparable at the confidence level of 80%. This confidence level is used primarily because SERS is a spectroscopy-based technique, in which peak position and peak height may vary due to substrate variations, laser focusing, and environmental geochemical conditions or interferences. Nonetheless, our goal is to establish a new SERS methodology that can be used for rapid screening and/or in-situ field monitoring of ClO_4^- in contaminated groundwater or surface water.

Table 3.1. Performance Objectives, Data Requirements, Success Criteria.

Performance Objective	Data Requirements	Success Criteria	Result
Quantitative Performance Objectives			
Development of a portable Raman sensor; SERS substrate optimization and commercial production	NA	• Field-ready meter and optimized substrates • Commercially produced SERS substrates	• A field-ready instrument was developed and commercial SERS substrates produced
Selective identification and detection of ClO_4^-	Raman spectra; peak intensities; common anions, cations, and co-contaminants	• Identification of ClO_4^- in the presence of common anions and cations at < 10 mM. • ClO_4^- detection in the presence of co-contaminants such as VOCs at < 1 ppm.	• ClO_4^- was readily identified in the presence of common anions, cations, and co-contaminants • However, the presence of interfering ions (>0.2 mM) made SERS detection less sensitive
Sensitive detection and quantification of ClO_4^-	Raman data; peak intensities; standard addition and calibration; IC data by EPA methods	• Quantitative analysis of ClO_4^- at LOD 3 ppb. • Analysis of ClO_4^- at wide concentration ranges from ~3 to 100,000 µg/L. • Measurement accuracy and precision at 20% or better • Quantitative comparison between IC and SERS ClO_4^- results at 80% confidence level	• The anticipated LOD for ClO_4^- was not achieved in site groundwater. The LOD was ~ 100 ppb for the method • Detection of ClO_4^- at >100 µg/L, and the precision may vary >20%, depending on interferences
Qualitative Performance Objectives			
Sensor methodology developed	Method development based on above data and analysis	• Method established for field monitoring and quantification • System robustness and ease of use	• Method established and easy to use

3.1 DEVELOPMENT OF PORTABLE RAMAN SENSOR AND SERS SUBSTRATE OPTIMIZATION/COMMERCIALIZATION

3.1.1 Data requirements for portable Raman sensor and optimized SERS substrates

There are no specific data requirements for this task.

3.1.2 Success criteria for portable Raman sensor and optimized SERS substrates

Success criteria for this task were the development and implementation of a field-ready portable Raman sensor and optimization of SERS substrates for commercial production. Both criteria were met in this case. A portable Raman instrument was developed and field-tested. Further work would be required to make this instrument "shippable" and more durable for commercialization due to the use of a fiber optic probe and SERS sensitivity to matrix interferences. However, the instrument was successfully demonstrated in the field on multiple occasions. Significant improvements were made in SERS substrates over the course of the project, leading to better sensitivity of ClO_4^- analysis in a laboratory setting, and successful commercial production of SERS substrates with acceptable quality and reproducibility.

3.2 SELECTIVE IDENTIFICATION AND DETECTION OF ClO_4^-

3.2.1 Data requirements for selective identification and detection of ClO_4^-

Data required to evaluate the performance objective of the selective identification and detection of ClO_4^- include collection of the Raman spectra for each individual sample so that the Raman peak and peak position at about 935 cm^{-1} can be used for the identification of ClO_4^-. As stated earlier, different chemical bonds give unique vibrational frequency shifts (or Raman peaks), which can be used for the identification or fingerprinting of the analyte molecule. Under idealized conditions (e.g., in purified water), this can be easily done. However, under realistic environmental conditions, groundwater often contains a variety of organic or inorganic anions (e.g., Cl^-, NO_3^-, SO_4^{2-}), cations (Ca, Mg, Na, K, Fe), and co-contaminants (such as VOCs), which can cause changes in the peak intensity and position making identification of the target molecule (ClO_4^- in this case) challenging. Therefore, the specificity of the methodology for the target molecule is important. We thus collected not only the Raman spectra of individual samples but also measured the concentrations of major organic or inorganic anions, cations, and co-contaminants (such as VOCs) so that the effects of these interfering ions on ClO_4^- identification could be evaluated. As described in Sections 4.1 and 4.2, multiple DoD sites with different groundwater characteristics were selected and used for the evaluation. Standard curves, data, and results of the standard addition were collected and analyzed. The measured ClO_4^- concentrations were also validated by parallel measurements using the standard EPA method.

3.2.2 Success criteria for selective identification and detection of ClO_4^-

The major success criteria are to resolve the peak position of ClO_4^- and thus identify ClO_4^- in complex groundwater matrices with common anions and cations at concentrations < 10 mM (typically observed in groundwater). Our results show that the sensor can selectively detect ClO_4^- in the presence of various inorganic anions (e.g., SO_4^{2-} and NO_3^-) and metal ions (see Fig. 3.1, and additional details described in Section 6.5). However, presence of major anions such as SO_4^{2-} and NO_3^- at relatively high concentrations (>200 µM) could significantly interfere with SERS analysis of ClO_4^-. Many DoD sites

are also contaminated with VOCs, albeit at low concentrations (usually < 1 ppm), which did not pose a significant issue for the sensor to selectively detect ClO_4^- in the presence of < 1 ppm VOCs. We thus partially met this criterion by selectively detecting ClO_4^- in the presence of interfering ions such as SO_4^{2-} and NO_3^- at < 200 µM.

3.3 SENSITIVE DETECTION AND QUANTIFICATION OF ClO_4^-

3.3.1 Data requirements for sensitive detection and quantification of ClO_4^-

In addition to the selectivity, sensitive detection and quantification of ClO_4^- at low concentrations (e.g., < 3 ppb) is another major performance objective of the project. Data required to evaluate this performance objective include those identified in Section 3.2.1. Additionally, perchlorate concentrations measured in the field by SERS sensor are compared with those obtained by a typical laboratory analysis using the standard EPA method using ion chromatography. Statistical analyses are used for comparisons of the results.

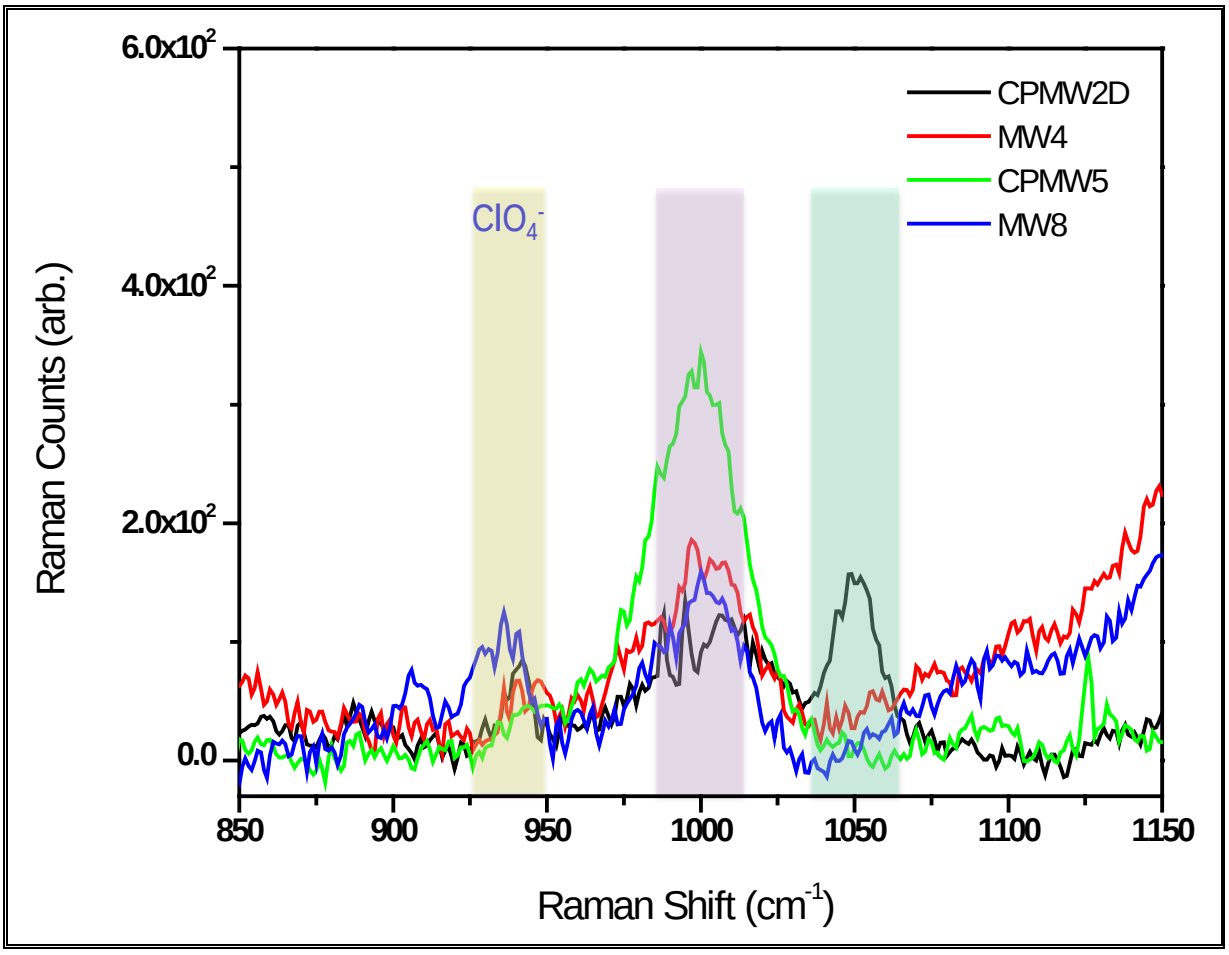

Figure 3.1. Illustration of Selective Detection of ClO4- by SERS in the Presence of Interfering Ions such as SO42- and NO3- in Groundwater Obtained from IHDIV Site.

Note that CPMW2D, MW4, CPMW5, and MW8 denote groundwater samples obtained from different sampling wells.

3.3.2 Success criteria for sensitive detection and quantification of ClO_4^-

The success criteria are quantification of ClO_4^- in complex groundwater matrices with a detection limit better than 3 μg/L ClO_4^-, and the method can be used in a wide range of ClO_4^- concentrations (from 3 to >100,000 μg/L) observed at various DoD contamination sites. Analytical variances between results obtained by the Raman sensor and the standard EPA method should be no more than 20%. The results show that the portable Raman sensor can detect ClO_4^- at concentrations above 10^{-6} M (or > 100 μg/L) in natural groundwater. This LOD is higher than what had been anticipated from laboratory studies, in part due to the presence of various interfering organic and inorganic ions in natural groundwater. Additionally, significant variations in SERS measurements (>30%) were observed, likely due to the sensitivity of SERS response to many interfering organic and inorganic ionic species in natural water (see additional details in Section 6.5).

3.4 ESTABLISH METHODOLOGY FOR ClO_4^- DETECTION BY THE RAMAN SENSOR

3.4.1 Data requirements for methodology

A qualitative performance objective is to establish the Raman sensor methodology for ClO_4^- detection and analysis at multiple DoD sites. Based on above three quantitative performance objectives, detailed analytical procedures, method LOD under field conditions, and potential interferences are documented by using the Raman sensor for ClO_4^- detection and analysis (see Sections 6.4 and 6.5).

3.4.2 Success criteria for methodology

The success criteria are that the methodology is established and can be understood and utilized by a field technician in less than 4 hours of onsite training. A step-by-step operating procedure is provided in Section 6.6. A field technician can easily understand and use the portable Raman sensor for ClO_4^- detection. The operating procedure also includes the method of standard addition to correct potential matrix interferences in natural groundwater, and quantification techniques.

4.0 SITE DESCRIPTION

Field testing of the Raman sensor technology was conducted at two different sites, the Indian Head Division (IHDIV) Naval Surface Warfare Center, in Indian Head, Maryland, and Redstone Arsenal (Redstone) outside of Huntsville, Alabama. Sections 6.5.2 and 6.5.3 details two field demonstrations at IHDIV between October 2015 and October 2016, and Section 6.5.4 provides details of the field demonstration at Redstone in November 2016. A field trial was also initially planned for Naval Surface Warfare Center, Dahlgren near Dahlgren, VA, primarily due to the co-existence of ClO_4^- and explosives, such as RDX and HMX in groundwater at an active range. However, after completing laboratory optimization work, the ClO_4^- concentrations at this site were deemed generally too low (10-80 ppb) to be readily detected by the field Raman instrument. The site characteristics of IHDIV and Dahlgren are provided below and the results from the demonstrations are provided in Section 6.5. We also initially planned to conduct a field test at the Fort Wingate Depot Activity (FWDA) site in Gallup, New Mexico, but this demonstration was abandoned due to the security and site access issues. We subsequently screened additional sites, including groundwater samples collected from West Texas and Kirtland Air Force Base in California. However, as shown in Tables 4.1 and 4.2 below, ClO_4^- concentrations at these sites were also too low to detect by the Raman sensor technique.

Table 4.1. Geochemical Characterization of Groundwater Samples from High Plains, West Texas.

Sample wells	Cl^-	$SO_4^=$	NO_3^-	Br^-	TDS	pH	ClO_4^-
	(mg/L)						(□g/L)
Bailey MW-1	1319.5	1783.4	n.a.	10.7	4830	8.00	0.0
Bailey MW-2	52.3	107.8	8.3	0.4	524	8.52	0.0
Gaines MW-1	444.4	999.1	12.9	2.9	2180	8.25	34.5
Gaines MW-3	649.1	1267.6	32.3	4.1	3320	8.25	52.5
Martin MW-1	975.9	781.7	12.4	7.6	3400	8.22	14.1

Table 4.2. Geochemical Characterization of Groundwater Samples from the Kirtland Air Force Base, California.

Kirtland samples	Cl^-	$SO_4^=$	NO_3^-	Br^-	TDS	ClO_4^-
	(mg/L)					□g/L
EOC-BH1	317	79.3	0.2	2.6	2730	0.5
EOC-BH2	332	81.9	0.2	2.4	2880	0.5

4.1 FIELD DEMONSTRATION AT INDIAN HEAD DIVISION, NAVAL SURFACE WARFARE CENTER

4.1.1 Site background

The IHDIV Naval Surface Warfare Center, is located near Indian Head, Maryland in Charles County. This facility, which is located approximately 50 km from Washington DC, manufactures explosives and tests energetic compounds for the US Navy. Fig. 4.1 shows the site location. The area where the Raman sensor was evaluated for this project is located on the southeast side of IHDIV Building 1419. Fig. 4.2 shows the site. Building 1419 is used to clean out or "hog out" solid propellant containing ammonium perchlorate from various devices, including rockets and ejection seat motors, that have exceeded their useful life span. The hog out process and former waste handling methods have impacted the groundwater near Building 1419. The presence of a former nitration plant in this area also has apparently resulted in high nitrate (NO_3^-) in some locations (as high as 14 mg/L as N).

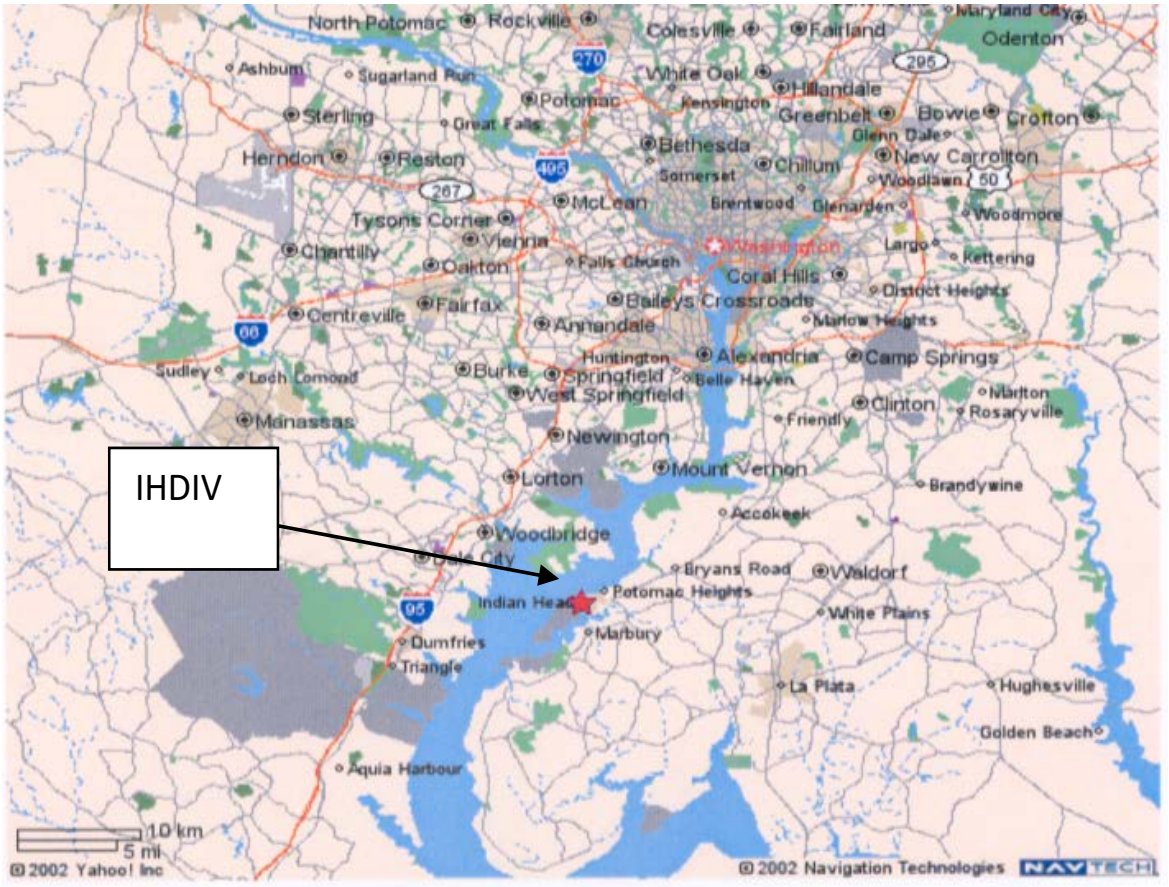

Figure 4.1. Location of the IHDIV Site, Maryland, USA.

Figure 4.2. Location of the Raman Sensor Field Demonstration at the IHDIV Site.

4.1.2 Geochemistry and contaminant concentrations

Site assessment work performed at Building 1419 is described in Hatzinger et al., (2006). Historical groundwater characterization data (samples collected January, 2002) are provided in Table 4.3 and Table 4.4. In summary, groundwater samples were collected from 17 Geoprobe borings to the southeast of Building 1419 and analyzed for ClO_4^-, NO_3^-, SO_4^-, pH, and dissolved oxygen (DO). Results of the chemical analyses from the Geoprobe borings are provided in Table 4.1. Groundwater samples collected from six monitoring wells present onsite were also analyzed for ClO_4^-, pH, and DO (Table 4.3). The field characterization data revealed a shallow, narrow plume of ClO_4^- contamination behind Building 1419 with levels ranging from below detection to approximately 430 mg/L. With a few exceptions, the pH of the site was below 5, and the dissolved oxygen levels were < 2 mg/L. In some instances, dissolved metal ions, such a Fe and Mn, were also elevated at this site.

Two previous demonstration plots, each consisting of 2 injection wells, 2 extraction wells and 9 groundwater monitoring wells were installed near Building 1419 in 2002, and a small field demonstration was conducted in which lactate was actively injected into one demonstration plot and another served as an unamended control plot. Full details of the demonstration are presented in Hatzinger et al. (2006). All groundwater wells for this demonstration as well as the wells installed for site assessment remain in place. A subset of these wells was selected for groundwater sampling during two field demonstrations of the Raman technology conducted at the IHDIV site. These data are described in Sections 6.5.2 and 6.5.3.

Table 4.3. Groundwater Chemistry at the IHDIV Demonstration Site (Hatzinger et al., 2006).

Boring	Perchlorate (mg/L)	Nitrate as N (mg/L)	Sulfate (mg/L)	pH	DO (mg/L)[1]
GP-1	120	0.6	66	4.67	NA[2]
GP-2	<2.5	3.0	220	8.08	NA
GP-3	8.2	1.9	280	5.23	NA
GP-4	57	0.3	110	4.54	NA
GP-5	65	0.1	130	4.21	1
GP-6	280	11	69	5.62	1
GP-7	35	1.5	66	4.21	0.1
GP-8	430	14	62	4.57	NA
GP-9	73	0.4	56	4.44	0.8
GP-10	300	12	70	4.31	1
GP-11	230	14	72	4.71	0.8
GP-12	55	2.0	110	6.46	NA
GP-13	230	3.8	64	4.61	1.5
GP-14	14	1.5	250	4.97	NA
GP-15	9.8	<0.2	160	5.34	0.2
GP-16	270	2.8	74	4.16	1
GP-17	<5	<0.2	140	4.83	0.2

[1] DO: Dissolved Oxygen: Analysis performed by colorimetric field method (CHEMetrics).

[2] NA: Not analyzed.

Table 4.4. Groundwater Chemistry and ClO_4^- Concentrations in Monitoring Wells 1-6 at the IHDIV Site (Hatzinger et al., 2006).

Monitoring Well	Perchlorate (mg/L)	pH	DO (mg/L)[1]
MW-1	84.7	5.02	1.49
MW-2	1.9	6.75	NA
MW-3	1.6	4.13	NA
MW-4	181	5.00	1.64
MW-5	82.8	6.20	1.13
MW-6	142.4	5.03	1.33

[1] DO: Dissolved oxygen.

4.2 REDSTONE ARSENAL

4.2.1 Site background

The Redstone Arsenal is an active US Army facility in northern Alabama, adjacent to Huntsville in Madison County (Fig. 4.3)**.** The current Redstone Arsenal originated as the Huntsville Arsenal in 1941, a facility built to produce chemical weapons for World War II, and the adjacent Redstone Ordnance Plant, used to manufacture grenades, bombs, and other ordnance (http://www. encyclopediaofalabama.org/face/Article.jsp?id=h-1882). The facilities were named Redstone Arsenal in 1943 (http://themilitarystandard.com/missile/redstone.php). After

World War II, the facility was reorganized to become a center for the US Army's rocket and missile projects, and now includes several different commands and centers involved with the testing and development of missiles. Redstone is also the home of the NASA Marshall Space Flight Center.

The demonstration was conducted using groundwater collected from the open burn/open detonation (OB/OD) area at Redstone Arsenal. The OB/OD Area is an active facility located within the RSA-151 groundwater unit in the southern portion of Redstone (Fig. 4.4). The OB/OD Area lies on topographically high ground surrounded by wetlands on three sides. The far northern boundary of the OB/OD Area is adjacent to a creek and wetland area. The far western boundary of the OB/OD Area is adjacent to wetlands and is approximately 250 feet from a lake located farther to the west. The OB/OD Area is located approximately 1,000 feet east of the Tennessee River. Portions of RSA-013 (Unlined Open Burn Pads) and RSA-014 (Waste Burn Trenches), currently inactive sites, are also located within the OB/OD Area site boundary.

Figure 4.3. Arial Map Showing the Location of Redstone Arsenal, Huntsville, Alabama, USA.

Upper red circle indicates CB&I building facility.

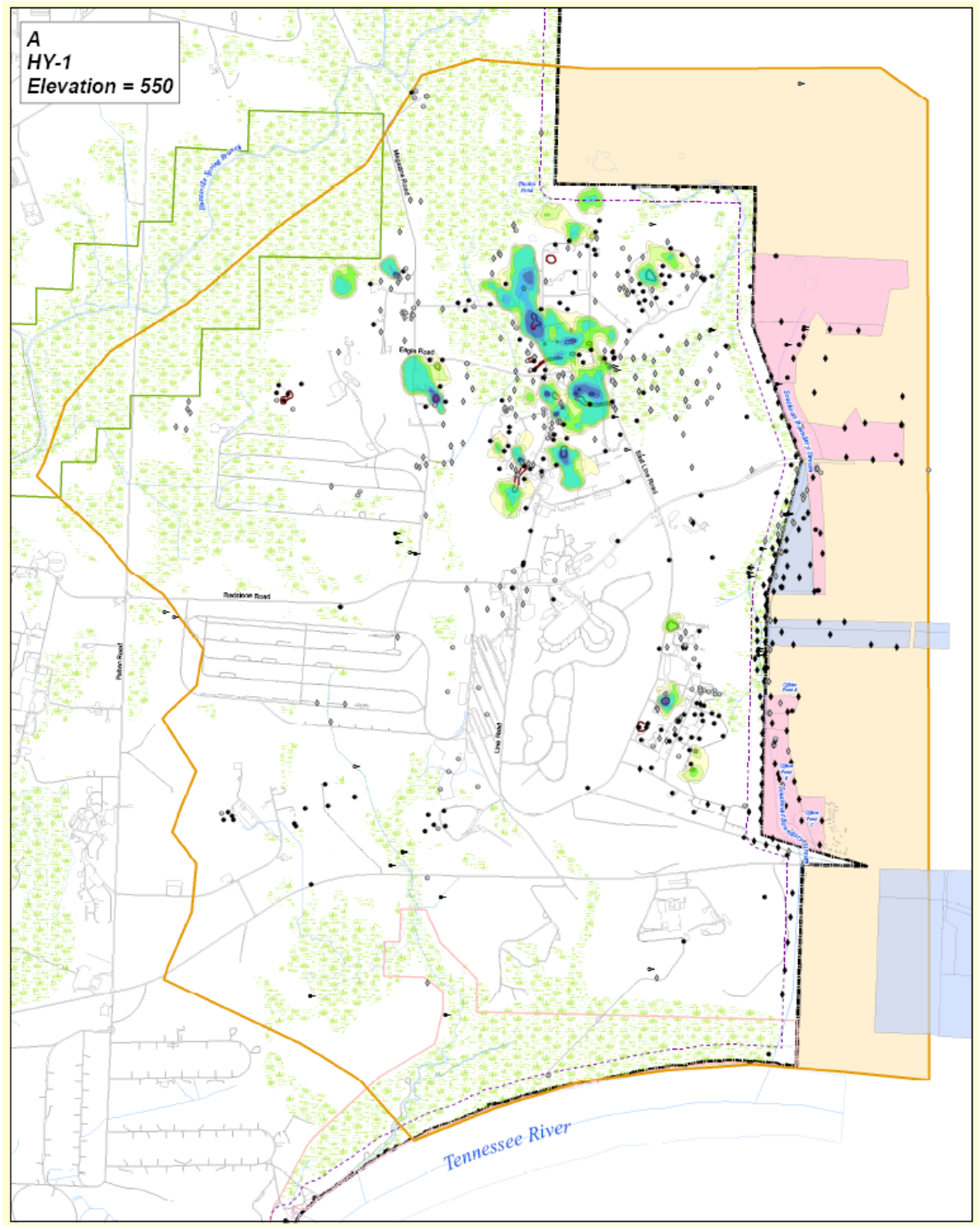

Figure 4.4. Location and Perchlorate Concentration Contours in Hydrostratigraphic Zone A of the Groundwater Unit at Redstone Arsenal, Alabama, USA.

4.2.2 Geochemistry and contaminant concentrations

The groundwater at the Redstone site has been previously characterized. In HY-zone 1, ClO_4^- concentrations in the site database range from ~ 0.05 µg/L to > 200 mg/L. A number of the wells also have trichloroethene (TCE) as a co-contaminant, at concentrations ranging from < 1 µg/L to > 800 mg/L. Tetrachloroethene (PCE) and lower-chlorinated degradation products of these two chlorinated ethenes, including 1,2-*cis* dichloroethene (cis-DCE), and vinyl chloride (VC) are also detected sporadically at the site. The groundwater across the large site is generally neutral in pH (~ 5.5 to 7.5), ORP values are variable with location and time, ranging about –200 to + 300 mV, similar to dissolved oxygen, which varies from < 1 to > 10 mg/L. Alkalinity is generally > 100 mg/L as $CaCO_3$. This site was selected as a test site for the Raman sensor primarily to evaluate the impact of VOCs such as TCE and possibly other chlorinated solvents, on ClO_4^- detection. The ORP, DO, alkalinity, pH and other parameters across the site will also be taken into consideration when selecting wells to sample in order to maximize the number of variables that can be tested.

In the OB/OD Area, eight wells are annually monitored. The pH in these wells is also variable, ranging from a low of 4.1 to a high of 6.9 in different wells during the 2015 sampling event. Wells across this pH range were sampled for this demonstration. The DO at the site ranged from 0 mg/L to 3.8 mg/L in 2015 and the ORP varied from -108 mV to + 242 mV in different wells. ClO_4^- concentrations ranged from 3 to 7580 µg/L in 2015. There are also variable levels of TCE present in several of the groundwater wells with concentrations ranging from 3 to 541 µg/L in 2015. The highest concentration was present in well PS12RS240, which also contained 187 µg/L of *cis*-DCE in 2015. This well was selected for Raman testing based on the elevated VOCs in addition to ClO_4^-. Other contaminants were present in select wells, including 1,4-dioxane and RDX, although the concentrations were generally below 15 µg/L in 2015. These wells also were tested, and detailed testing results are provided in Section 6.5.4.

Page Intentionally Left Blank

5.0 TEST DESIGN AND EVALUATION

5.1 EXPERIMENTAL DESIGN

Unlike many ESTCP ER projects for which a single demonstration site is chosen to test a remediation approach, this project is being conducted to test the performance of the SERS sensor as an instrument for ClO_4^- detection. As such, the basic testing procedures and experimental design are the same, except that the test was performed multiple times at two sites, covering a general range of geochemical and contaminant conditions. The field testing was conducted following initial characterization of the groundwater samples and a significant amount of optimization and testing of both the field Raman instrument and the SERS substrates that are required for contaminant analysis by the SERS technology. Those results are described in Section 6.5. In addition, laboratory studies were completed in conjunction with the field demonstration(s) to better understand the potential interferences with the SERS technique that are likely to be encountered in the field. Those results are presented in Section 6.4. Additional field sites were considered but field trials were not conducted, partly due to the low or non-detect ClO_4^- concentrations found in these groundwaters and to the time and budget constraints, as described earlier.

5.2 GROUNDWATER SAMPLING

5.2.1 Sample collection

Groundwater samples were collected for this project. In general, low-flow sampling procedures were followed (USEPA, 2010). Groundwater sampling was performed using pumps appropriate to the well depth and desired flow rate. For shallow groundwater (< 10 ft) a peristaltic pump was used to collect samples. New tubing (or dedicated well tubing) was used depending on site conditions. For deeper groundwater (> 10 ft), a Grundfos submersible pump (or equivalent) was used to collect groundwater samples. After the appropriate pump was installed/set-up, groundwater was passed through a field meter (e.g., YSI multi-parameter meter or equivalent) at a low flow rate, and geochemical parameters were measured with time, including dissolved oxygen, pH, conductivity, temperature, and oxidation-reduction potential. When these parameters stabilized according to the specifications in low-flow groundwater sampling guidance (USEPA, 2010), groundwater samples for ClO_4^- analysis were collected. Sampling for other desired chemical analyses were also performed at this time.

In addition to ClO_4^-, geochemical parameters including major anions (e.g., Cl^-, SO_4^{2-}, NO_3^-) dissolved metal ions, pH, TDS, or alkalinity were measured for most of the samples collected for the demonstration. Other more specialized analyses for explosives (EPA 8330) or volatile organic compounds (EPA 8260), were performed on a site-by-site basis based upon the expected co-contaminants in groundwater.

5.2.2 Supporting analytical methods

5.2.2.1 Perchlorate analysis

Perchlorate concentrations measured by the portable Raman sensor were compared with those determined by the reference EPA Method 314.0 (ion chromatography with conductivity detection; USEPA, 1999) performed in the CB&I Analytical Laboratory in Lawrenceville, NJ. IC analysis was also conducted at ORNL for some samples for comparison.

5.2.2.2 Field parameters

Typical geochemical parameters were collected at each well during sampling using a field meter (e.g., YSI multi-parameter meter). The parameters, which provide a basic geochemical baseline for each well, include temperature, dissolved oxygen, oxidation-reduction potential, conductivity, and pH. The stabilization of these parameters with time was also used to determine when to collect field samples, according to USEPA guidelines on low-flow sampling (USEPA, 2010).

5.2.2.3 Anions and cations

Common anions, including Cl^-, $SO_4^=$, NO_2^-, and NO_3^- were measured by EPA Method 300.0 (Ion chromatography with conductivity detection) in the CB&I Analytical Laboratory in Lawrenceville, NJ, as well as in laboratories at ORNL. Common metal cations, including Ca, Mg, K, Na, Fe, Al, Mn, and Cu were measured at ORNL by EPA Method 6020A using inductively coupled plasma - mass spectrometry (ICP-MS).

5.2.2.4 Co-contaminants

Contaminants other than ClO_4^- were not expected at IHDIV, and no other analyses were conducted. At Redstone, a variety of other contaminants are potentially present in groundwater wells in the OB/OD Area, including explosives, pesticides, and chlorinated volatile organic compounds (cVOCs), among others. Because our SERS demonstration was coordinated with the annual OB/OD groundwater sampling event at this location, a variety of analyses were conducted on the groundwater samples based upon permit. The analyses, which were performed by Empirical Analytical in Nashville, were conducted in accordance with the U.S. Environmental Protection Agency's (EPA) *Test Methods for Evaluating Solid Waste, Physical/ Chemical Methods* (SW-846), and included the following:

Nitroaromatic compounds by SW-846 Method 8330A
cVOCs by SW-846 Method 8260B
sVOCs and PAHs by SW-846 Method 8270D
Pesticides and PCBs by SW-846 Methods 8081B and 8082A
Herbicides by SW-846 Method 8151A
Dioxin/furans by SW-846 Method 8280B
TAL metals and tin by SW-846 Methods 6010C and 7470A

5.3 FIELD TESTING

5.3.1 Instrument and operating parameters

A portable Raman sensor (shown in Fig. 5.1) was utilized throughout the field demonstration. The application of the technology requires the following: (1) preparation of nano-structured SERS substrates (pre-prepared in the laboratory); (2) interface the SERS substrate with the Raman probe through a SERS module (pre-fabricated); (3) collection of the groundwater sample; (4) pipette a small drop of the groundwater sample onto the SERS substrate; (5) spectral collection and analysis of ClO_4^- by the SERS Raman probe; (6) calculation of ClO_4^- concentrations against standard calibration curves; and (7) statistical analysis, interpretation, and correlation of data with those obtained by standard EPA methods. Multiple wells at each of the test sites were used for analysis, and multiple analyses (usually triplicate) were performed for select samples.

A standard addition method was employed for some samples due to matrix interferences with unknown background organic or inorganic ions in the groundwater. In brief, the method involves the addition of varying amounts of ClO_4^- (standard solutions in deionized water) to a fixed amount (e.g., 5 mL) of the same groundwater. The samples (with ClO_4^- standards) were made up to a fixed final volume (e.g., 10 mL) so that all these samples contain the same matrix interferences, except the ClO_4^- concentration differs. Samples were then analyzed, and the characteristic Raman intensities for ClO_4^- (Y-axis) were plotted against the final added ClO_4^- concentration (X-axis). A linear regression was then used to calculate the absolute value of the X-axis intercept, which corresponds to the true concentration of ClO_4^- in the unknown groundwater sample.

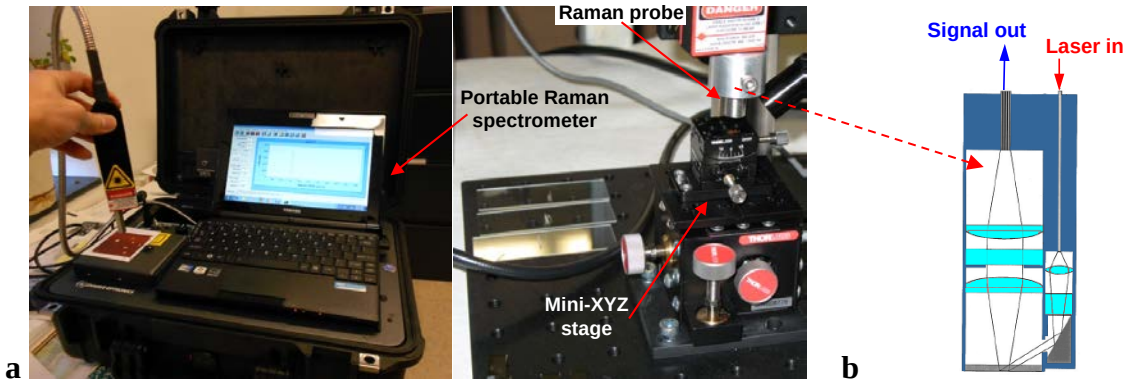

Figure 5.1. (a) A Portable Raman Sensor Equipped with a Fiber-optic Raman Probe was used to Detect ClO_4^-. (b) A Schematic, Enlarged View of the Raman Probe with Optical Lens and Fibers for the Incident Laser and Signal Collection.

5.3.2 Sampling time

Sampling and analysis at each site lasted from 1 to 3 days depending on the number of wells requiring sampling, site conditions, analytical parameters to be collected. At the IHDIV site, field demonstrations were performed in October 2015 and October 2016. For the Redstone site, the field demo was performed in coordination with the schedule of the field crew performing annual groundwater sampling in the OB/OD in November 2016.

5.3.3 Residuals handling

Site regulations or guidance concerning disposal of groundwater were followed. Since no chemicals or pre-treatments are necessary for the demonstration of the Raman sensor, there were no other residuals or chemicals requiring disposal.

5.3.4 Health and safety

Site specific Health and Safety Plans (HASP) were followed during the demonstrations.

5.4 DATA ANALYSIS

5.4.1 Data analysis, interpretation and evaluation

Selective identification of ClO_4^- from complex groundwater matrices was a key measure of the success of the portable Raman sensor. This is accomplished by the collection of the Raman spectra, in which characteristic Raman peak at about 935 cm^{-1} is obtained and analyzed under varying environmental conditions or groundwater matrices. The peak position may shift slightly depending on the groundwater chemistry since the vibrational frequency of the Cl-O bond could be affected by its neighboring atoms or the bonding environment and the co-existing ions. The peak height or intensity can then be used for the quantification of ClO_4^- in unknown samples through calibration standards. The response of the sensor to ClO_4^- concentration defines the analytical detection limit, which is another key measure of the success of the project. In many cases, we utilized the standard addition technique (see section 5.3.1), in which ClO_4^- standards are added to the same groundwater matrix and spectra collected, so that the ClO_4^- concentration in the unknown samples can be determined more accurately.

5.4.2 Statistical analysis

An evaluation of the new Raman technique for ClO_4^- analysis vs the traditional EPA 314.0 method was conducted using multiple techniques. A subset of split samples (at least two wells for each site) were analyzed multiple times by each technique giving a measure of method variability. The means for each sample set were then compared by a standard two-sample *t*-test. Raman peak position and peak intensity changes with groundwater characteristics (e.g., pH and anion concentrations) was used for assessing their influence on ClO_4^- detection. Analyzing the sample multiple times also shows the repeatability of the analysis.

The dataset was also evaluated according to the basic procedures described in Bland and Altman (1986) for comparing two different measurement techniques. The data from all wells for which samples were analyzed by both analytical methods were initially plotted against each other on a correlation plot (Raman on the y axis and IC on the x axis), and the data were compared. In instances where the sample was analyzed multiple times by both methods, error bars were displayed for the points. This analysis shows the correlation between the data or any bias. A correlation coefficient (R) for the data was calculated. To further measure agreement between the data, the means of analysis by both methods for each sample were plotted against their differences (see additional details in Section 6.5).

6.0 PERFORMANCE ASSESSMENT

6.1 CONSTRUCTION OF A PORTABLE RAMAN SENSOR

A SERS-based portable Raman sensor was constructed in our laboratory (Fig. 5.1). The sensor consists of a Raman analyzer equipped with a 300-mW near infrared laser and a fiber-optic probe for laser excitation and signal collection (Fig. 5.1a). A key component of the sensor probe is the interface where the nanostructured SERS array substrate is attached, and the Raman signal becomes substantially enhanced (Hatab et al., 2010b; Hatab et al., 2011b). A diode laser operated at 785 nm is used as the excitation source with a high Rayleigh rejection fiber optic probe, which serves three purposes: 1) transmission of the incident laser to the SERS substrate or the sample, 2) collection of the scattered Raman signal to the spectrograph, and 3) removal of unwanted background signals through an optical filtering device. The incident laser is focused onto the SERS substrate, which is mounted on a xyz stage to allow precise focusing to obtain maximal signal. The scattered SERS signals are then collected through a separate optical fiber to the spectrograph/detector system. A schematic drawing of the Raman probe is provided in Fig. 5.1b.

To facilitate the field analysis, a focal-length adjustable SERS probe module (Fig. 6.1) was designed and fabricated by Nanova Inc., which was intended to be used with the portable Raman sensor for field demonstration. The module allows the vertical adjustment of the focal length so that the excitation laser beam can be better focused on the SERS substrate for optimal detection of ClO4-. Subsequent laboratory and field tests indicated that, while the module performed as designed, the adjustment was not smooth, partly due to the fact that module gears were made with plastic materials (with relatively high frictions). The design was later improved by using a metallic fine-threaded bolt. Both units have been successfully used to measure spectra using the portable Raman sensor. Additional adjustments can be made to further improve the ergonomics and repeatability for SERS detection. Fig. 6.2 illustrates the use of an active SERS substrate mounted on a glass slide, which is then inserted into the SERS module, allowing collection of Raman signal via a fiber optic SERS probe to the Raman analyzer.

Figure 6.1. (Top) Initial and (Bottom) Improved Design and Fabrication of a SERS Module, Allowing for Vertical Adjustment of the SERS Probe Focal Point for Optimal Performance.

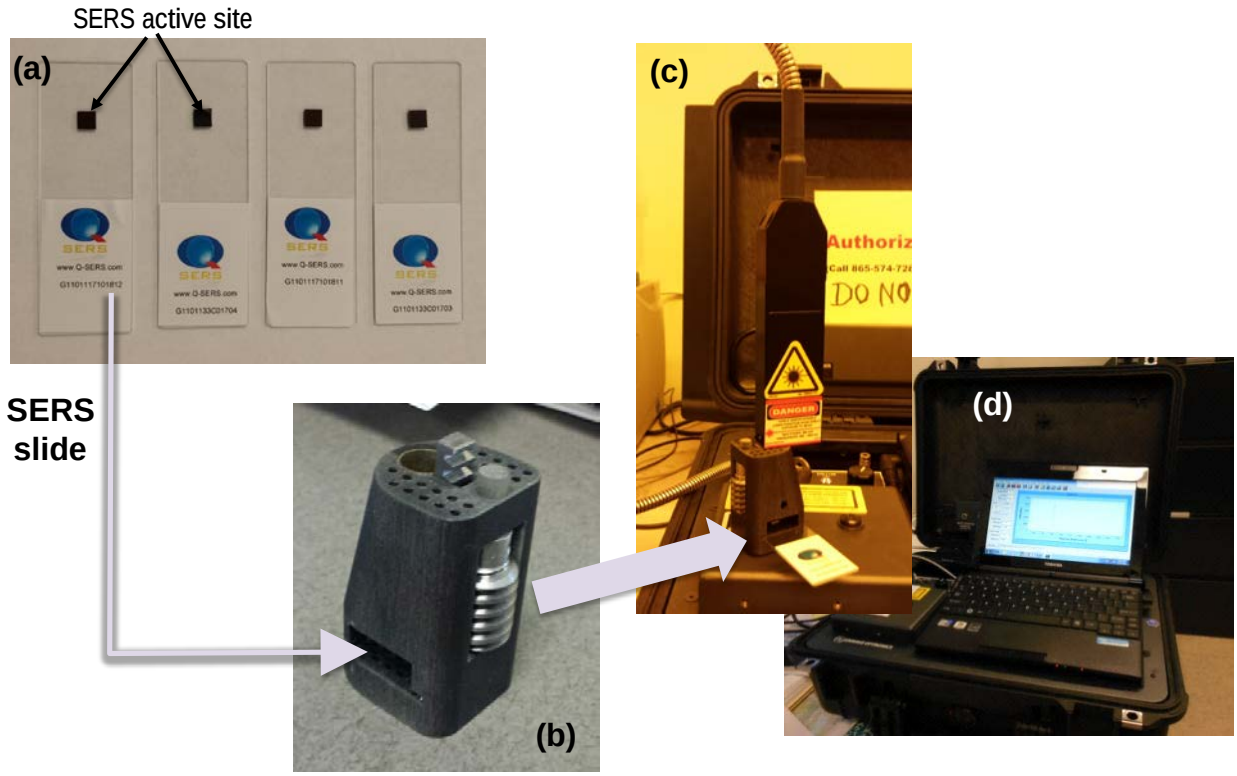

Figure 6.2. Illustration of SERS Detection Using a Portable Raman Analyzer.

(a) Glass slides mounted with active SERS substrates, (b) a SERS module for holding the glass slide and (c) the fiber optic SERS probe, and (d) signal collected via fiber optics by a portable Raman analyzer.

6.2 SERS SUBSTRATE FABRICATION AND OPTIMIZATION

To optimize SERS detection sensitivity, we designed uniform and sensitive novel SERS template based on elevated gold ellipse dimers with 10±2 nm gaps. Elevating the SERS active structures from the underlying substrate has been previously demonstrated to offer greater signal enhancements for both bowtie and mushroom geometries compared to SERS structures in direct contact with the substrate (Hatab et al., 2010b; Hatab et al., 2011a; Jubb et al., 2016; Polemi et al., 2011; Wells et al., 2011). Here we extend this reasoning to ellipse dimer geometries. The ellipse dimers with 10±2 nm gap size are fabricated by electron beam lithography and subsequent gold deposition following lift-off.

The effect of tuning the ellipse aspect ratio on the plasmon resonance frequency is studied, and a shift in the LSP resonance frequency is observed, consistent with theoretical predictions (Hatab et al., 2010b; Jackson and Halas, 2004; Jain et al., 2007a; Zhao et al., 2006a). This tunability enables a more flexible SERS substrate design and a systematic control of the resulting SERS signal intensity compared to our previously reported elevated gold bowtie arrays (Hatab et al., 2010b; Hatab et al., 2011a). The SERS response following excitation by two common Raman excitation wavelengths, 633 nm and 785 nm, are tested and compared. When optimized for 785 nm excitation, the elevated gold ellipse dimer substrates were found to have an enhancement factor (EF) up to 10^9 for adsorbed *p*-mercaptoaniline (*p*MA) molecules.

6.2.1 Experimental approach

6.2.1.1 Materials

The ZEP520A photoresist (ZEON, Tokyo, Japan) and *p*-mercaptoaniline (*p*MA) (97% wt) were used as received. All solvents used during SERS substrate fabrication were reagent grade or better. Deposited Cr and Au were from sources with 99.995% and 99.99% wt purity, respectively. Deionized water (18.2 MΩ cm^{-1}) was produced in house using a MQ water purification system. Q-SERS substrate for enhancement factor comparison was obtained from Nanova Inc. (Columbia, Missouri, USA) and used as received.

6.2.1.2 Fabrication of elevated gold ellipse dimer arrays

The fabrication process of the elevated gold ellipse arrays is schematically illustrated in Fig. 6.3. The complete details for the fabrication process are available in a previous publication from this laboratory and is only briefly described here (Hatab et al., 2010b; Hatab et al., 2011a; Jubb et al., 2016). Electron beam lithography (EBL) was used to expose patterns of ellipse dimer arrays into a ~300 nm thick ZEP520A e-beam resist which had been spin coated on silicon wafers and baked at 180˚C for 2 min. Samples were developed in xylenes for 30 s and subsequently descummed for 6 s in an oxygen plasma to completely remove the exposed resist. All dimer arrays were patterned with a center-to-center distance (CCD) between dimers of ~800 nm and a row-to-row distance (RRD) of ~330 nm following previous work that demonstrated greatest SERS response for substrates with CCD dimensions on the order of the excitation laser wavelength. After the development and descum process, a 10-nm thick Cr layer was deposited on both exposed and non-exposed regions with an electron beam evaporator. In the lift-off step the Cr-covered non-exposed resist areas were removed via sonication in an acetone bath followed by an isopropyl alcohol rinse (photo-resist lift off). Cr deposits, adhered to silicon in the previously developed ellipse patterns, served to promote Au adhesion and acted as a hard mask for subsequent anisotropic silicon etching. Reactive ion etching (RIE) was used to form Si nanoposts with ~100 nm height, in line with previously demonstrated SERS responses from suspended structures with nanopost heights of this magnitude. In the final step, an Au layer was deposited by electron beam evaporation forming the elevated ellipse dimer arrays with variable nanogaps. By controlling the Au deposition it is possible to tune the nanogap between the elevated ellipse dimers. For all substrates reported here an Au thickness of 40 nm was used.

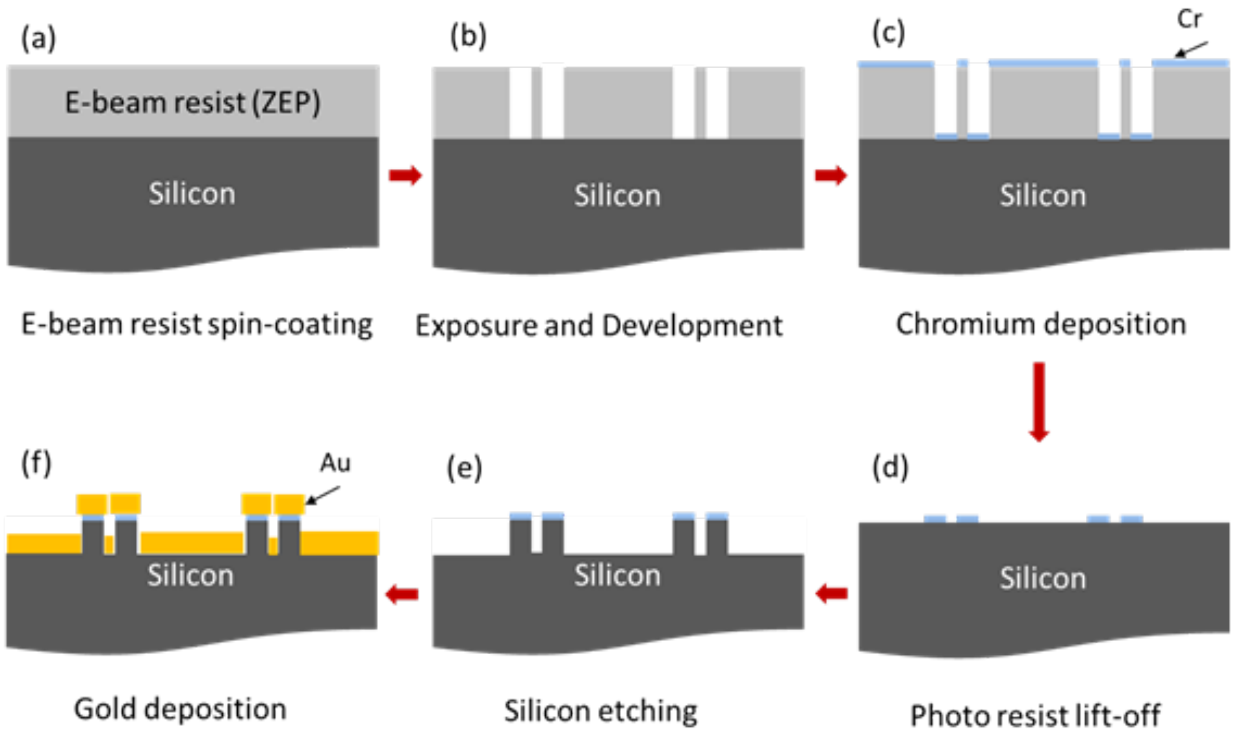

Figure 6.3. Schematic of the Fabrication Process for Elevated Gold Ellipses.

(a) 300 nm photoresist (ZEP520A) is spin coated on a silicon wafer. (b) Designed patterns are transferred via e beam exposure followed by 30 s development in xylenes. (c) A 10 nm thick Cr layer is deposited on developed samples. (d) Photoresist is lifted off in acetone bath with sonication. (e) Silicon is etched to form nanoposts. (f) 40-nm gold layer is deposited.

Scanning electron microscope (SEM) images of single gold ellipse dimers with increasing dimensions (aspect ratios) of approximately 1.3:1, 1.6:1, 2.2:1, 2.4:1, and 3:1 are shown in Figs. 6.4a-e, respectively, from the top down perspective. For all ellipses, the lithographic y-axis was fixed at 50 nm which resulted in final widths of ~70 - 80 nm (measured from SEM images) following Au deposition. Fig. 6.4f shows a large area 30˚ tilted view of an ellipse dimer array with ~100 nm post height and a periodicity of ~800 nm along the x-axis (CCD) and ~330 nm along the y-axis (RRD). A zoomed in 30˚ tilted view of a single ellipse dimer with an aspect ratio of 1.1:1 and a post height of ~100 nm is shown in Fig. 6.4g.

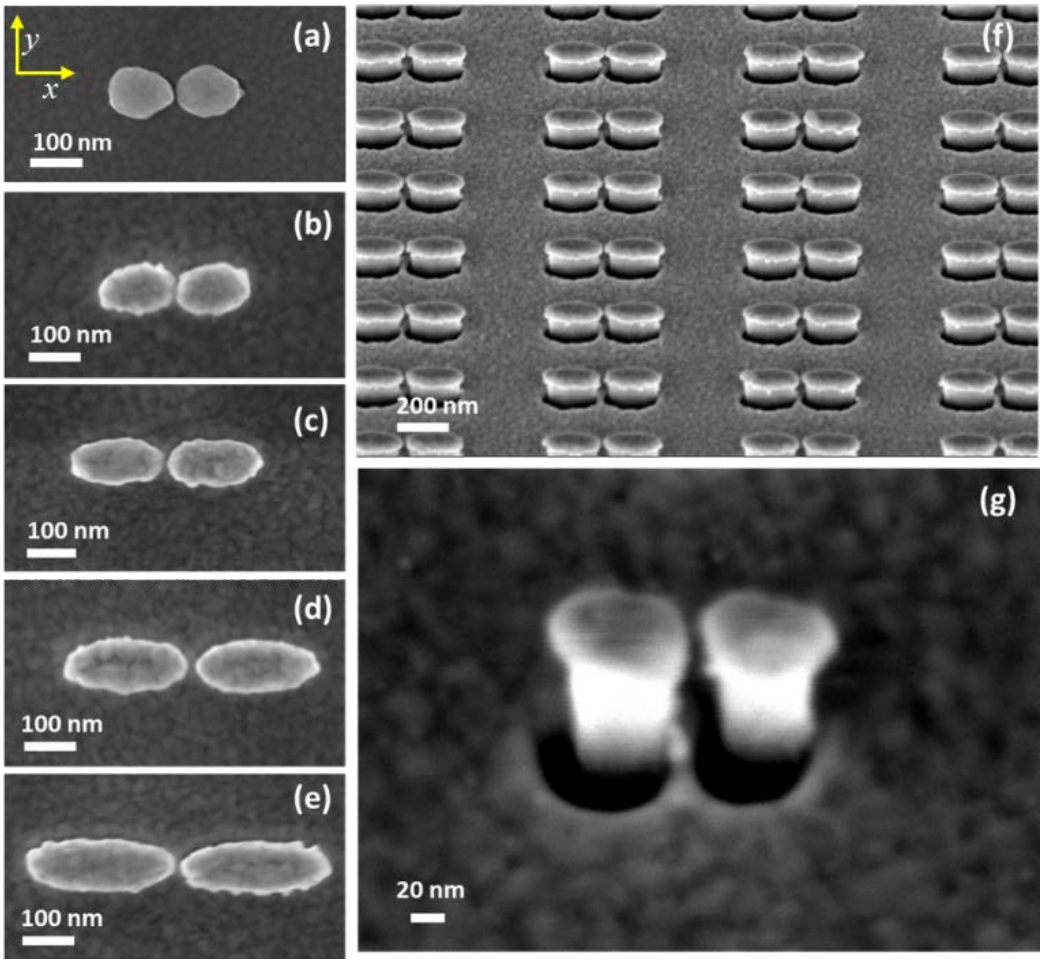

Figure 6.4. SEM Images of Single Elevated Gold Ellipse Dimers with Various Aspect Ratios.

(a) 1.3:1, (b) 1.6:1, (c) 2.2:1, (d) 2.4:1, and (e) 3:1, respectively. (f) Large area, 30-degree tilted SEM image of elevated gold ellipse arrays with an aspect ratio of 2.4:1 and a post height of ~100 nm. (g) The 30-degree tilted SEM image of a single gold ellipse dimer (1.1:1 aspect ratio) with a 10±2 nm gap and ~100 nm post.

6.2.1.3 SERS measurements

The SERS enhancement factor (EF) provided by the ellipse dimer arrays was investigated through the detection of adsorbed *p*MA molecules (Hatab et al., 2010b; Jackson and Halas, 2004; Jubb et al., 2016). Each substrate sample was immersed in a saturated (~5 mM) *p*MA solution in water for 1 h; the samples were subsequently rinsed with a 10% (vol.) ethanol solution and dried under a N_2 stream. SERS spectra were collected using two Renishaw Raman InVia instruments. The majority of the SERS spectra were taken with a Raman instrument equipped with a 50× microscope objective (0.5 NA) and a 785 nm diode laser as the excitation source. The 785 nm excitation beam energy was attenuated to ~1 mW (measured at the sample stage) and had a vertical line-shape beam profile with dimensions of ~20 × 1.5 µm and a focal depth of ~2 µm. The other instrument used to collect the 633 nm spectra was also equipped with a 50× microscope objective with a beam spot diameter of ~633 nm and focal depth of ~2 µm. The energy of the 633 nm beam was attenuated to ~250 µW measured at the sample stage.

The phonon band at ~520 cm^{-1} from crystalline Si was used to calibrate the SERS spectra. All SERS spectra were collected with one 10 s scan. The ellipse dimers were oriented with their X-axis parallel to the polarization of the excitation beam at the sample stage for all SERS measurements excluding the polarization dependence tests.

SERS EFs were calculated according to Eq. 1 (Hatab et al., 2010b; Jubb et al., 2016):

$$\mathrm{EF} = \frac{N_{BULK}}{N_{SERS}} \times \frac{I_{SERS}}{I_{BULK}} \quad (1)$$

where N_{BULK} is the number density of molecules in a conventional Raman sample, N_{SERS} is the number density of molecules excited by the localized field existing in the ellipse dimer gap, I_{SERS} is the intensity of the SERS signal, and I_{BULK} is the intensity of a conventional Raman signal. N_{BULK} was determined using a focal volume of 60 μm^3 for the 785 nm beam and 0.63 μm^3 for the 633 nm beam along with a *p*MA density of 1.18 g cm^{-3} (Hatab et al., 2010b; Jubb et al., 2016). N_{SERS} was determined based on a packing density for *p*MA of 0.2 nm $molecule^{-1}$ and the assumptions that the enhanced signal comes primarily from *p*MA molecules that are adsorbed in the nanogap region of the ellipse dimers and that *p*MA molecules are evenly distributed within this region. As such, the surface area covered by *p*MA which contributes to N_{SERS} can be calculated as two half-cylinders with a height of 40 nm and a radius of curvature estimated to be 15 nm via SEM images. Finally, the number of ellipse dimers within the beam spot, ~60 for the 785 nm beam and ~3 for the 633 nm beam, based on a CCD of 800 nm and a RRD of 330 nm, is required for the N_{SERS} determination. Both I_{SERS} and I_{BULK} were taken from the peak area of the band centered at ~1587 cm^{-1} determined by fitting representative spectra with a sum of Lorentzian peaks (Figs. 6.5 and 6.6).

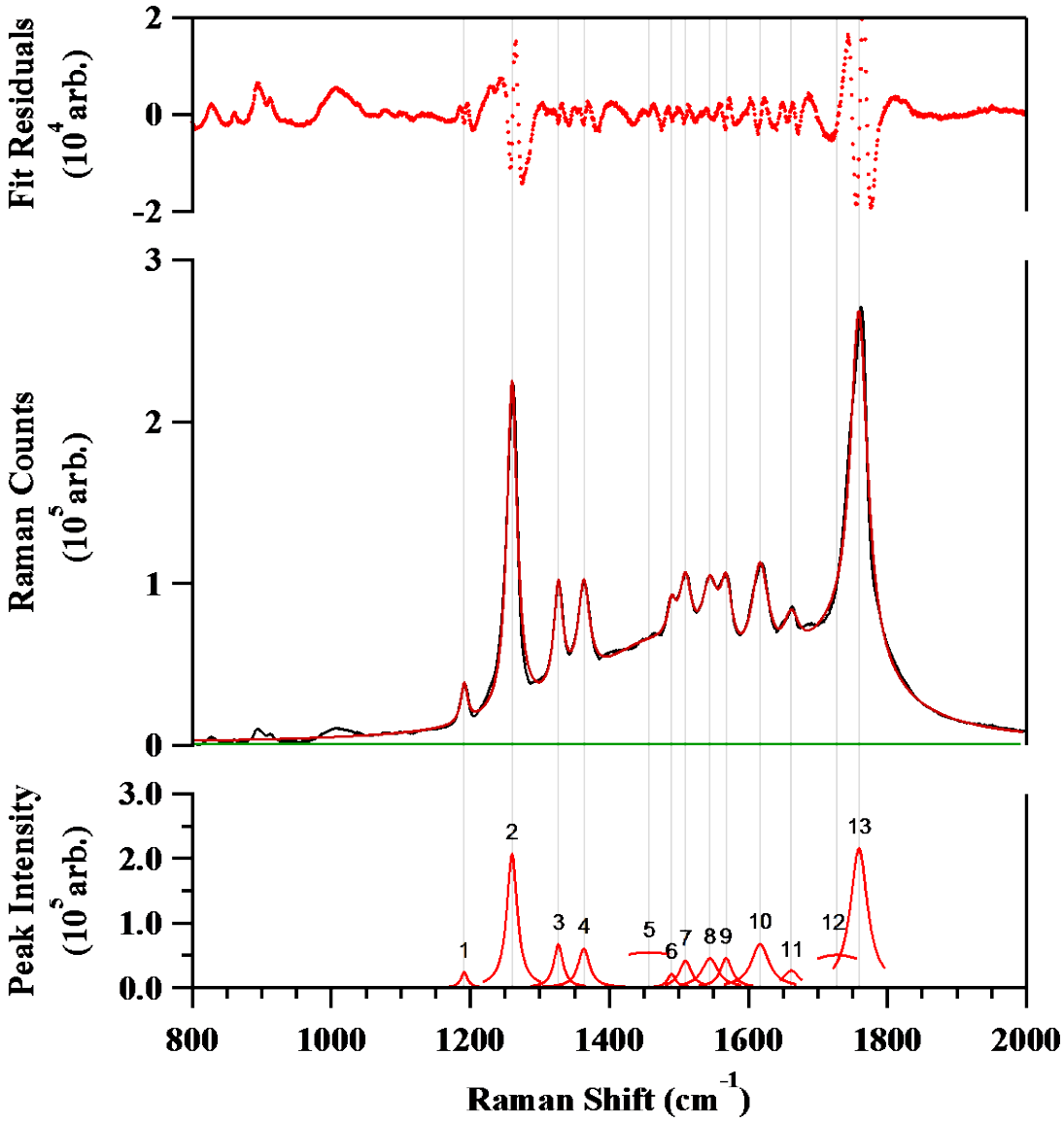

Figure 6.5. Fitting Analysis of a Representative SERS Spectrum of *p*MA Adsorbed on an Elevated Au Ellipse Dimer Substrate (1.3 aspect ratio, 10 nm nanogap, 100 nm post height, 0˚ polarization) Collected with One 10 s Scan and 1 mW 785-nm Laser Excitation.

Top panel: Fit residuals (red markers). Middle panel: raw data (black trace), composite fit (red trace), and baseline (green trace). Bottom panel: Lorentzian peak components (red traces) with corresponding peak number. Solid grey lines indicate fit peak centers. Peak 13 area used for enhancement factor determination.

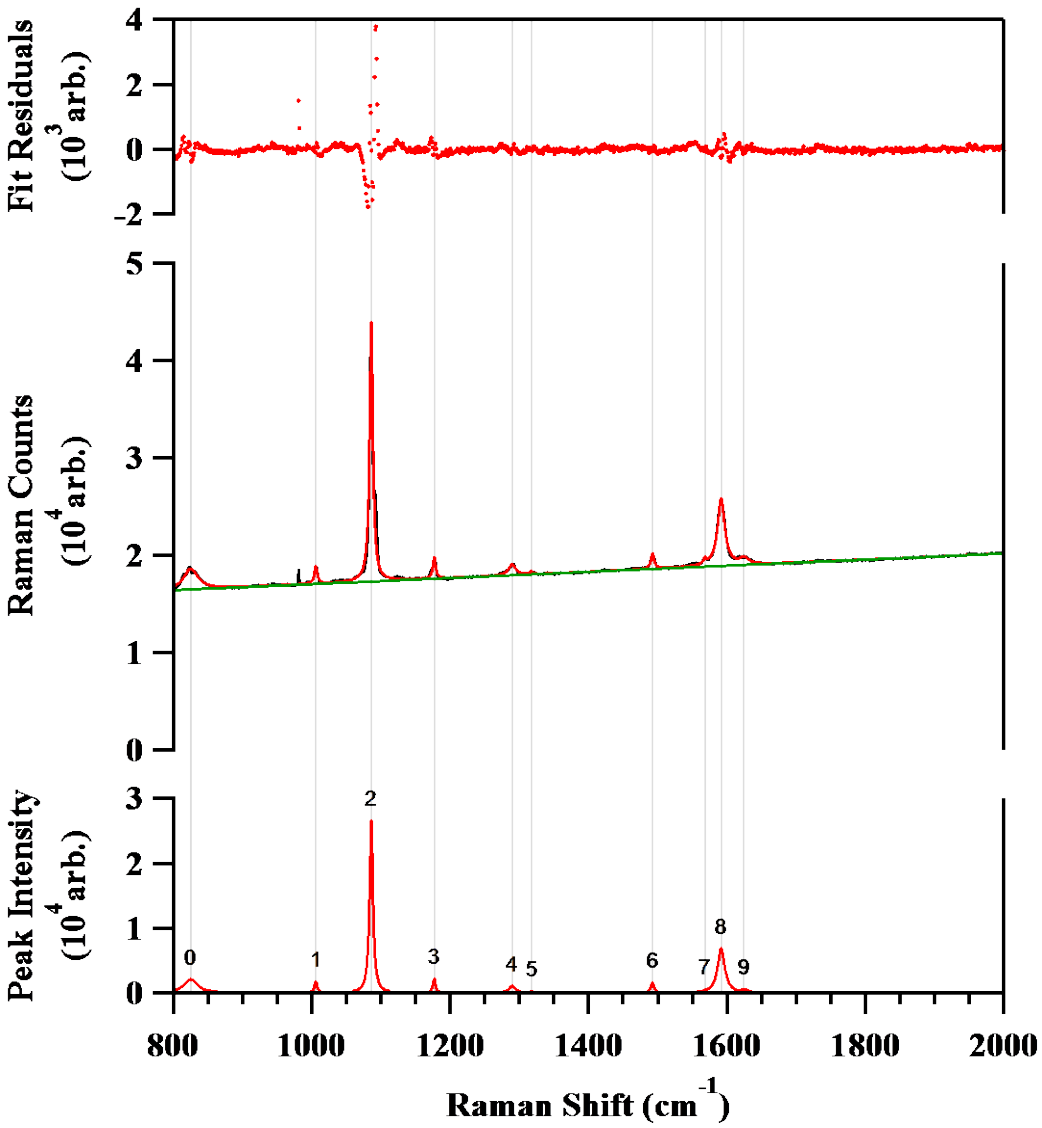

Figure 6.6. Fitting Analysis of a Representative Spectrum of a *p*MA Particle on Au Mirror Collected with One 10 s Scan and 1 mW 785 nm Excitation.

Top panel: Fit residuals (red markers). Middle panel: raw data (black trace), composite fit (red trace), and baseline (green trace). Bottom panel: Lorentzian peak components (red traces) with corresponding peak number. Solid grey lines indicate fit peak centers. Peak height area used for enhancement factor determinations.

6.2.1.4 Infrared measurements

Infrared spectra were collected on substrates with various aspect ratios in order to probe the effect of the ellipse aspect ratio on the frequency for the plasmon resonance. The infrared spectra were all collected with 100 co-added scans and 4 cm^{-1} resolution using a Bruker Hyperion 2000 Fourier transform infrared (FTIR) microscope equipped with a liquid-N_2 cooled mercury-cadmium-telluride (MCT) detector in the reflection mode. Individual background spectra were collected prior to each sample from a clean Au mirror.

6.2.1.5 FDTD computational algorithm and simulations

Lumerical FDTD Solutions software was used to simulate the electromagnetic field intensity as described previously in our lab for elevated bowtie dimer arrays (Hatab et al., 2010b; Jubb et al., 2016; Lumerical Solutions, 2003). For all simulations, the Y-axis of the ellipses was fixed at 50 nm, the gap size was 10 nm, and the Si post height was 100 nm. The FDTD near field intensity, $|E|^2$, for 785 nm excitation was simulated for ellipse aspect ratios of ~1:1 to 4:1. These elliptical disks were simulated with a 50 nm metal layer thickness (40 nm Au on top of 10 nm Cr) suspended on a Si post which was aligned with the origin of the elliptical disk.

6.2.2 Experimental results and technical discussion

6.2.2.1 Influence of gap size

SEM images of various elevated ellipse dimer substrates with the four nanogap sizes tested (0, 10, 15, and 24 nm) are given in Fig. 6.7. The SERS EFs corresponding to substrates with the four nanogap sizes are shown in Fig. 6.8a with representative SERS spectra for each case in Fig. 6.8b. It is clear from the EFs reported in Fig. 6.8a that with a decrease of gap size from 24±2 to 15±2 nm the SERS signal is enhanced dramatically, indicating that the LSP resonance coupling efficiency has increased.

As the nanogap size is decreased further to 10±2 nm the reported SERS EF reaches a maximum value of ~10^9 for 785 nm excitation. The spectra collected with gap sizes on the order of 10 nm generally had ~2× more signal than spectra taken from substrates with slightly larger (15±2 nm) gaps indicating that the LSP coupling efficiency is optimized with a decrease in nanogap size, as expected. When compared to the larger nanogap arrays with 24±2 nm nanogaps the optimized arrays with 10±2 nm gaps are found to have greatly enhanced EFs, typically by factors ≥35. Consistent with previous reports (Hatab et al., 2010b; Jackson and Halas, 2004; Zhao et al., 2006b) on SERS structures featuring a nanogap, the observed EF values increase exponentially with a decrease in the ellipse dimer nanogap distance.

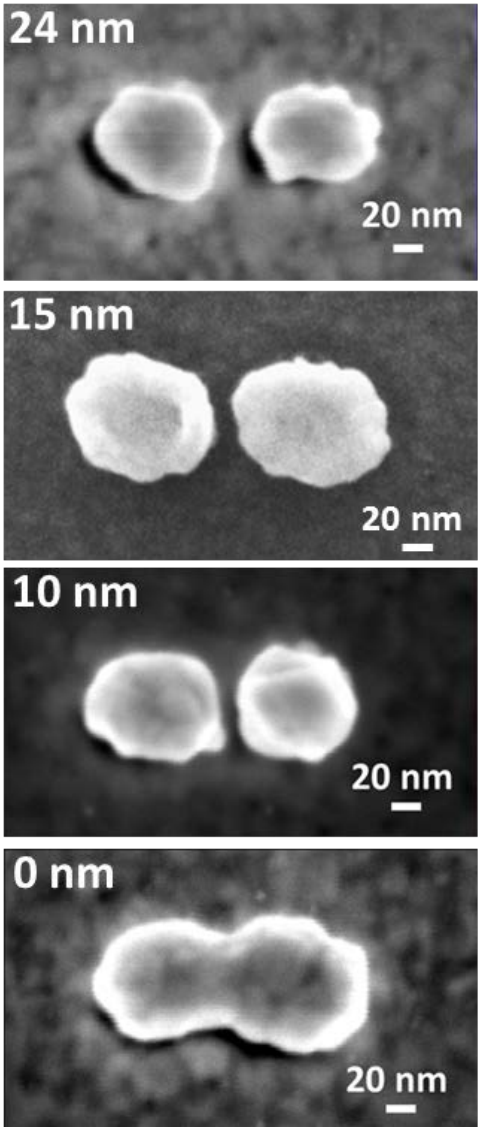

Figure 6.7. SEM Images of Single Elevated Au Ellipse Dimers (1.3:1 aspect ratio, 100 nm post height) with 0 nm, 10 nm, 15 nm, and 24 nm Gap Sizes.

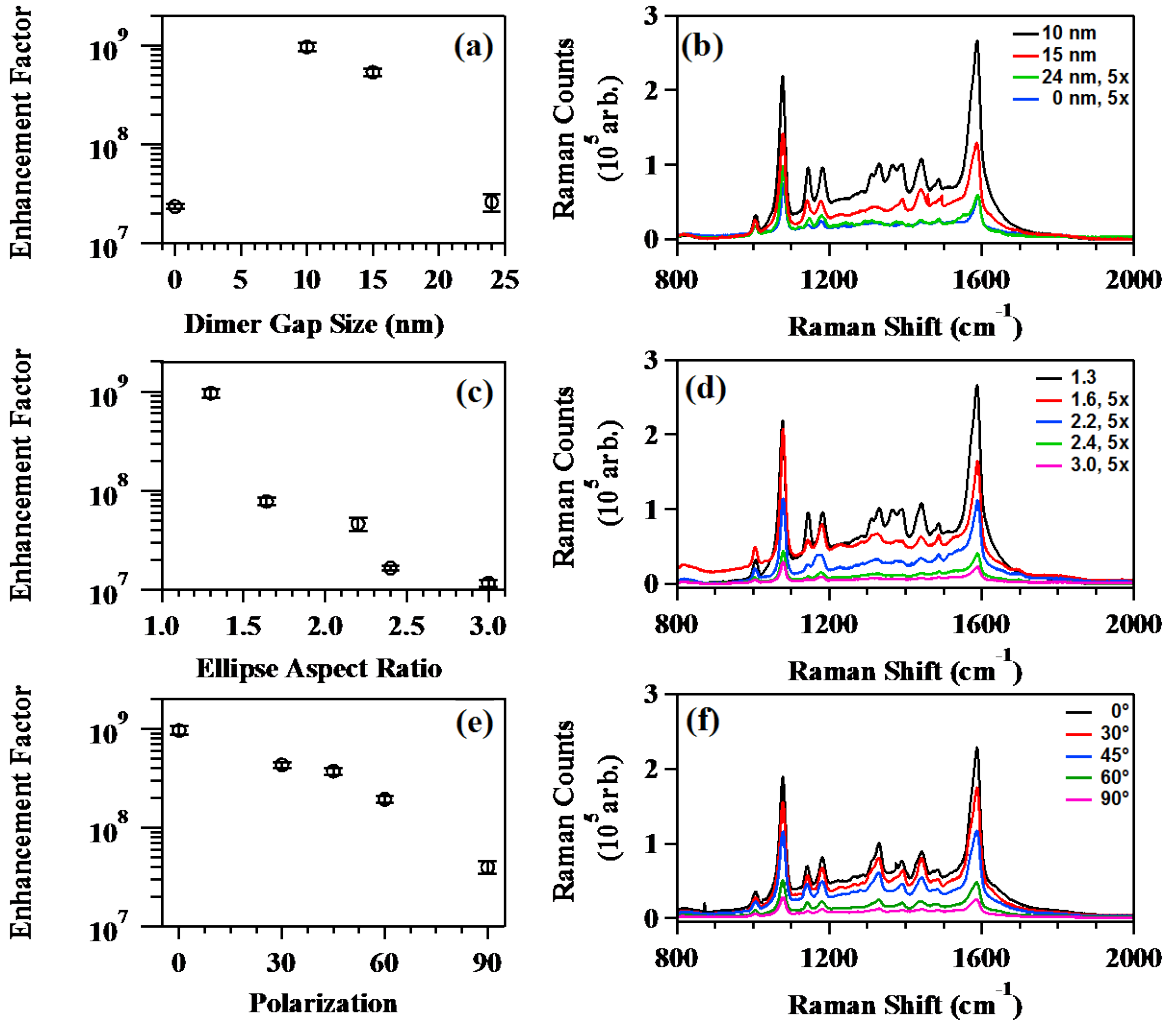

Figure 6.8. SERS Enhancement Factors (EFs) Following 785 nm Excitation for the Elevated Au Ellipse Dimer Substrates as a Function of Changing Parameters as well as Corresponding Representative SERS Spectra.

(a) EFs with changing dimer nanogap size for substrates with ellipse aspect ratio of 1.3, post height 100 nm, and 0˚ polarization. (b) SERS spectra with changing dimer nanogap size (1.3 aspect ratio, 100 nm post height, and 0˚ polarization): 10 nm (black trace), 15 nm (red trace), 0 nm (blue trace), and 24 nm (green trace). Spectra corresponding to the 0 nm and 24 nm nanogap substrates have been multiplied by a factor of 5 for clarity. (c) EFs with changing ellipse aspect ratio for substrates with 10 nm nanogap, post height 100 nm, and 0˚ polarization. (d) SERS spectra with changing ellipse aspect ratio (10 nm nanogap, 100 nm post height, and 0˚ polarization): 1.3:1 (black trace), 1.6:1 (red trace), 2.2:1 (blue trace), 2.4:1 (green trace), and 3.0:1 (pink trace). Spectra corresponding to all substrates with aspect ratios other than 1.3:1 have been multiplied by a factor of 5 for clarity. (e) EFs with changing substrate orientation with regards to excitation beam polarization for substrates with 10 nm nanogap, ellipse aspect ratio of 1.3, and post height 100 nm. (f) SERS spectra with changing orientation relative to the polarization of the 785 nm beam (10 nm nanogap, aspect ratio 1.3:1, and 100 nm post height): 0˚ (black trace), 30˚ (red trace), 45˚ (blue trace), 60˚ (green trace), and 90˚ (pink trace). All EF values were determined from an average of 3–8 SERS spectra where error bars represent the 2σ level of uncertainty. All representative SERS spectra have been baseline corrected.

The strong influence of the dimer gap size is further confirmed by comparing the SERS response from dimers with no gap (0 nm) to dimers with a large gap (24±2 nm). When the gap is closed (i.e. two ellipses are touching or are fused together) the SERS enhancement decreases sharply with the removal of the LSP coupling between the ellipse dimers. While the *p*MA spectra collected from the substrates with a 24±2 nm gap have a slightly higher overall signal-to-noise level than spectra from dimers with no gap (Fig.6.8b), the overall signal intensity, and hence EF, between the two samples is quite similar (Fig. 6.8a). This indicates that a 24 nm gap is large enough to effectively decouple the LSP resonances in the dimer structure such that there is little advantage to a dimer array versus a monomer arrangement.

Previous studies have indicated that the SERS response from nanofabricated substrates with closely spaced features increases greatly as the gap distance decreases, with greatest enhancement predicted for gaps that approach bridging (Hatab et al., 2010b; Zhao et al., 2003). The results on the nanogap size effect on the SERS response from the elevated ellipse dimers confirms that this phenomenon applies to the structures under study here. It is expected that the SERS response from the elevated gold ellipse dimer substrates could be further optimized if the nanogap size was decreased below 10 nm. Efforts to produce gaps much smaller than 10 nm are a delicate function of the electron beam patterning fidelity and the Au deposition rate.

6.2.2.2 Influence of aspect ratio

Following optimization of the nanogap distance for the elevated ellipse dimers the influence of ellipse dimension/aspect ratio on the SERS response was experimentally determined for a series of substrates with different aspect ratios. The SERS spectra from *p*MA molecules adsorbed on elevated Au ellipse dimer substrates with aspect ratios of 1.3, 1.6, 2.2, 2.4, and 3.0 (measured from SEM images), respectively, are shown in Fig. 6.8d. The SERS EFs determined for each of these substrates are given in Fig. 6.8c which demonstrates that the SERS response for 785 nm excitation decreases dramatically as the ellipse dimer aspect ratio increases. For 785 nm excitation, the optimal ellipse aspect ratio was observed to be ~1.3; where the observed SERS enhancement for ellipse dimers with a ~1.3 ratio was almost 100× greater than dimers having a 3:1 aspect ratio.

The decrease in SERS response with an increase in ellipse aspect ratio is attributed to a red-shift for the LSP resonance which results in weaker coupling between the surface plasmon resonance and the input 785 nm light, in agreement with previous studies on the effects of nanoparticle aspect ratio for SERS studies (Jubb et al., 2016; Weber et al., 2011). The red-shift for the plasmon resonance with increasing aspect ratio was probed by infrared reflection from uncoated substrates with three different aspect ratios (Fig. 6.9a). The spectra shown in Fig. 6.9a illustrate the large degree that the plasmon resonance shifts with an increasing aspect ratio; on the order of 3000 cm^{-1} as the aspect ratio increases from ~1:1 to 3:1. These results reiterate the importance of the geometry of the SERS substrate on determining the LSP resonance response to an excitation laser beam. It is important to note that the spectra given in Fig. 6.9a do not show the peak plasmon resonance of the ellipse dimer substrates as this lies above the cut-off frequency (~8000 cm^{-1}) for the FTIR microscope used to collect the spectra. However, the spectral red-shift of the plasmon resonance with an increase in ellipse aspect ratio is clear from these spectra.

These results support the conclusion that by tuning the aspect ratio of the elevated ellipse dimers it becomes possible to optimize the SERS response for a specific excitation wavelength. This is further confirmed by considering the SERS EF determined following 633 nm excitation for an

array of elevated ellipse dimers with conditions optimized for 785 nm excitation, i.e. aspect ratio ~1.3. The EF value determined at 633 nm is ~2 orders of magnitude lower, ~10^7, than what is determined for the arrays optimized for 785 nm excitation. While this result is somewhat surprising given the trend in EF magnitudes observed here with decreasing ellipse aspect ratios, it indicates that the peak plasmon resonance for ellipses with aspect ratios of ~1.3 lies closer to 785 nm than 633 nm. This tunability exhibited by the elevated ellipse dimer geometry toward excitation at different wavelengths highlights the increased flexibility available when adopting this approach.

The observed trend in the experimentally determined spectra with changing ellipse aspect ratio for 785 nm excitation was additionally established theoretically via finite difference time domain (FDTD) simulations. In the FDTD simulations the spatial distribution of the electric field density for ellipse dimers with various aspect ratios was calculated using the Lumerical software suite (Lumerical Solutions, 2003). In all simulations the Y-axis of the ellipses was fixed at 50 nm and the gap size was fixed at 10 nm. The FDTD simulated near field intensity, $|E|^2$, for 785 nm excitation of Au ellipse dimers with aspect ratios that range from ~1:1 to 4:1 are shown in Fig. 6.9b. For all ellipse dimers simulated the electric field is primarily confined within the nanogap region due to strong LSP coupling.

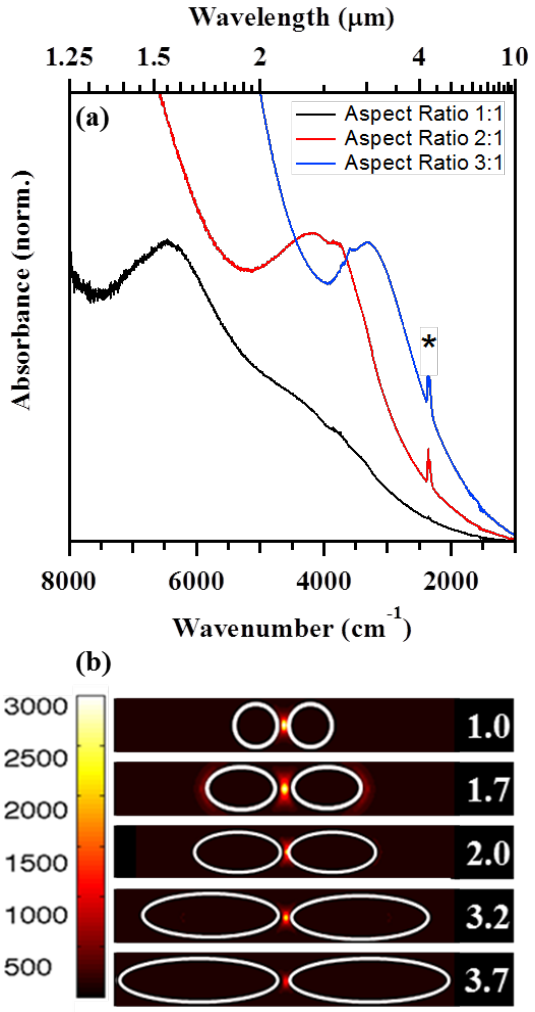

Figure 6.9. (a) Normalized Fourier Transform Infrared Spectra of Three Elevated Au Ellipse Dimer Substrates with Increasing Aspect Ratios: ~1:1 (*black trace*), ~2:1 (*red trace*), and ~3:1 (*blue trace*). (b) FDTD Simulation Intensity Color Maps for Ellipse Dimer Arrays with Aspect Ratios Ranging from ~1 to 4 Following Excitation at 785 nm.

(a) Peak LSP resonance is observed to strongly red-shift with increasing aspect ratio. No data is shown below 1.25 μm (8000 cm^{-1}) as this is the cut-off limit for the infrared instrument. Peak indicated by asterisk corresponds to CO_2 adsorption. (b) The Y-axis of the ellipses is fixed at 50 nm and the gap at 10 nm for all simulations. The intensity of SERS signal is proportional to the fourth power of the electric field, $|E|^4$, while the simulation output is proportional to the square of the electric field, $|E|^2$.

Critically, with the increase in the simulated ellipse aspect ratio, the calculated electric near field intensity decreases, in agreement with the experimental results presented in Fig. 6.8c. The simulated intensity decrease with the increase of ellipse aspect ratio is attributed to a red-shift in the optimal excitation wavelength for generating a strong LSP resonance, as demonstrated in Fig. 6.9a. It is important to note that the experimentally detected SERS signal is proportional to the fourth power of the electric field, while the simulation output is given in the square of the electric field; however the trend is generally the same between the experimental and simulated results.

6.2.2.3 Polarization dependency

As plasmon effects are known to be strongly polarization reliant (Homola, 2008; Kneipp et al., 1999; Mayer and Hafner, 2011; Stewart et al., 2008), the polarization dependency of a representative elevated Au ellipse dimer substrate (10±2 nm gap, 1.3:1 aspect ratio, 100 nm post) was examined for 785 nm excitation by rotating the SERS substrate orientation with respect to the polarization of the laser beam (Fig. 6.10). The polarization angle from 0˚ to 90˚ was rotated with respect to the x-axis of the ellipse dimers and a significant decrease (~50%) in the SERS intensity was observed following a small change of 30˚ (Figs. 6.8e and 6.8f). Following a 90˚ rotation the observed SERS EF decreased by a factor of 20.

While there is a strong polarization dependency to the SERS response exhibited by these structures, the enhancement factor determined for the substrates following a 90˚ rotation is still high, ~10^7. This illustrates that the elevated Au dimer substrates should exhibit strong SERS performance regardless of the substrate orientation. However, for optimal performance during SERS applications, the orientation of the elevated ellipse dimer's X-axis should be aligned with the polarization of the excitation beam.

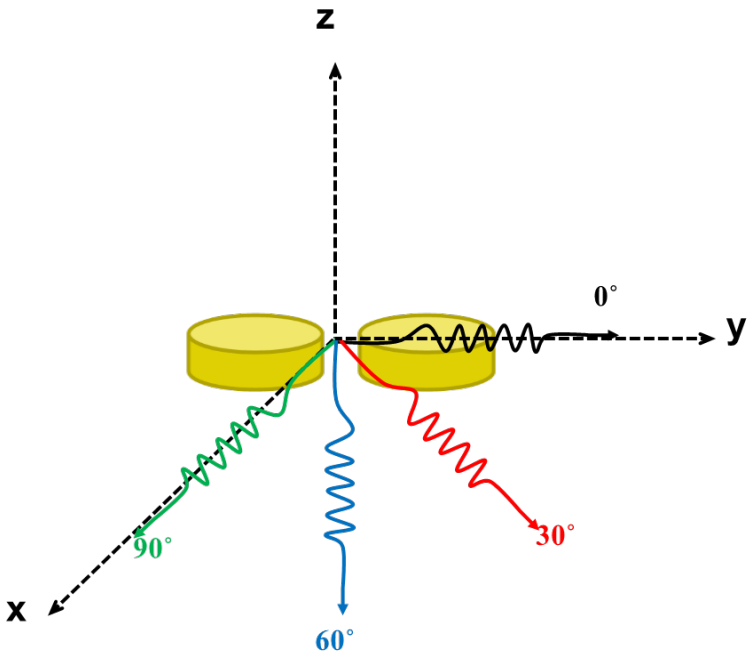

Figure 6.10. Schematic Illustrating the Polarization Orientation Relative to an Elevated Au Ellipse Dimer.

6.2.2.4 Reproducibility and performance of optimized substrates

A key advantage to the lithography based SERS substrate fabrication approach taken here is the ability to produce large arrays of well-ordered SERS active structures. As discussed above, this obviates the need to search for SERS active hot-spots. To demonstrate the SERS reproducibility of the elevated Au ellipse dimer structures 10 spectra were collected in 10 µm steps from a 100 µm line scan with 785 nm excitation across a representative *p*MA coated substrate with an aspect ratio of 1.3:1, a 10 nm nanogap, post height of 100 nm, and 0˚ polarization rotation, Fig. 6.11a.

The average EF calculated from the spectra shown in Fig. 6.11a was determined to be (9.6 ± 0.9) × 10^8 at the 2σ uncertainty level. This degree of reproducibility is similar to results for our previously reported elevated Au bowtie SERS structures (Hatab et al., 2010b; Hatab et al., 2011a), indicating that the lithographic technique used to fabricate these classes of SERS structures is effective at generating large areas possessing high SERS activity.

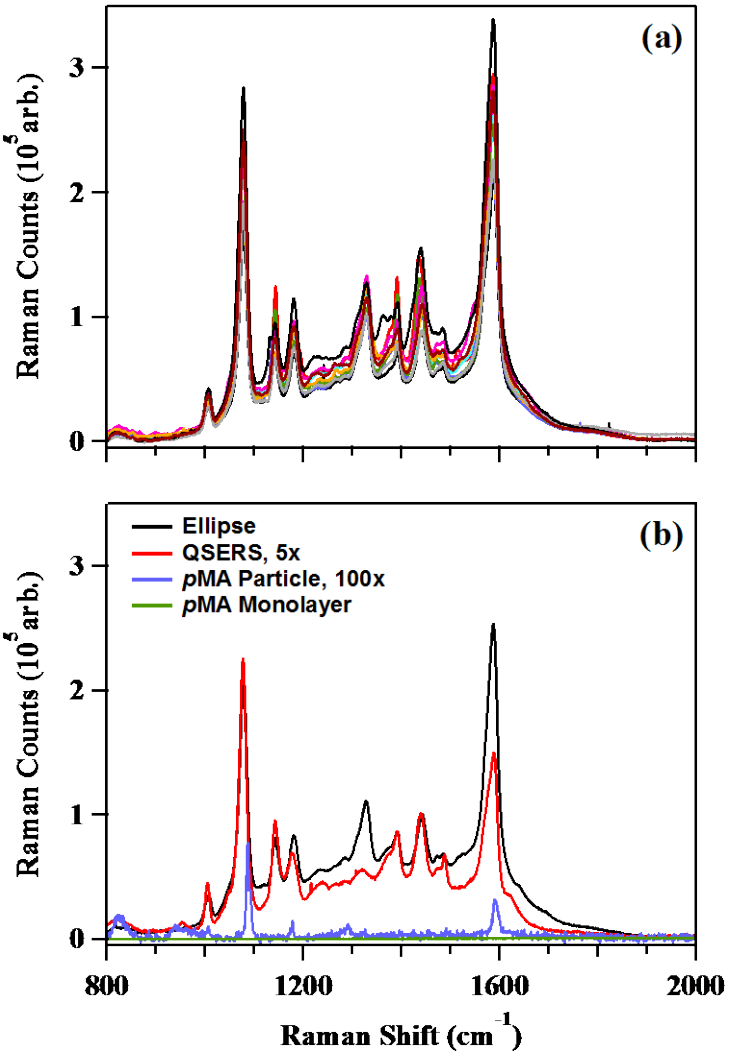

Figure 6.11. (a) SERS reproducibility test showing representative 785 nm SERS spectra from a *p*MA coated elevated Au ellipse dimer substrate (1.3:1 aspect ratio, 10 nm nanogap, 100 nm post height, and 0˚ polarization rotation) collected in 10 µm steps over a 100 µm line-scan. (b) Comparison of 785 nm SERS response for *p*MA from an optimized elevated Au ellipse dimer (*black trace*) with 1.3:1 aspect ratio, 100 nm nanogap, 100 nm post height, and 0˚ polarization orientation, a commercially available SERS substrate, Q-SERS, (*red trace*), and the conventional Raman spectra of a bulk pMA particle (*blue trace*) and a *p*MA monolayer adsorbed on a gold mirror (*green trace*).

The Q-SERS and pMA spectra have been multiplied by 5× and 100×, respectively, for clarity. All spectra shown in (a) and (b) were collected with the same experimental conditions and have been baseline corrected.

We also compared the SERS performance of the above fabricated Au ellipse dimer substrates with a commercially available SERS substrate (Q-SERS, made by Nanova Inc.) based on a dispersion of 60 nm and 15 nm Au nanoparticles. From the spectra shown in Fig. 6.11b it is observed that the SERS response from the elevated Au ellipse dimers is approximately 1 order of magnitude greater than the commercially available substrate. However, if a N_{SERS} value for the Q-SERS substrate is calculated based on an assumed efficient packing scheme for the 60 nm and 15 nm Au spheres within the 785 nm excitation beam spot, the resulting EF value determined for the Q-SERS substrate is ~10^6. An EF of this magnitude is ~1000× less than those determined for optimized elevated Au ellipse dimer structures. This is a promising result as it demonstrates that the optimized elevated Au ellipse dimer structures reported here are capable of providing greatly enhanced performance for SERS applications compared with currently available commercial SERS substrates.

6.2.3 SERS substrate fabrication and optimization summary

The influence of dimer nanogap size, ellipse aspect ratio, and substrate orientation relative to the excitation beam polarization on the SERS response for elevated Au ellipse dimers was investigated for 785 nm laser excitation. The optimized SERS substrate conditions were found to be a gap of 10±2 nm, an aspect ratio close to 1:1, and the polarization of the 785 nm excitation beam aligned with the ellipse x-axis. With increasing aspect ratio the LSP resonance for the elevated Au ellipse dimers was shown to red-shift. These results were compared with another commonly used Raman excitation wavelength, 633 nm, to demonstrate the flexibility of this SERS geometry.

The tunability of the ellipse geometry provides a rational basis for the design of SERS substrates based on the elevated ellipse dimer platform for matching a desired excitation wavelength. Total SERS enhancement factors on the order of 10^9 for a layer of adsorbed *p*-mercaptoaniline as a probing molecule were determined for arrays with parameters optimized for 785 nm laser excitation. Additionally, the tunability of the ellipse dimers make them an attractive practical choice for a broad range of SERS applications including chemical and biological sensing (Hatab et al., 2011a; Jubb et al., 2017; Ruan et al., 2006a; Xu et al., 1999). It is subsequently utilized for perchlorate detection in environmental samples.

6.3 COMMERCIAL FABRICATION OF SERS SUBSTRATES

6.3.1 Substrate production by nanoimprinting

While EBL technique has been successfully used for the fabrication of desired SERS substrates, it requires the use of a high-resolution electron microscope and a nanometer pattern generator. The fabrication process also requires specialized skills and is a rather slow process. To reduce the cost of fabrication and lead to commercialization, we teamed with Nanova Inc. and its partner NIL Technology for the commercial production of optimized ORNL SERS substrates based on the elevated Au ellipse dimer architectures. Here nanoimprinting technology is utilized for large-scale production. Nanoimprinting lithography is based on pressure-induced transfer of a topographic pattern (e.g., ellipses in this case) from a rigid mold into a thin thermoplastic polymer film or resist heated above its glass transition temperature (Veres et al., 2010; Weiss et al., 2011). It is a physical process that does not use any energetic beams and is under rapid development to meet the needs of

the new generation of applications extended into the nanoscale arena. Imprint molds can be fabricated with multiple layers of topography stacked vertically. Resulting imprints replicate both layers with a single imprint step, which reduces SERS substrate fabrication costs and improve product throughput. A broader range of materials with varying properties are also available for use with imprint lithography, thus increasing the potential range of SERS substrates for Raman SERS applications. Its high resolution, high throughput, and relatively low cost have made nanoimprint lithography one of the leading nanofabrication techniques. The simplified requirements of the technology lead to its easy production at relatively low costs.

A mold designed for high throughput, nanoimprint fabrication of SERS substrates was made at ORNL Center for Nanophase Materials Science (CNMS) and shipped to Nanova Inc. for commercial testing and production in March 2014. The mold was made with about 100 desired nanostructural arrays on a 4-in Si wafer (Fig. 6.12). The mold was later used to transfer topographic patterns (e.g., ellipses) from a rigid mold into a thin thermoplastic polymer film or resist heated above its glass transition temperature (so-called "nanoimprinting"). Once the imprinted materials are fabricated (or patterns transferred), they are processed through the usual lift-off and gold deposition to obtain the elevated gold ellipse nanoarrays for SERS detection.

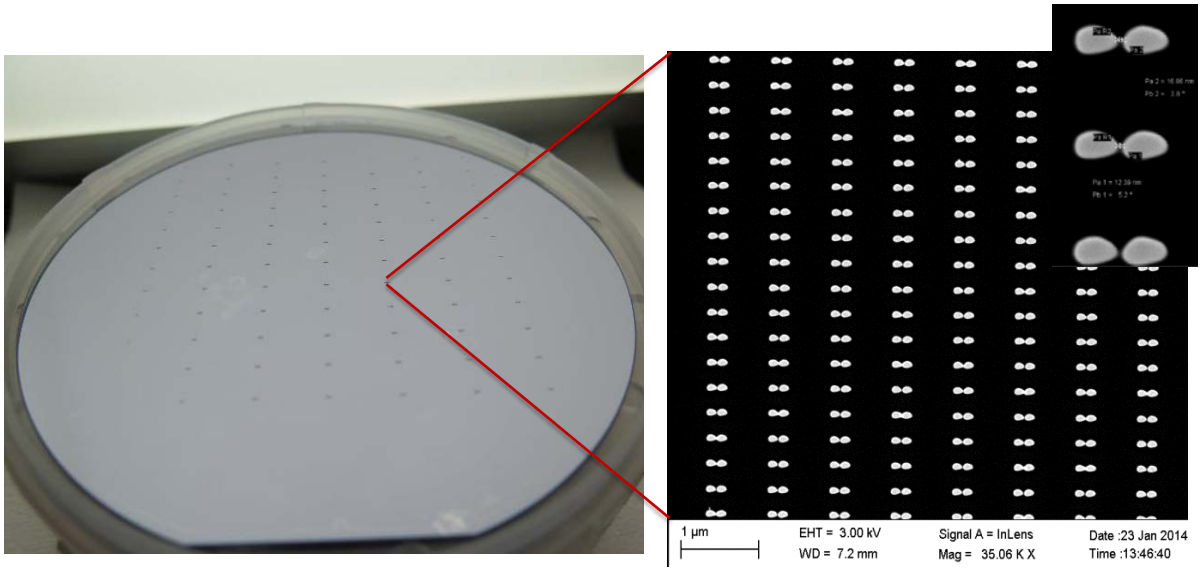

Figure 6.12. A Mold Designed for High Throughput, Nanoimprint Fabrication of SERS Substrates was Made at ORNL CNMS.

The mold was used to transfer topographic patterns (e.g., ellipses in this case) by a commercial company, resulting in substantially decreased SERS chip fabrication costs and improved product throughput.

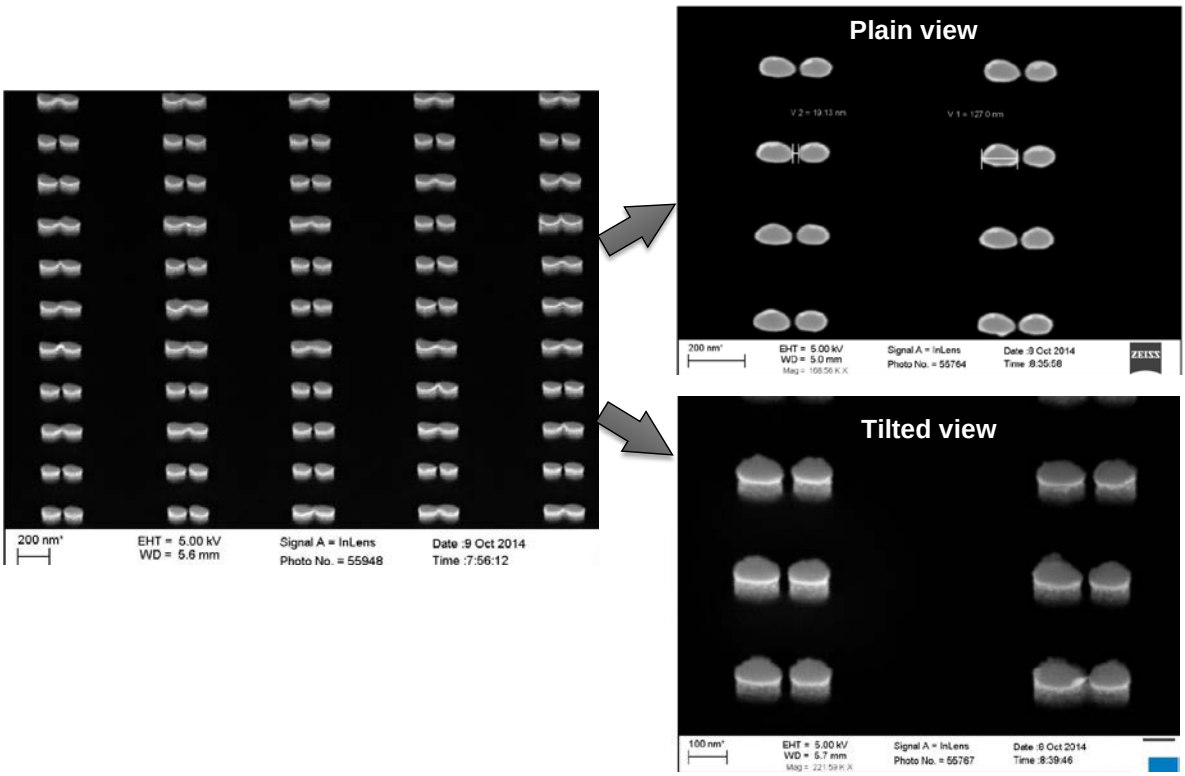

Figure 6.13. SEM Images of Commercially Fabricated SERS Substrates via High Throughput Nanoimprinting (without Cr and Au coatings).

The topographic patterns (i.e., ellipses) were successfully transferred.

As shown in Fig. 6.13, despite some difficulties encountered initially, we were able to successfully transfer topographic patterns from the mold onto a thin thermoplastic polymer film or resist, and subsequently to the Si wafer ("nanoimprinting"). The transfer and integrity of the ellipse dimer architectures were verified by scanning electron microscopy (SEM) analysis (e.g., Fig. 6.13) and atomic force microscopy (AFM) analyses (e.g., Fig. 6.14).

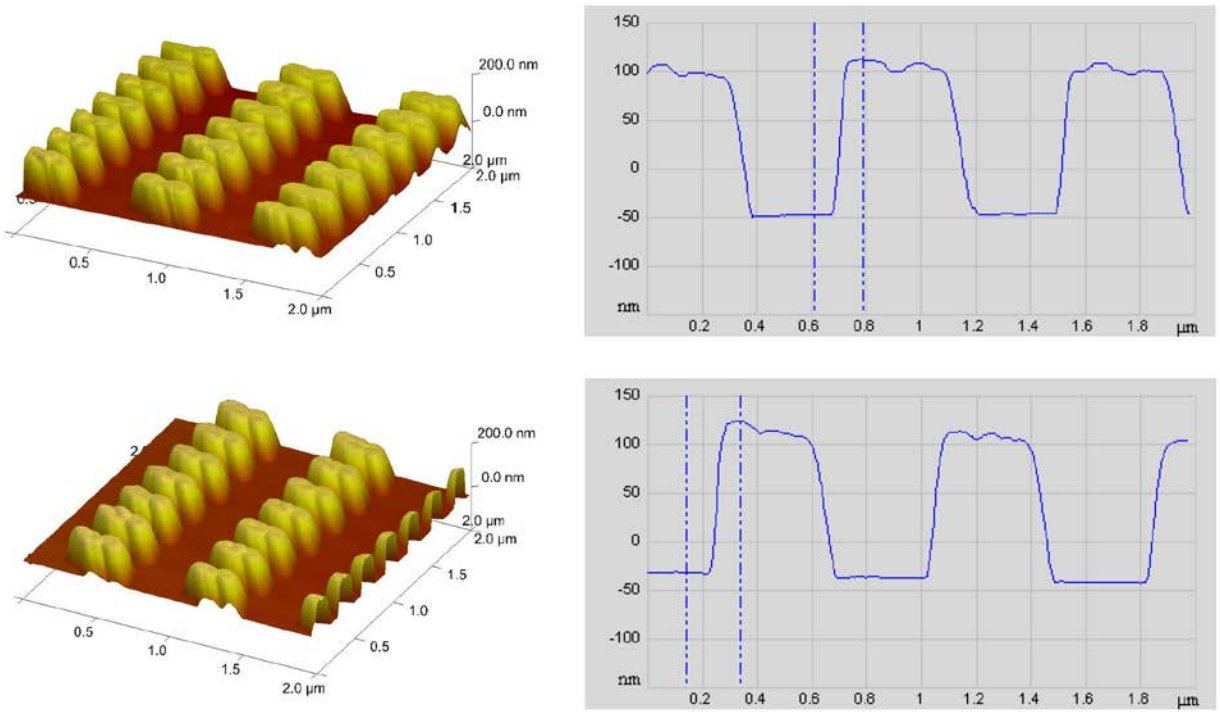

Figure 6.14. Representative AFM Images Showing Topographic Features of the Commercially Fabricated SERS Substrates by High Throughput Nanoimprinting after Lift-off and Etching to 150 nm Depth by NIL Technology.

6.3.2 Substrate optimization

Following successful transfer of the topographic features, the imprinted SERS substrates were coated with a thin layer of Cr (8 – 10 nm, as an adhesion layer) and subsequently coated with Au at various thicknesses for performance evaluations. Extensive studies were then carried out to evaluate the performance and sensitivity of the commercially produced SERS substrates for ClO_4^- detection. For example, we varied the Au coating thicknesses, 20, 30, 40, 60, 80, 110, and 140 nm and studied the effect of Au thickness on ClO_4^- detection at various concentrations in water (Fig. 6.15 and 6.16). Peak intensities at ~ 928 cm^{-1} for ClO_4^- analyte (at 10 and 1 mg/L) for these substrates were recorded and plotted in Fig. 6.15. Results suggest that the optimal Au coating thickness is ~ 60 nm. Quality control testing these commercial substrates with a model thiol compound, *p*-mercaptoaniline ($C_6H_4NH_2SH$) and with ClO_4^- standards in nanopure (MQ) water was also performed, and results show performance comparable, in most cases, to the SERS arrays fabricated at ORNL using electron beam lithography. This is a substantial step forward toward the commercialization of these sensors.

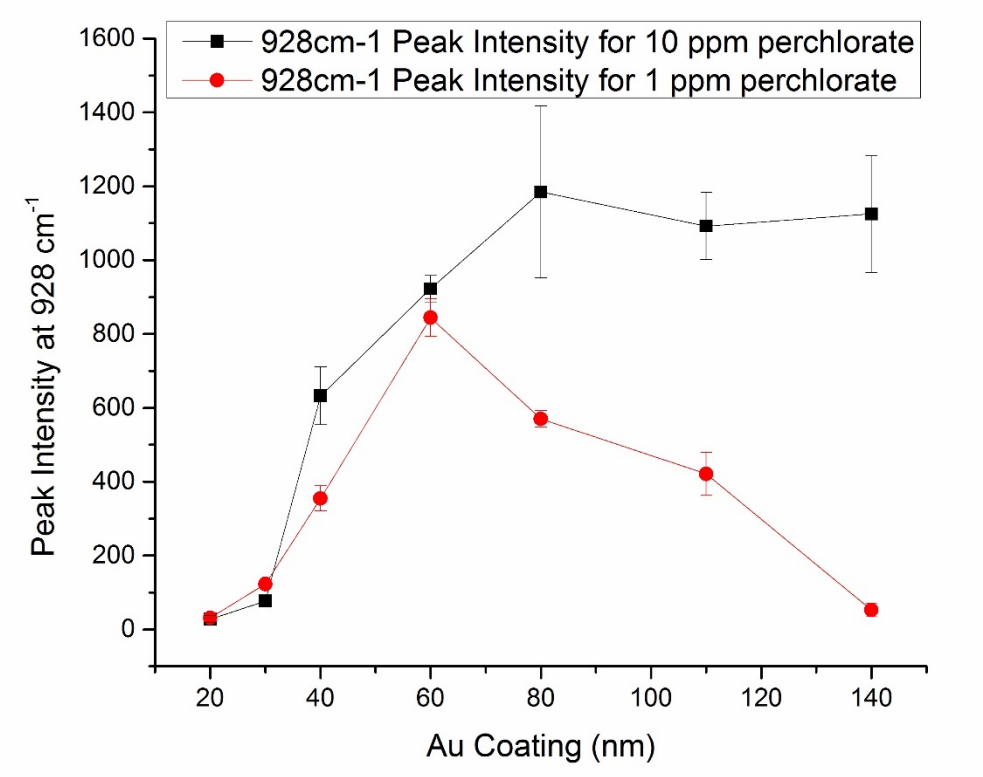

Figure 6.15. Peak Intensities of 10 and 1 ppm Perchlorate as a Function of Au Coating Thickness Using Commercially Fabricated SERS Substrates.

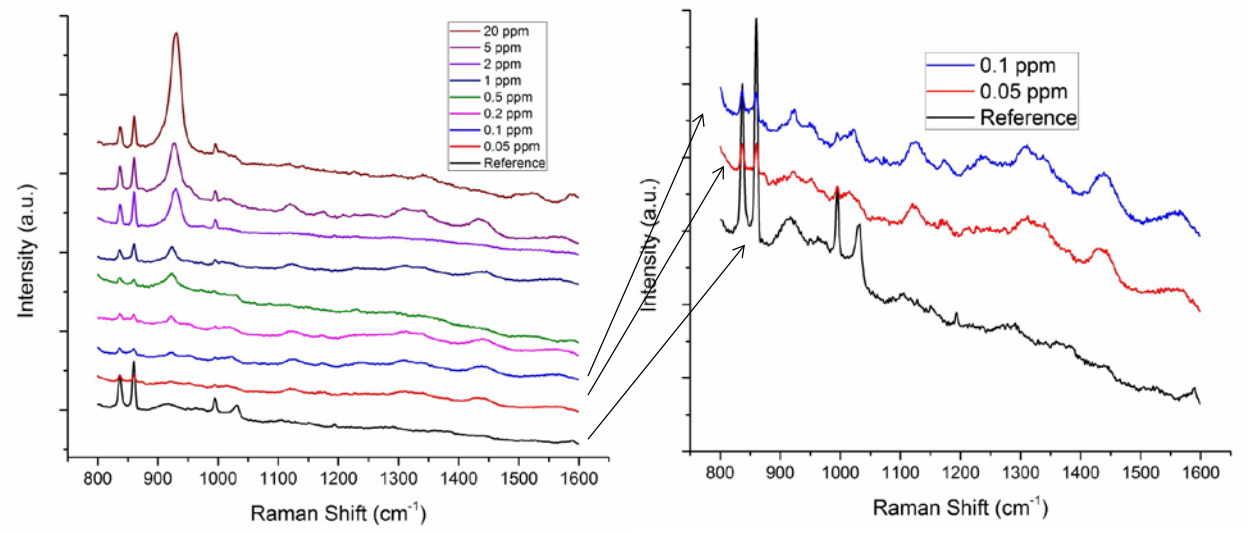

Figure 6.16. SERS Spectra Acquired on the Nanoimprinted Substrates for a Series of Perchlorate Analytes.

One source of variation in the detected ClO_4^- signal is the inhomogeneous distribution of ions across the active SERS substrate surface. This arises due to the inherently random nature of drying the sample droplet in which surface tension forces effectively pull ions toward the outer edge of the drop. One approach to lessen this effect is to functionalize the surface of the SERS arrays with an agent that attracts ClO_4^- ions. Toward this end, laboratory investigations were performed with coating the elevated Au ellipse dimer SERS substrates with dimethyl-amino-ethane-thiol (DMAET) which can form a monolayer on the Au surface through the thiol moiety while leaving the positively charged dimethyl amino group pointed into the sample solution. One concern with this approach is the added baseline signal from SERS enhanced vibrational modes of the DMAET. Our results show that this is not a significant issue, in line with previous literature reports which have taken this approach with colloidal Au spheres SERS substrates (Gu et al., 2009). We found that coating the SERS substrates with DMAET had the benefit of increasing the detection efficiency as it enhances the adsorption of ClO_4^- to the SERS active region (Fig. 6.17).

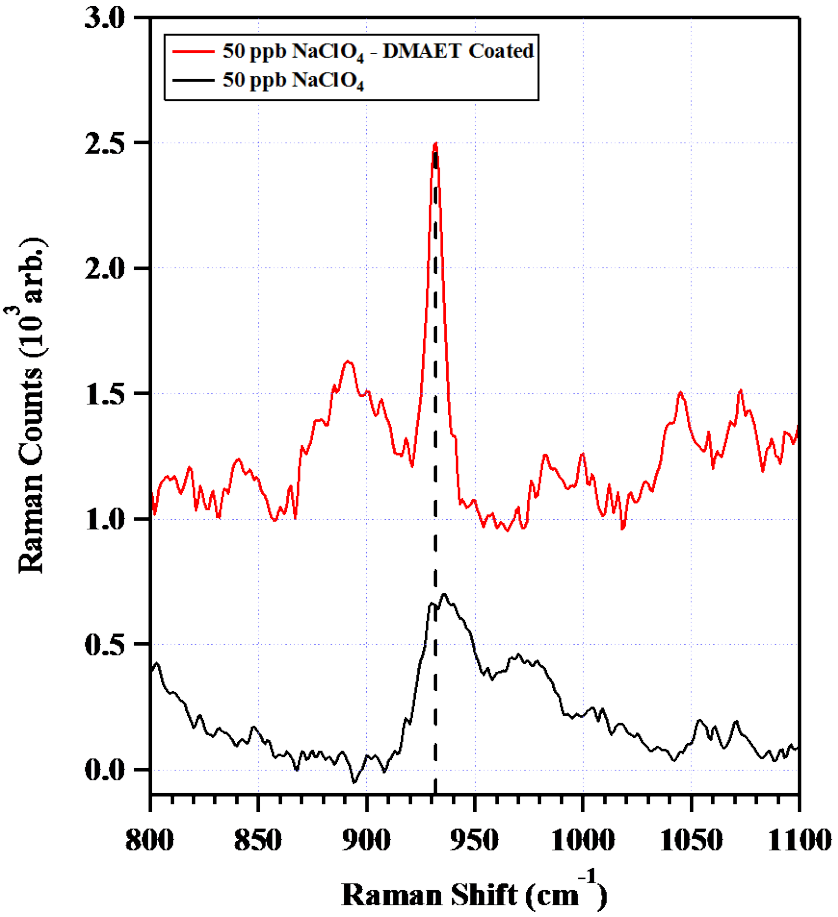

Figure 6.17. Comparison between a DMAET Coated SERS Array (*red trace*) and a Blank SERS Array (*black trace*) with 50 ppb $NaClO_4$ Standard.

Dashed vertical line represents ClO_4^- symmetric stretching peak. All spectra have been baseline corrected and scaled for clarity. DMAET coated SERS array has ~3× higher signal compared to uncoated array.

6.3.3 Commercial SERS substrate production summary

Despite some difficulties encountered initially during commercial fabrication of SERS substrates via nanoimprinting, we were able to successfully transfer topographic ellipses patterns from the mold (made with EBL at ORNL) onto a Si wafer by nanoimprinting. The integrity and gap sizes of the ellipse dimers were verified by SEM and AFM analyses. This is a substantial step forward toward the commercialization of the SERS sensors.

We also evaluated the functionalization of the substrates with DMAET to minimize variations in inhomogeneous distribution of ClO_4^- ions across the active SERS substrate surface. We found that coating the SERS substrates with DMAET had the benefit of increasing the detection efficiency as it enhances the adsorption of ClO_4^- to the SERS active region. Their performance was comparable to the SERS substrates fabricated using EBL at ORNL.

6.4 EVALUATION OF INTERFERENCES ON SERS PERFORMANCE

To determine potential interference effects present in natural groundwater or surface water, we further investigated the sensitivity of commercially produced SERS substrates based on elevated Au ellipse dimers for rapid detection of ClO_4^-. These dimers were observed to provide higher sensitivity than previously reported elevated Au bowtie geometries (Hatab et al., 2010b; Hatab et al., 2011a). Additionally, we systematically explored the interference effects of other common ions (e.g., chloride (Cl^-), nitrate (NO_3^-), and sulfate (SO_4^{2-}) typically found in environmental samples) on SERS detection of ClO_4^-. The systematic quantification of interferences in SERS is vital for analyzing complex samples as the SERS technique is non-specific and will report on any Raman active compounds within the working region of the sensor.

6.4.1 Experimental approach

6.4.1.1 Materials

$NaClO_4$, NaCl, $NaNO_3$, and Na_2SO_4 were ACS grade or higher and were used as received. The 25 mM 2-(dimethylamino)ethane-thiol (DMAET) hydrochloride (>98% wt) solutions used to functionalize the SERS substrate surface as well as all salt solutions were prepared in deionized water. Deionized water (18.2 MΩ cm^{-1}) was produced in house using a MQ water purification system. The ZEP520A photoresist (ZEON, Tokyo, Japan) was used as received. All solvents used during SERS substrate fabrication were reagent grade or better. Deposited Cr and Au were from sources with 99.995% and 99.99 wt% purity, respectively.

6.4.1.2 Fabrication of SERS architectures

Complete details on the fabrication of the elevated gold ellipse dimer SERS substrates are provided in previous section and are only briefly described here (Hatab et al., 2010b; Hatab et al., 2011a; Jubb et al., 2016). All SERS substrates used in this study were patterned with an optimized aspect ratio of 1.3:1, a center-to-center distance of 800 nm and a row-to-row distance of 330 nm. Following the patterning process, the wafer substrates were developed in xylenes for 30 s, rinsed with isopropyl alcohol, and 'descummed' for 6 s in oxygen plasma. A Cr layer (10 nm) was subsequently deposited onto the samples using an electron beam evaporator. Post-Cr deposition the samples were subjected to photo-resist lift off by sonication in an acetone bath followed by an isopropyl alcohol rinse. Reactive

ion etching was then used to form 100 nm posts capped by the 10 nm Cr deposits. In the final step, 40 nm Au was deposited on the sample substrates using electron beam evaporation which produced ellipse dimers with a nanogap distance of 10 ± 2 nm. A scanning electron microscopy (SEM) image of a representative elevated Au ellipse dimer array is shown in Fig. 1.2f where the array has been tilted at 30° such that the nanoposts are visible. The final size of the SERS arrays measured 0.5 × 1 mm with ~100 arrays fabricated per 4-in Si wafer.

6.4.1.3 SERS measurements

All SERS measurements were taken with a portable TSI EZRaman-I system equipped with a thermoelectrically cooled charge-coupled device operated at –50° C, a 785 nm diode laser, and an InPhotonics fiber optic Raman probe, which was used to both direct the 785 nm excitation beam to the sample stage as well as collect the scattered Raman signal. The sample stage was adjustable in the *xyz* directions and was equipped with a miniaturized camera focused on the 785-nm laser focal spot in order to achieve optimal beam focusing and overlap between the SERS array and the excitation beam. Each SERS spectrum was collected with one 60 s scan and ~75 mW laser power measured at the sample stage. The 785 nm beam diameter was typically 300 μm at the sample stage. The Si phonon mode at 520 cm^{-1} was used to calibrate each SERS spectrum following a spectral acquisition. All data were analyzed in the IGOR Pro software suite.

In a typical SERS measurement, the SERS substrate surface was first functionalized with DMAET to ensure homogeneous ClO_4^- dispersion through interaction with the dimethyl-amino moiety of the thiol compound, as previously demonstrated (Gu et al., 2009). This was accomplished by soaking the SERS substrate in 25 mM DMAET solution for an hour followed by rinsing in copious amounts of deionized (18.2 MΩ) water and drying the substrate in a N_2 stream. Post functionalization, 3 μL of sample solution was pipetted onto a SERS array and subsequently dried in air at 50 °C on a benchtop hot plate. The analyte coated array was then placed on the portable Raman spectrometer sample stage, the 785 nm excitation beam was brought into overlap with the array, and a spectral acquisition was initiated. Spectra were collected from 3–5 distinct locations on a single array in order to account for spot-to-spot variations in the SERS detection efficiency across the array as well as sample distribution inhomogeneity.

6.4.2 Testing results and discussion

6.4.2.1 Perchlorate detection sensitivity

The ClO_4^- detection efficiency of the DMAET-coated Au ellipse dimer SERS substrates was first determined in the absence of interferences with $NaClO_4$ solutions ranging in concentration from 0.4 – 80 μM (~0.04 – 8 mg L^{-1} ClO_4^-). DMAET binds to the surface of the SERS substrate through the well characterized affinity for Au possessed by thiol compounds. Functionalization of the substrate surface with DMAET serves a dual purpose: 1) the homogeneity of ClO_4^- dispersion across the sensor surface is increased by the attraction between the dimethyl-amino moiety and anionic ClO_4^- molecules and 2) the adsorption of ClO_4^- within the SERS active region located between the elevated ellipse dimers is enhanced after functionalization. This approach has been previously reported to increase the performance of SERS sensors for ClO_4^- detection (Gu and Ruan, 2007; Gu et al., 2009; Jubb et al., 2017; Mosier-Boss and Lieberman, 2003; Ruan et al., 2006b). One concern with functionalization of SERS sensors is the increased baseline that may occur due to enhanced Raman signal originating from DMAET vibrational modes. While this issue is unavoidable, it did not interfere significantly with the detection of ClO_4^- (Fig. 6.18a).

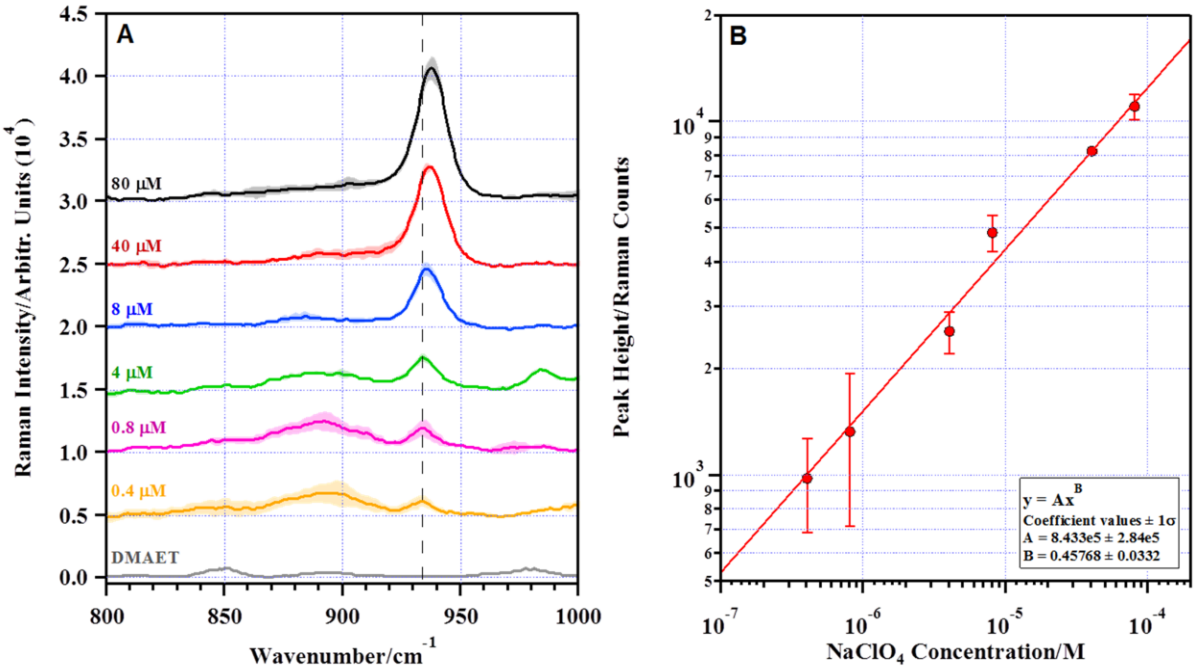

Figure 6.18. (a) Representative SERS spectra of $NaClO_4$ solutions varying in ClO_4^- concentration from 0.4 – 80 µM. (b) Log-log plot of the ν_{SS}-ClO_4^- peak height versus $NaClO_4$ concentration. Data (*red markers*) and power law fit to the data (*red trace*) are provided.

a) A spectrum of the DMAET-coated SERS substrate is given (gray trace) showing minimal contributions to the SERS spectrum from DMAET vibrational modes within the ν_{SS}-ClO_4^- region. Data are represented by solid traces while shaded regions represent ±1σ standard deviation. All spectra are the average of 3-5 spots and have been baseline corrected. Spectra are offset (Y-axis) for clarity. The vertical dashed line represents the peak center of the ν_{SS}-ClO_4^- mode for the 0.4 µM spectrum (orange trace). Note shift of the ν_{SS}-ClO_4^- mode wavenumber with increasing concentration. b) Error bars on data correspond to ±1σ standard deviation between peak height values determined from the Lorentzian fitting analysis (see Fig. 6.19) for the spectra acquired at each ClO_4^- concentration.

The SERS response to trace levels of ClO_4^- can be seen in the spectra shown in Fig. 6.18a. These spectra clearly exhibit the symmetric stretching peak of ClO_4^- (ν_{SS}-ClO_4^-) molecules at ~935 cm^{-1} for solution concentrations as low as 0.4 µM (~40 µg L^{-1}). With a concentration increase, the ClO_4^- signal increases correspondingly, and the relationship is well fit with a power law expression (Fig. 6.18b). It may be reasonable to expect the SERS signal increase to scale linearly with the increased concentration, however, this is clearly not the case; deviations from linearity are common in quantitative SERS studies (Gu et al., 2009; Hatab et al., 2011a; Mosier-Boss and Lieberman, 2003). This is due to saturation of adsorption sites within the SERS substrate active regions at higher ClO_4^- concentrations as well as the large dynamic range of concentrations used in the current study. Regardless, the clear ClO_4^- signal apparent for solution concentrations as low as 0.4 µM demonstrates that the elevated Au ellipse dimer SERS architecture is well suited for the detection of trace quantities of ClO_4^-.

A detection limit of 0.4 μM corresponds to a SERS enhancement factor (EF) of ~10^7 for the elevated ellipse dimer architectures, Eq. 1. For the ClO_4^- EF calculations N_{BULK} can be calculated from the density of $NaClO_4$, given to be 2.52 g cm^{-3}, and the focal volume of the excitation beam, assumed here to be a sphere with a radius equal to 150 μm. N_{SERS} can be determined by considering that the SERS signal originates only from ClO_4^- molecules within the active region between the elevated ellipse dimers. The volume of this region can be calculated for a single dimer possessing a 10 nm nanogap as a cylinder with a radius of 5 nm and a height of 40 nm. Using this active site volume, the density of $NaClO_4$, and the number of elevated ellipse dimers within the beam spot, an N_{SERS} value can be determined; this value represents an upper-limit estimate for the ClO_4^- molecules contributing to the detected SERS signal since not all of the deposited ClO_4^- will be located within the SERS active region. Both I_{SERS} and I_{BULK} were taken as the peak height of the ν_{SS}-ClO_4^- mode determined by fitting the SERS spectrum with a sum of Lorentzian profiles (Fig. 6.19).

The EF equal to ~10^7 calculated for the elevated Au ellipse dimer substrates is 10^2 – 10^3× higher than most previous reports for the SERS detection of ClO_4^-, including those that take advantage of similar nanofabricated architectures, such as elevated Au bowties (Gu et al., 2009; Hatab et al., 2011a; Mosier-Boss and Lieberman, 2003; Ruan et al., 2006b). Simultaneously, the SERS architectures reported here demonstrate good reproducibility, i.e. spot-to-spot variation across a SERS array of ±10% and array-to-array variation of ±10% for a typical reproducibility of ±15% at the ±1σ standard deviation level of uncertainty (Gu et al., 2009; Hatab et al., 2011a). The standard deviation for the two lowest tested ClO_4^- concentrations (0.4 and 0.8 μM) was slightly higher (±30% in both cases). This is attributed to the very small amount of ClO_4^- actually deposited onto the SERS sensor surface in these low concentration tests which increases the sample distribution inhomogeneity; e.g., in the 0.4 μM tests, only ~150 pg (1.5×10^{-10} g) of ClO_4^- is on the surface.

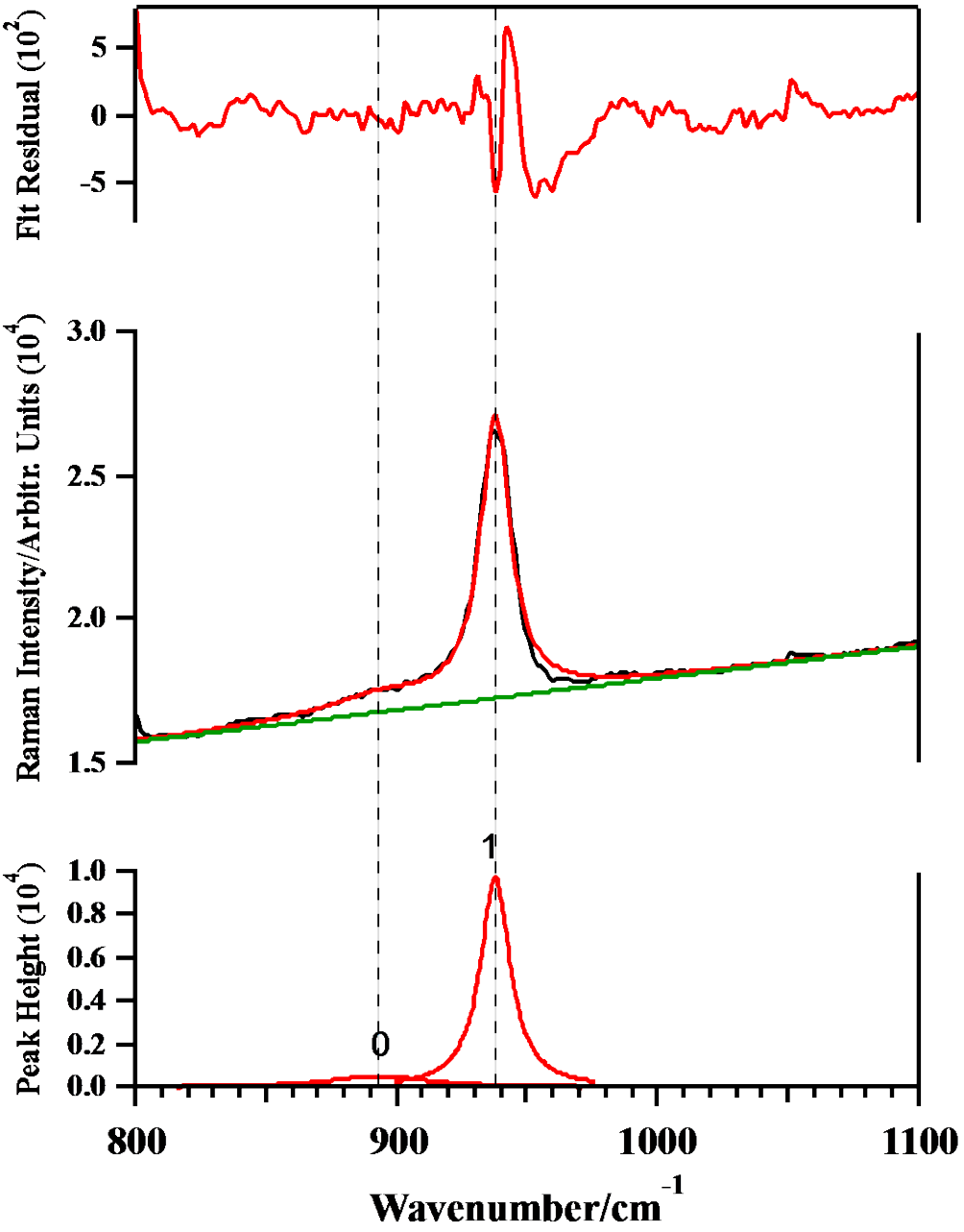

Figure 6.19. Lorentzian Fitting Analysis of Representative 80 µM ClO_4^- SERS Spectrum.

Top Panel – Fit residuals (red trace). Middle Panel – raw spectrum (black trace), composite fit (red trace), and baseline (green trace). Bottom Panel – individual Lorentzian peaks used in fitting analysis (red traces) numbered 0 and 1. Dashed vertical lines indicate Lorentzian peak center frequencies.

There are several literature reports of ClO_4^- detection by SERS at a detection limit lower than or equal to the 0.4 μM level observed for the elevated Au ellipse dimer structures; e.g. Hao et al. (2015) report a detection limit of 5 μg L^{-1} (~0.05 μM) using cysteamine functionalized Ag films on roughened Cu foil. However, the performance of the elevated Au ellipse dimer architectures reported here was determined with a portable Raman instrument, as the ultimate goal of this approach is to demonstrate field-scale measurements, which has inherently lower detection efficiency than the bench-top Raman microscopes typically used in SERS measurements (Fig. 6.20). Additionally, the good reproducibility of the reported SERS architectures is in contrast to SERS substrates based on random geometries where SERS active hot-spots must be located.

The ν_{SS}-ClO_4^- peak wavenumber is observed to increase slightly with an increase in concentration from ~932 cm^{-1} to 940 cm^{-1}, towards the Raman wavenumber observed for solid bulk $NaClO_4$ salt (see Fig. 6.21), in the Fig. 6.18a spectra. The origin of this frequency shift is unclear; however, it may correspond to ion-pairing phenomena between ClO_4^- molecules and other ions or the dimethyl-amino head group of the DMAET coating within the active region of the SERS sensors. This frequency shift has been previously observed for the SERS detection of ClO_4^- and does not impede the successful detection of ClO_4^- (Gu et al., 2009; Hao et al., 2015; Hatab et al., 2011a; Ruan et al., 2006b). Further study is needed to fully elucidate the origin of this behavior.

6.4.2.2 Impact of ion interferences on perchlorate detection

One issue with using a SERS approach to measure ClO_4^- in groundwater is the potential interference effects of other ions and solutes on the ClO_4^- detection efficiency. This issue was examined for SERS sensors based on colloidal Au nanoparticles functionalized with DMAET by Gu et al. in simulated groundwater where ClO_4^- existed concomitantly with Cl^-, NO_3^-, SO_4^{2-}, and PO_4^{3-} ions (Gu et al., 2009). For these solutions, NO_3^- was observed to interfere with ClO_4^- detection, based on detection of the NO_3^- symmetric stretch at ~1045 cm^{-1}, while SO_4^{2-}, PO_4^{3-}, and Cl^- ions were not observed to impact ClO_4^- detection. These observations were attributed to the high hydration energies of SO_4^{2-} and PO_4^{3-} compared to ClO_4^- which may inhibit their adsorption/ion-pairing at the DMAET-modified SERS active site surface, while an explicit explanation on the effect of Cl^- was not given.

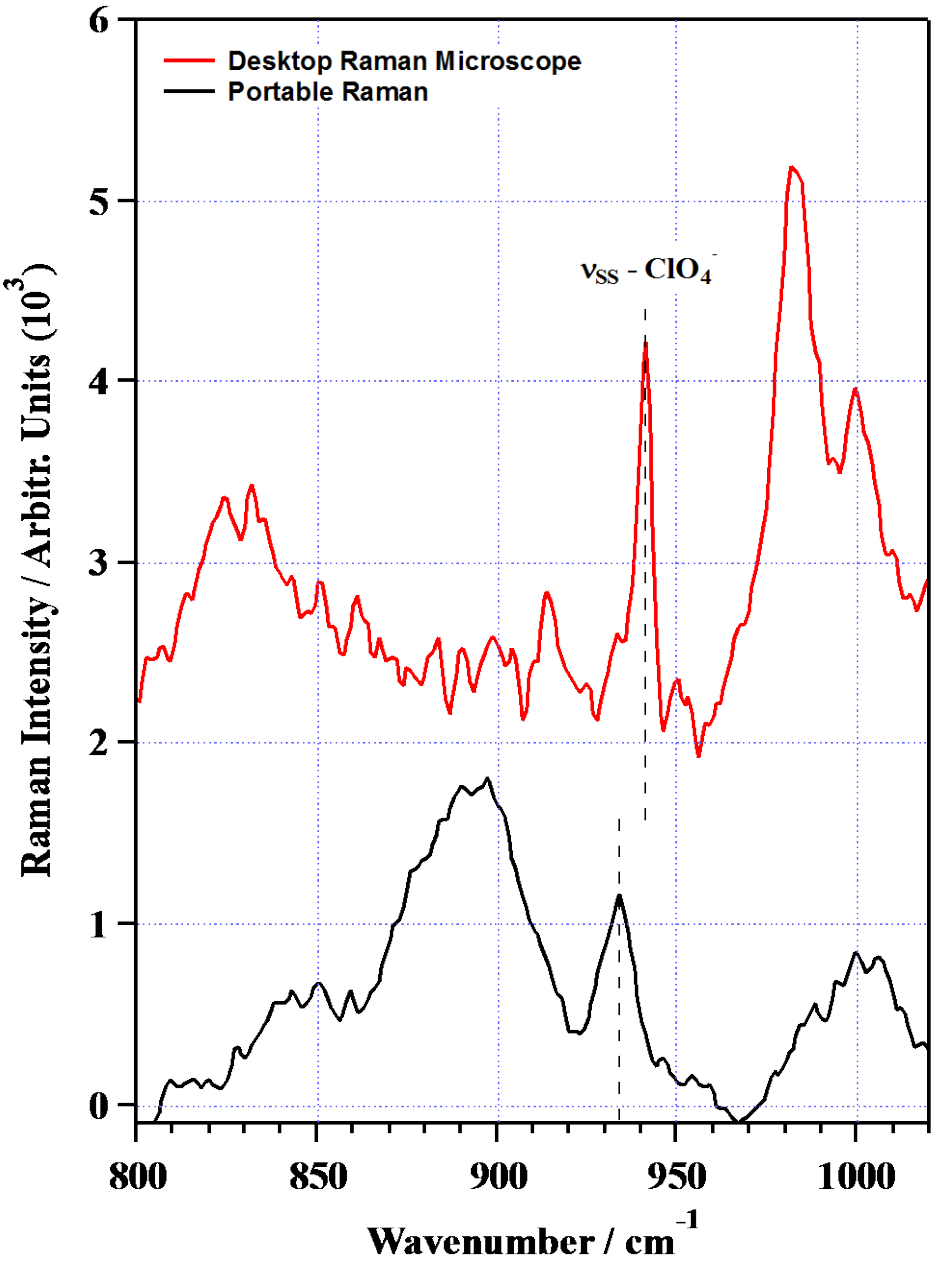

Figure 6.20. Comparison between Raman Spectra from a SERS Sensor with 4×10^{-7} M (~40 µg L^{-1} ClO_4^-) Solution Deposited (3 µL), and Spectra Collected with a Benchtop Raman Microscope (*red trace*) and the Portable Raman Instrument (*black trace*).

Experimental conditions used to collect spectra are as follows; Desktop Raman: 60 s, 1 scan, 1 mW of 785 nm excitation at sample surface, beam size 1.5 × 20 µm. Portable Raman: 60 s, 1 scan, 75 mW of 785 nm excitation at sample surface, beam diameter 300 µm. Spectra are the average of 3 collections, have been baseline corrected, and are scaled for clarity. Dashed vertical line indicates the ν_{SS}-ClO_4^- mode.

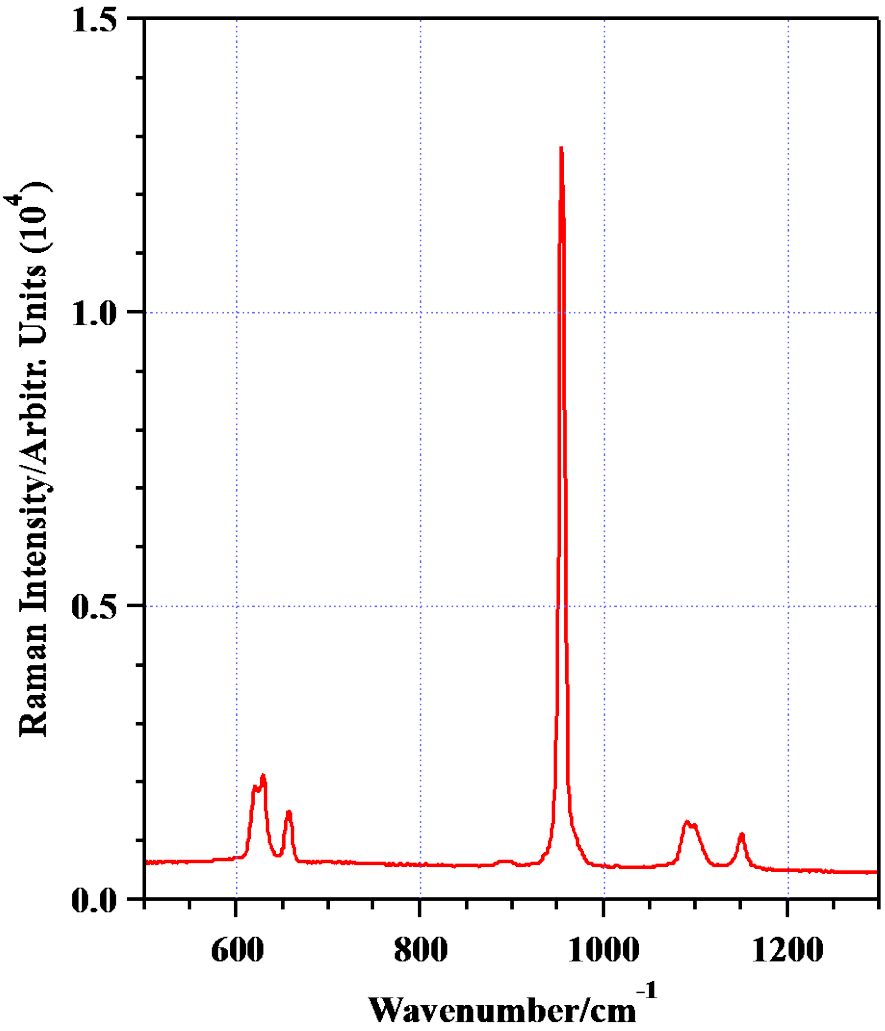

Figure 6.21. Conventional Raman Spectrum of Solid $NaClO_4$ Salt (*red trace*).

Strong peak centered at 955 cm^{-1} corresponds to the ν_{SS}-ClO_4^- mode.

More recently, the interference effect of ions on SERS detection of ClO_4^- for DMAET coated substrates was investigated by Mosier-Boss and Putnam who determined ion-pairing constant strengths between DMAET and a suite of ions including: ClO_4^-, Cl^-, NO_3^-, SO_4^{2-}, HPO_4^{2-}, and $H_2PO_4^-$ (Mosier-Boss and Lieberman, 2003). While the ion-pairing strengths suggest that SO_4^{2-} should be a significant interference to the SERS detection of ClO_4^-, only NO_3^- and Cl^- appeared to impact the detection efficiency of their SERS sensor, in agreement with the earlier findings of Gu et al. (2009). However, neither of these studies evaluated the interferences provided by coexisting solution ions at the individual level and, as such, it is not possible to distinguish between ion specific effects (e.g. ion-pairing) versus macroscopic interferences such as physical displacement of ClO_4^- ions from SERS active sites with an increase in solution ionic strength. Additionally, the ClO_4^- concentration used by Mossier-Boss and Putnam in their interference tests was quite high, 25 mg L^{-1} (~250 μM); as this ClO_4^- concentration is at least two to three orders of magnitude higher than those typically found in many impacted groundwaters, determining the SERS interference of co-existing ions with lower ClO_4^- concentrations is warranted

The effect of individual coexisting ions on the SERS detection of ClO_4^- has been explored in detail by Hao et al. for a SERS architecture involving a cysteamine functionalized Ag nanoparticle film on roughened Cu foil (Hao et al., 2015; Hao et al., 2010). They reported that SO_4^{2-} exhibited the greatest interference effect of the five ions tested (HCO_3^-, NO_3^-, $H_2PO_4^-$, Cl^-, and SO_4^{2-}) which is well explained by the earlier ion-pairing constants reported by Mosier-Boss and Lieberman for these anions with cysteamine (Mosier-Boss and Lieberman, 2003). While the findings of Hao et al. are very informative for predicting the interferences from individual ions on the SERS detection of ClO_4^-, their results differ slightly from the earlier reported findings of Gu et al. and Mosier-Boss and Putnam, both of whom did not observe interference from SO_4^{2-} for DMAET functionalized SERS sensors, even though the ion-paring constant between DMAET and SO_4^{2-} is greater than the value for DMAET - ClO_4^-. In order to rationalize these differences, as well as explore interference effects for the new developed elevated Au ellipse dimer SERS architecture, we further investigated the impact of Cl^-, NO_3^-, and SO_4^{2-} ions on the SERS detection of ClO_4^-.

The influence of Cl^-, NO_3^-, and SO_4^{2-} ions on the ClO_4^- SERS signal from ~8 µM $NaClO_4$ solutions is shown in Fig. 6.22 spectra. The concentration of the interfering ions ranged from 7 – 1500 µM (~1 – 100 mg L^{-1}). For all three interferences tested there was clear ClO_4^- signal detected, even at millimolar concentrations of the competing ions. Fig. 6.23a presents the ClO_4^- peak height versus the interfering ion concentration normalized to the peak height determined from an 8 µM $NaClO_4$ solution in the absence of interferences. These data are replotted in Fig. 6.23b where the normalized peak heights versus the log of the interfering ion concentration is shown for clarity. The influence of Cl^-, NO_3^-, and SO_4^{2-} on the detected ClO_4^- SERS signal all follow a similar pattern where there is a drastic initial decline (~50%) in detected ClO_4^- SERS signal for the lowest concentration of interfering anions tested, followed by a more gradual decline in signal intensity for intermediate interference concentrations until, finally, a sharp drop in signal for the two highest interfering ions tested is observed (Fig. 6.23a).

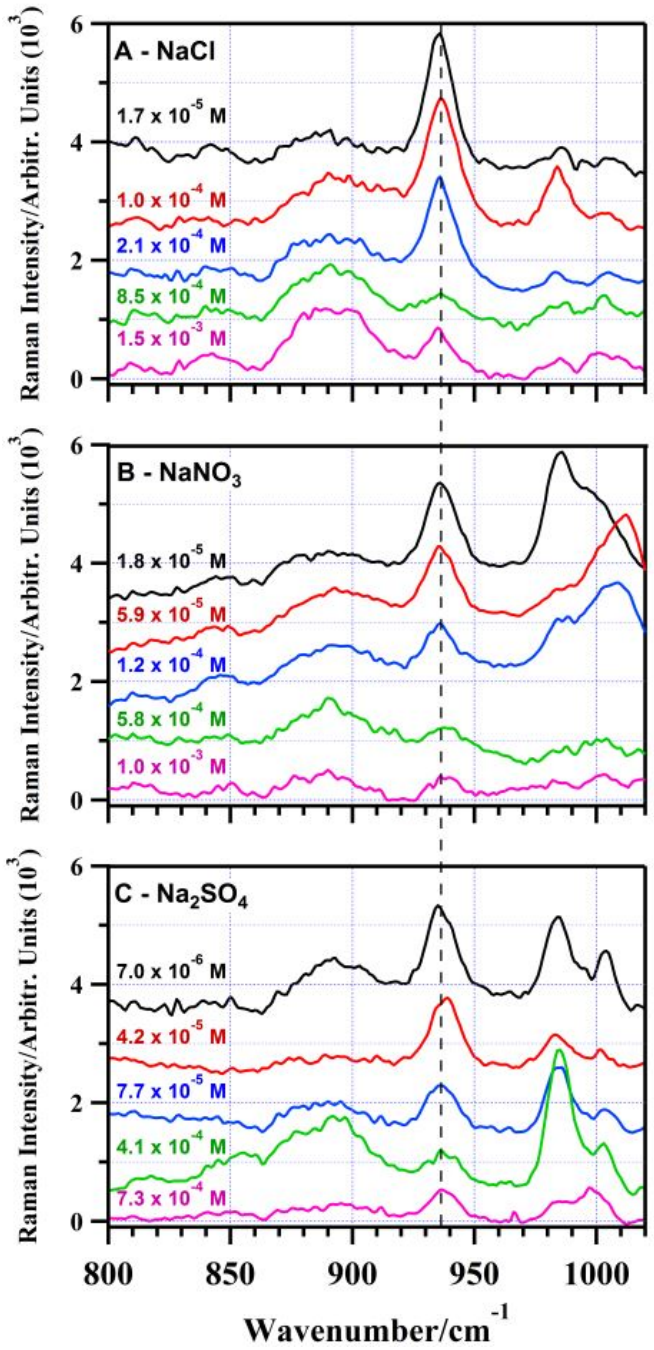

Figure 6.22. SERS Spectra from the Ion Specific Interference Tests Where a) NaCl, b) $NaNO_3$, and c) Na_2SO_4 Were Added to ~8 µM ClO_4^- Solutions.

Interfering ion concentrations were varied from ~10^{-6} – 10^{-3} M. All spectra are the average of 3 – 5 spots, have been baseline corrected, and are offset (Y-axis) for clarity. Dashed vertical line represents the center wavenumber for the ν_{SS}-ClO_4^- peak.

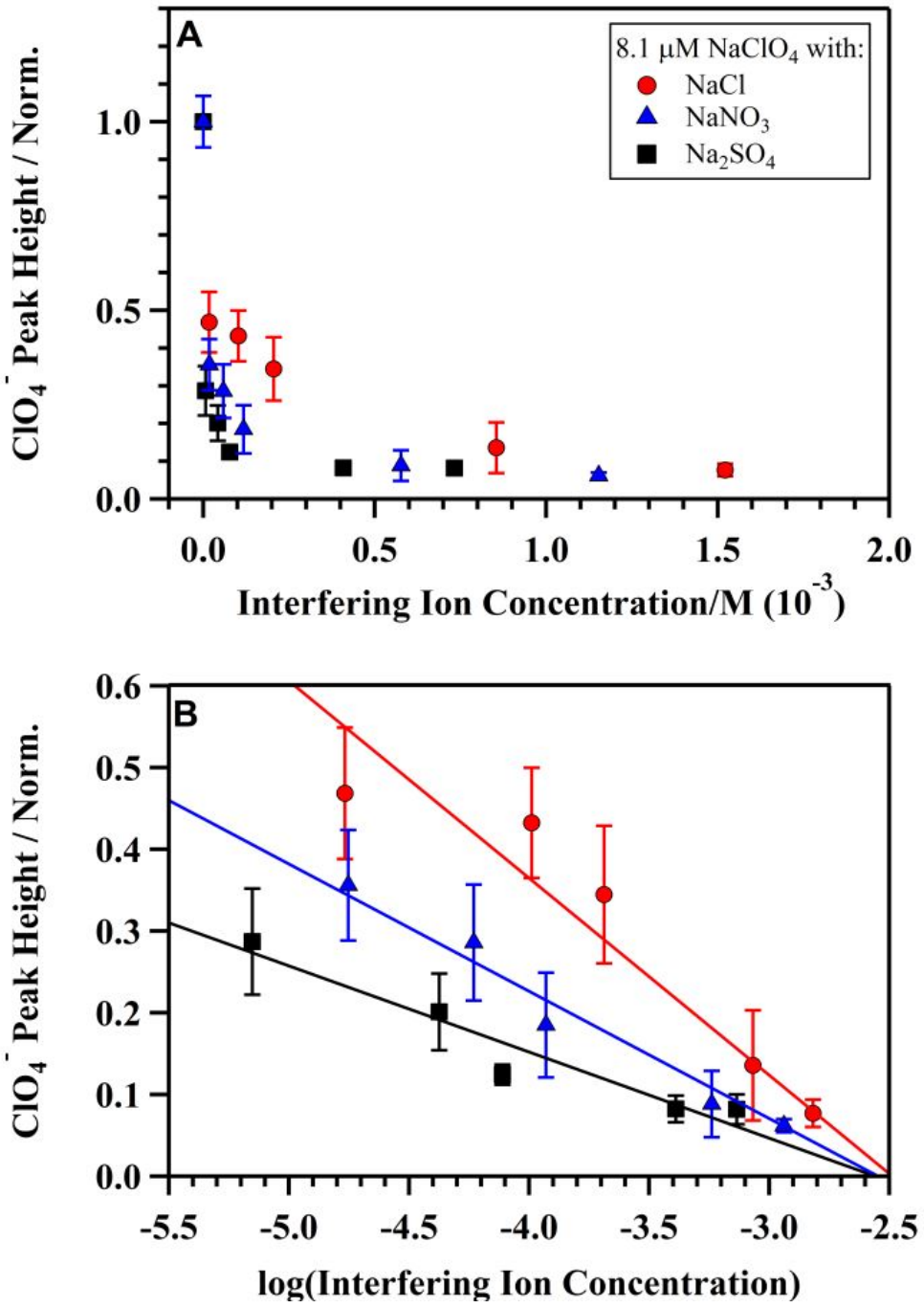

Figure 6.23. (a) Normalized SERS ν_{SS}-ClO_4^- peak heights for an 8 μM ClO_4^- solution determined in the presence of NaCl (*red circles*), $NaNO_3$ (*blue triangles*), and Na_2SO_4 (*black squares*) versus the concentration of the respective interference species. (b) The same data *(markers)* as shown in (a) only plotted against the log of the interfering ion concentration.

Solid traces are linear regression fits to the data. Error bars represent ±1σ standard deviation. Peak heights have been normalized to the ν_{SS}-ClO_4^- peak height from an 8 μM ClO_4^- solution in the absence of any interfering ions.

By fitting the normalized peak heights versus the log of the interfering ion concentration with linear regressions, it is possible to compare the relative effects of the different interfering species on ClO_4^- detection (Hao et al., 2010). From the linear regression fits shown in Fig. 6.23b, it is clear that, at low and intermediate concentrations of interfering ions (i.e., ≤ 200 µM), the interference strength is ion specific with the effect decreasing as: SO_4^{2-} > NO_3^- > Cl^-, in agreement with the findings of Hao et al. (2010). However, at higher ion concentrations (> 200 µM) the identity of the interfering ion seems to play less of a role in determining the overall interference effect; this can be seen in Fig. 6.23b where the linear regression curves intersect. This is attributed to physical displacement of ClO_4^- ions from the SERS active region within the nanogap of the elevated Au ellipse dimers by the much more prevalent interfering ions. This behavior has not been observed previously in studies examining interference effects on the SERS detection of ClO_4^-, likely due to the major differences between typical nanoparticle SERS substrates with much larger surface areas able to accommodate higher ion loadings than those of the elevated Au ellipse dimer architectures used here. These finding would imply that efforts to use these SERS architectures for ClO_4^- analysis in highly saline environmental samples may be complicated by the ability to actually deposit ClO_4^- molecules within the active region of the sensor.

Additionally, the impact of ferrous ions (Fe^{2+}) on the SERS detection of ClO_4^- anions was investigated; this is shown in Fig. 6.24 compared against the results for Na_2SO_4 interference. With low levels of Fe^{2+} concentration the SERS response from ClO_4^- is dramatically depressed. However, unexpectedly, as Fe^{2+} concentrations increased above 500 µM the ClO_4^- SERS signal was enhanced somewhat but decreased again with further increasing Fe^{2+} concentrations. Signal suppression and smearing effects at high Fe^{2+} concentrations are expected due to oxidation of Fe^{2+} leading to precipitation of iron oxyhydroxides. Further work is needed to confirm and elucidate the mechanisms of either the enhancement or inhibition effects by Fe^{2+} ions.

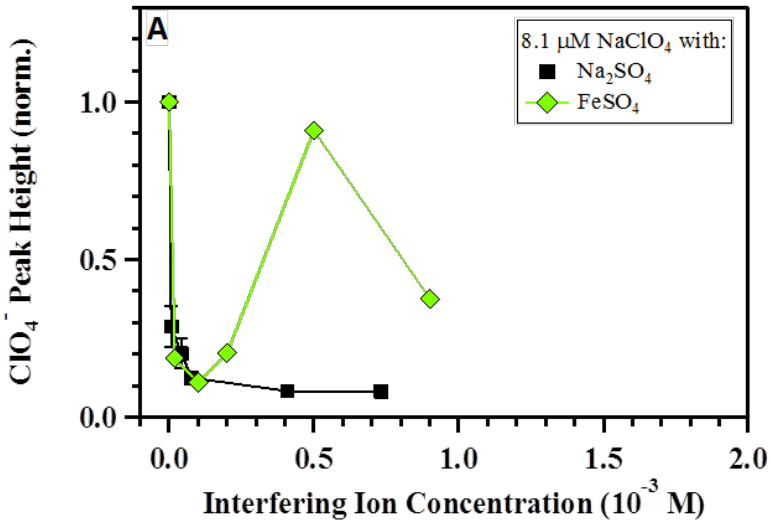

Figure 6.24. Influence of Na_2SO_4 (*black squares*) and $FeSO_4$ (*green diamonds*) Interferences on the SERS Detection of ~8 µM ClO_4^-.

6.4.3 SERS performance and interference evaluation summary

Commercially produced SERS substrate sensors based on elevated Au ellipse dimer architectures were demonstrated to detect ClO_4^- at levels below 1×10^{-6} M using a portable Raman analyzer. The systematic evaluation of interference effects on the SERS detection efficiency for ClO_4^- ions from Cl^-, NO_3^-, and SO_4^{2-} ions was carried out. It was determined that for low interference concentrations ($< 2\times10^{-4}$ M) the interference strength is ion specific with SO_4^{2-} exhibiting the largest effect. For interference concentrations above $\sim2\times10^{-4}$ M the identity of the interfering species does not play a major role, likely due to physical displacement of the much less abundant ClO_4^- ions from the SERS active region of the sensors. Taken together, the results presented in this study make a case for the applicability of the SERS-based portable Raman sensor for rapid field measurements of trace levels of ClO_4^- in contaminated water.

6.5 FIELD DEMONSTRATION AND EVALUATION

6.5.1 Detection and analysis of perchlorate at field sites

To evaluate the applicability of the elevated Au ellipse dimer SERS substrates to detect ClO_4^- within impacted groundwater, where multiple interferences exist, groundwater samples were collected from multiple DoD sites. The ClO_4^- concentrations were determined with a portable SERS sensor in the field, and the samples were subsequently tested again for ClO_4^- by IC. Sections 6.5.2 and 6.5.3 detail two field demonstrations at the Indian Head Division, Naval Surface Warfare Center (IHDIV) near Indian Head, MD, between October 2015 and October 2016, and Section 6.5.4 provides details of another field demonstration at Redstone Arsenal (Redstone) outside of Huntsville, AL, in November 2016. The data for the Indian Head 2015 visit was taken with uncoated SERS substrates, as detailed in Section 4.5.2, while commercially fabricated SERS substrates coated with dimethyl-aminoethane thiol were used to for the 2016 field demonstrations at IHDIV and Redstone sites, respectively.

As previously noted, a field demonstration was also planned initially at the Naval Surface Warfare Center Dahlgren site in Dahlgren, VA, but the ClO_4^- concentrations at this site were deemed generally too low (20-80 ppb) to be detected by the field Raman instrument. A second field demonstration, with optimized commercial SERS substrate, was performed at IHDIV in place of the Dahlgren field trial. We also surveyed additional sites, including High Plains in West Texas and Kirtland Air Force Base in California, and groundwater samples were collected and analyzed (Tables 4.1 and 4.2). However, ClO_4^- concentrations at these sites were also non-detect or too low to conduct meaningful field trials.

6.5.2 IHDIV demonstration 1

6.5.2.1 IHDIV Field Demonstration

An initial field demonstration of the portable Raman sensor for ClO_4^- detection was conducted at IHDIV in October 2015. Site background was provided previously in Section 4.5. Groundwater samples were collected from six representative monitoring wells behind the perchlorate hog-out facility (Figs. 6.25 and 6.26) for on-site SERS analysis as well as further laboratory analysis by both ion chromatography (IC) and SERS. Of the six groundwater samples collected, four were analyzed on-site with the portable Raman system, including samples CPMW-2D, MW-4, CPMW-5, and MW-8.

These four were selected since they were the first four wells sampled. MW-1 and MW-11 were not analyzed on-site with the portable SERS system due to time constraints at the IHDIV site but were analyzed later in the laboratory.

The experimental procedure used for the on-site SERS analysis is briefly described below. Following collection of the ground water samples an aliquot of sample, typically 1-5 µl, was placed on a previously fabricated SERS sensor based an elevated Au ellipse dimer substrate template which had been taped onto a glass microscopy slide (illustrated in Fig. 6.2) (Jubb et al., 2017; Jubb et al., 2016). The sample aliquot was subsequently dried onto the SERS array and placed on the portable Raman sample stage under the laser excitation beam spot. A SERS spectrum was then collected. SERS spectra were collected with six 10 s scans using either 75 mW or 300 mW of 785 nm laser light. At the lower laser power (75 mW), most spectra featured a broad strong background signal (Fig. 6.27). This is attributed to fluorescence from potential naturally dissolved organic compounds within the groundwater samples as well as the non-specificity of the SERS response (to other interfering ions), which also "report" on chemical compounds with Raman active vibrational modes. In the frequency region relevant for ClO_4^- detection, 850 – 1100 cm^{-1}, three peaks are observed which can be assigned to ClO_4^-, SO_4^{2-}, and NO_3^-. The symmetric stretch of the ClO_4^- ion should occur at ~940 cm^{-1}; this can be seen clearly for CPMW-2D and to a lesser extent for the other three well waters tested (Fig. 6.27).

The symmetric stretches of SO_4^{2-} and NO_3^-, likely interferences due to their environmental ubiquity, occur at ~990 cm^{-1} and 1050 cm^{-1}, respectively. Peaks are observed in several of the groundwater spectra at these frequencies and are attributed to the presence of these chemical compounds. When the laser power of the SERS excitation beam is increased to ~300 mW the presence of ClO_4^- within CPMW-2D is very clear with a signal to noise ratio > 50 (Fig 6.28). While increasing the power of the excitation beam increases the SERS response, and hence the detection limit, incident powers of ~300 mW are typically to be avoided as it is possible to damage the SERS array through heating effects which may lead to non-reproducibility. These results indicate that the portable Raman sensor worked as expected.

We also tested on-site standard addition (described in Section 5.3.1) to construct calibration curves from previously generated standard solutions of ClO_4^- as well as standard solutions of ClO_4^- with known amounts of interfering compounds (e.g. SO_4^{2-}, NO_3^-, etc.).

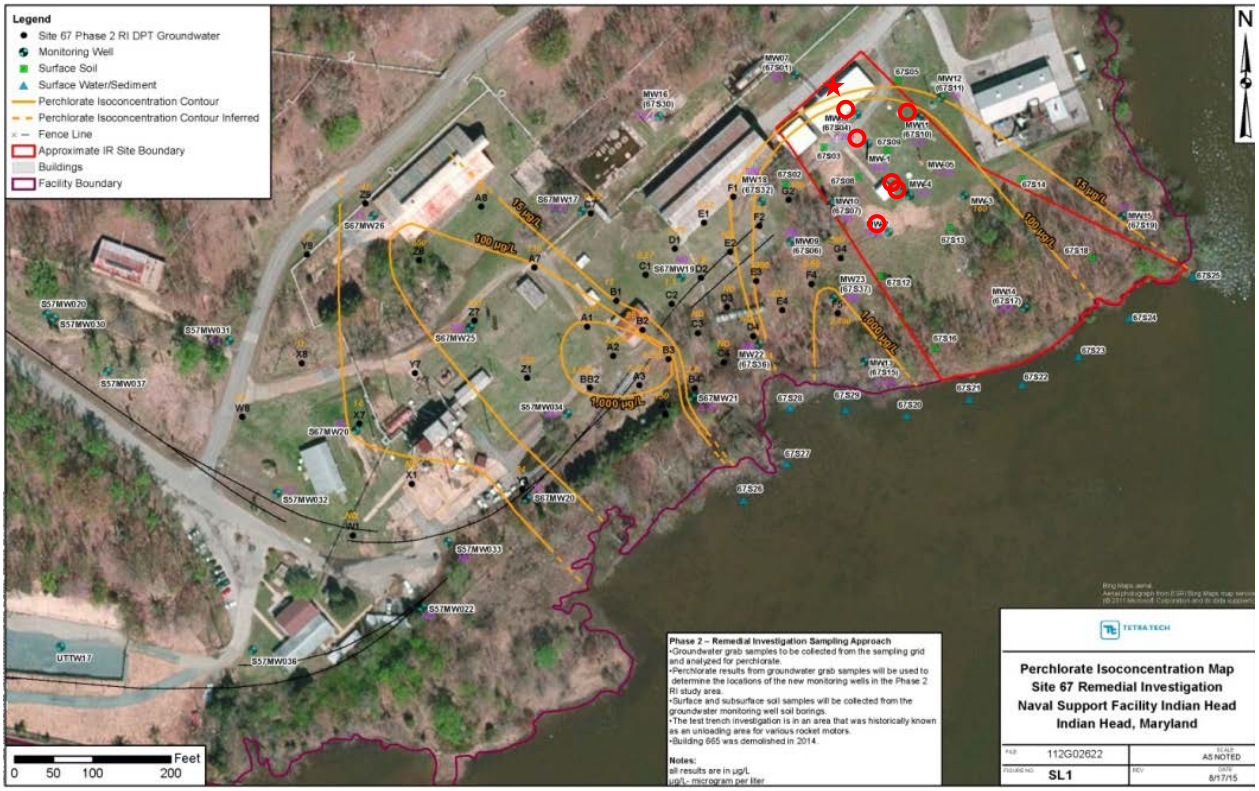

Figure 6.25. Aerial Map of Perchlorate Ground Water Collection Wells at Indian Head Naval Surface Warfare Center.

Perchlorate hog-out facility is indicated by red star while the six ground water wells sampled are circled in red. Yellow lines represent ClO_4^- concentration contours.

Figure 6.26. Photograph of Portable Raman Instrument Deployed at Indian Head Naval Surface Warfare Hog-out Site with Groundwater Wells in Background.

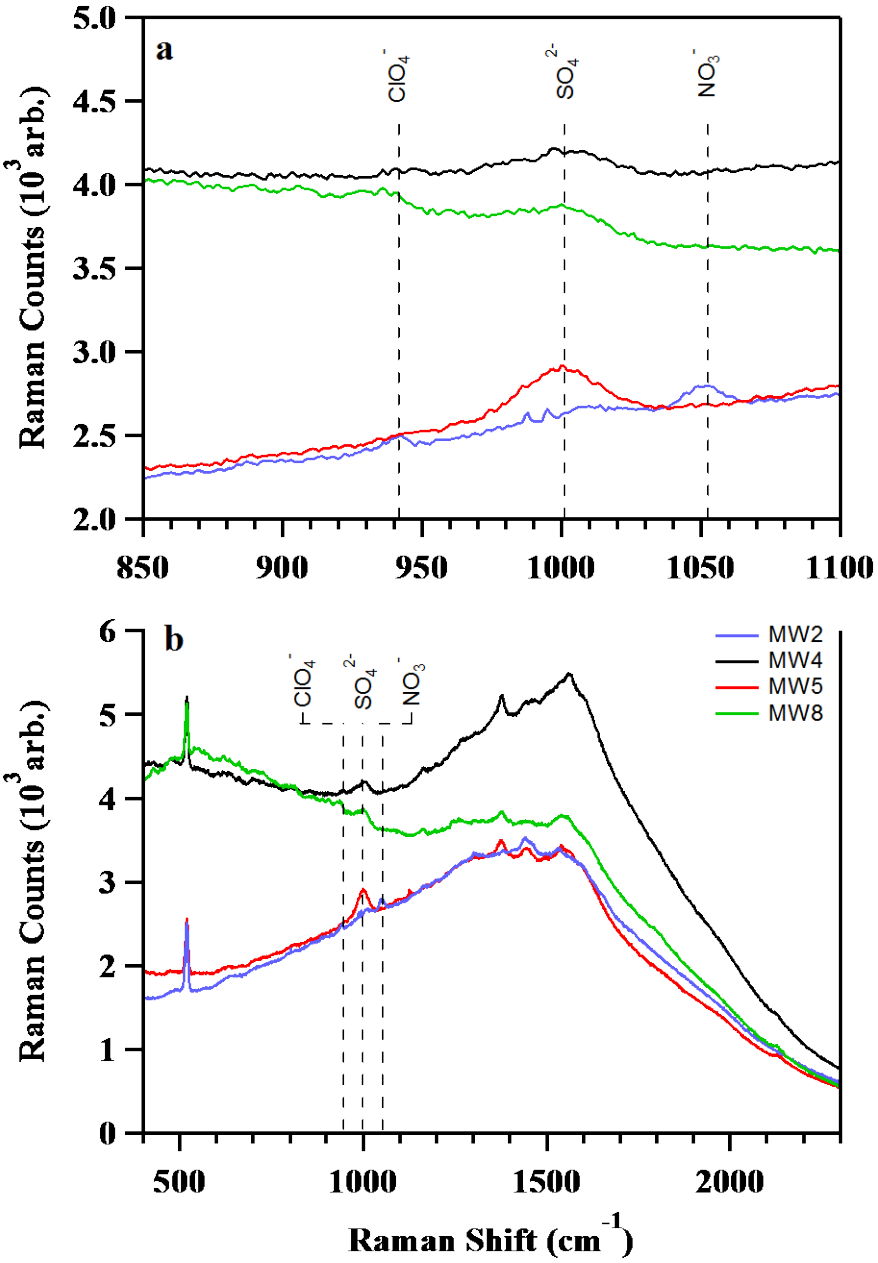

Figure 6.27. SERS Spectra of Four Groundwater Samples Collected at Indian Head Naval Surface Warfare Center: CPMW-2D (MW2) (*blue trace*), MW4 (*black trace*), CPMW-5 (MW5) (*red trace*), and MW8 (*green trace*).

(a) SERS spectra of the four groundwater samples in the perchlorate symmetric stretching region. (b) Full SERS spectra of the four groundwater samples. Vibrational signatures of perchlorate (ClO_4^-), sulfate (SO_4^{2-}), and nitrate (NO_3^-) ions indicated by dashed lines and annotations.

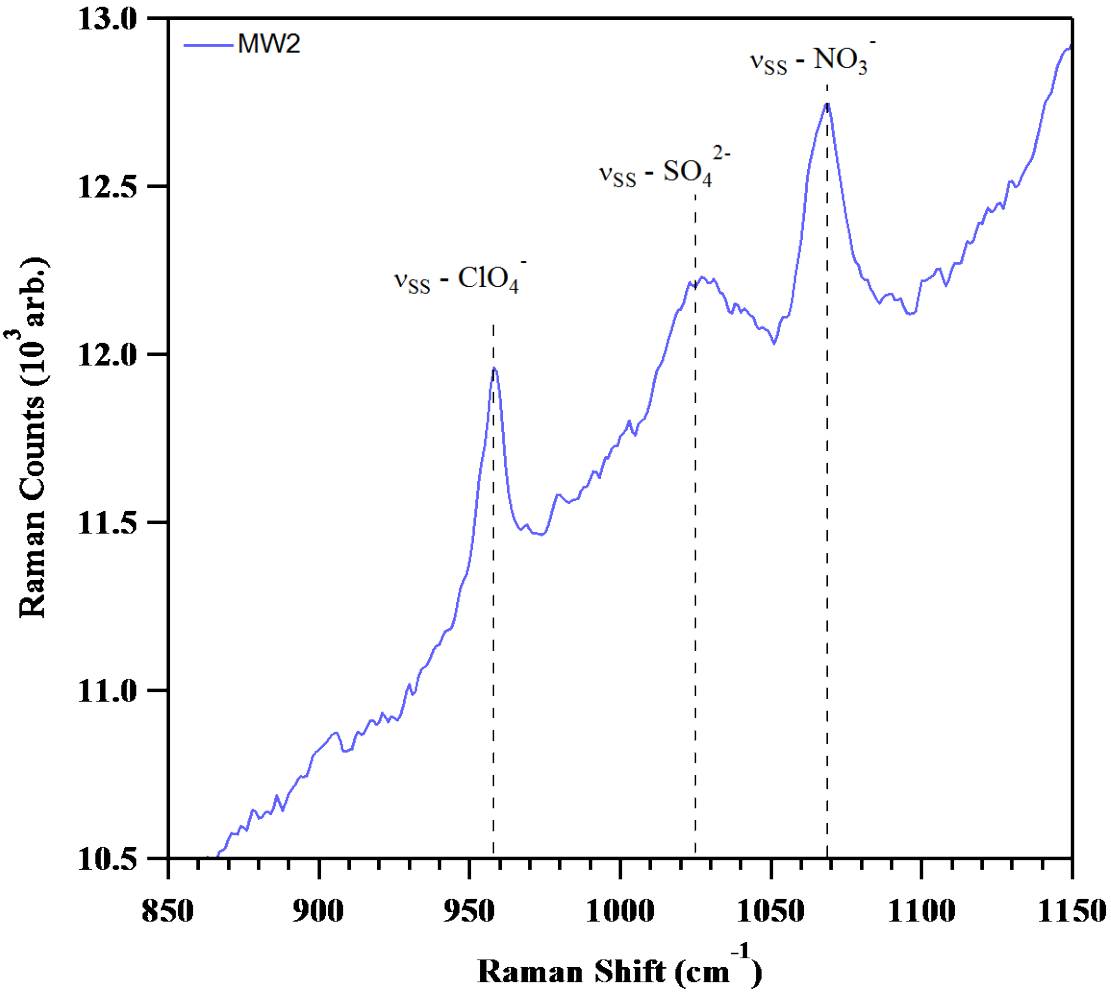

Figure 6.28. SERS Spectrum of CPMW-2D (MW2) Groundwater with ~300 mW Incident 785 nm Power.

Perchlorate, sulfate, and nitrate vibrational features are clearly present and indicated with dashed lines and annotations.

The six ground water samples collected from the Indian Head Naval Surface Warfare Center site were also analyzed for ClO_4^- by ion chromatography following EPA method 314.0 at ORNL and at CB&I (Table 6.1). The agreement between the two laboratory IC analyses is within ±10% for five of the six ground waters tested. For CPMW-2D the deviation between the two labs is higher, ~20%, which is likely caused by its relatively high ClO_4^- concentration in this sample exceeding the linear region of the calibration curve used. Each standard deviation is the result of triplicate analyses of split samples (i.e., from the same individual sample bottle).

Table 6.1. Perchlorate Concentrations of the Six Ground Water Samples Determined via Ion Chromatography (IC) by CB&I and ORNL in October 2015.

Perchlorate (mg/L) determination with IC					
	CB&I		ORNL		
	Average	Standard deviation	Average	Standard deviation	% Deviation
MW-01	627	9	611.5	5	-2.5
CPMW-2D	2060	26	2468	18	19.8
MW-4	73.0	0.7	73.4	1	0.5
CPMW-5	261	6	269.0	2	3.1
MW-08	375	5	376.5	3	0.3
MW-11	98.9	0.3	91.9	1	-7.6

In addition to determine ClO_4^- concentration with IC, we also determined the concentration of a suite of other inorganic cations and anions as well as total dissolved solids (TDS). This is important in the context of SERS detection of perchlorate as other anions, especially oxyanions, are vital to quantify as they can provide possible interferences due to their molecular vibrations. The major anions present in the six ground-water samples were Cl^-, SO_4^{2-}, and NO_3^-. Both SO_4^{2-} and NO_3^- appeared to interfere with the SERS detection of ClO_4^-, additionally they are present at levels equal to or greatly exceeding the amount of ClO_4^- within the samples. These IC results also confirm the earlier assignments of peaks at ~990 cm^{-1} and ~1050 cm^{-1} in the SERS spectra collected on-sight to sulfate and nitrate, respectively. The results for major anions are given in Table 6.2.

The six groundwater samples previously collected from the IHDIV Naval Surface Warfare Center on 08/16/2015 (MW-1, CPMW-2D, MW-4, CPMW-5, MW-08, and MW-11) were further analyzed with the portable SERS instrument in a laboratory setting following an identical procedure as was used in the field, i.e., an aliquot of sample, ~1 uL, was placed on a Au ellipse dimer nanoantennae SERS sensor, dried, placed on the portable Raman sample stage, and a SERS spectrum collected. The SERS spectra of a series of ClO_4^- standard solutions made in 18.3 MΩ water were also collected in a similar manner. The SERS spectra collected from the ClO_4^- standard solutions indicate that the detection limit of the SERS technique is ~100 ppb.

Table 6.2. Results of Anions and Total Dissolved Solids (TDS) from October 16, 2015 Sampling Event at IHDIV.

All results are presented in mg/L.

	F^-	Cl^-	NO_2^-	SO_4^{2-}	Br^-	NO_3^-	ClO_3^-	PO_4^{3-}	TDS
W-01	0.2	**61.9**	0.2	**28.4**	0.2	**2.52**	0.2	0.2	**227**
CPMW-2D	0.2	**30.3**	0.2	**64.3**	0.2	**1.07**	0.2	0.2	**189**
MW-4	0.2	**9.12**	0.2	**57.7**	0.2	0.2	**0.51**	0.2	**156**
CPMW-5	0.2	**6.96**	0.2	**71.9**	0.2	0.2	0.2	0.2	**214**
MW-08	0.2	**79.7**	0.2	**52.8**	0.2	**0.61**	0.2	0.2	**229**
MW-11	0.2	**32.0**	0.2	**55.4**	0.2	**0.23**	0.2	0.2	**177**

The SERS spectra from two groundwaters, CPMW-2D and CPMW-5, collected from separate sampling wells are shown in Fig. 6.29. While these spectra exhibit both a different number of peaks as well as relative intensity differences, the ν_{SS}-ClO_4^- is clearly visible at ~935 cm^{-1} for each groundwater spectrum. Ion chromatography was used to establish the concentration of ClO_4^- within each groundwater sample along with several common coexisting ions that potentially interfere with the SERS detection of ClO_4^- (Tables 6.1 & 6.2). A standard addition approach was also used to validate the identification of ClO_4^- and to determine its concentration in the two groundwater samples. As the groundwaters had differing matrix compositions and concentrations of co-existing ions, it was necessary to use individual standard addition curves for each groundwater sample (Fig. 6.30). The determined ClO_4^- concentrations from the SERS analysis for CPMW-2D and CPMW-5 are given in Table 6.3 and agree well with the IC ClO_4^- concentrations.

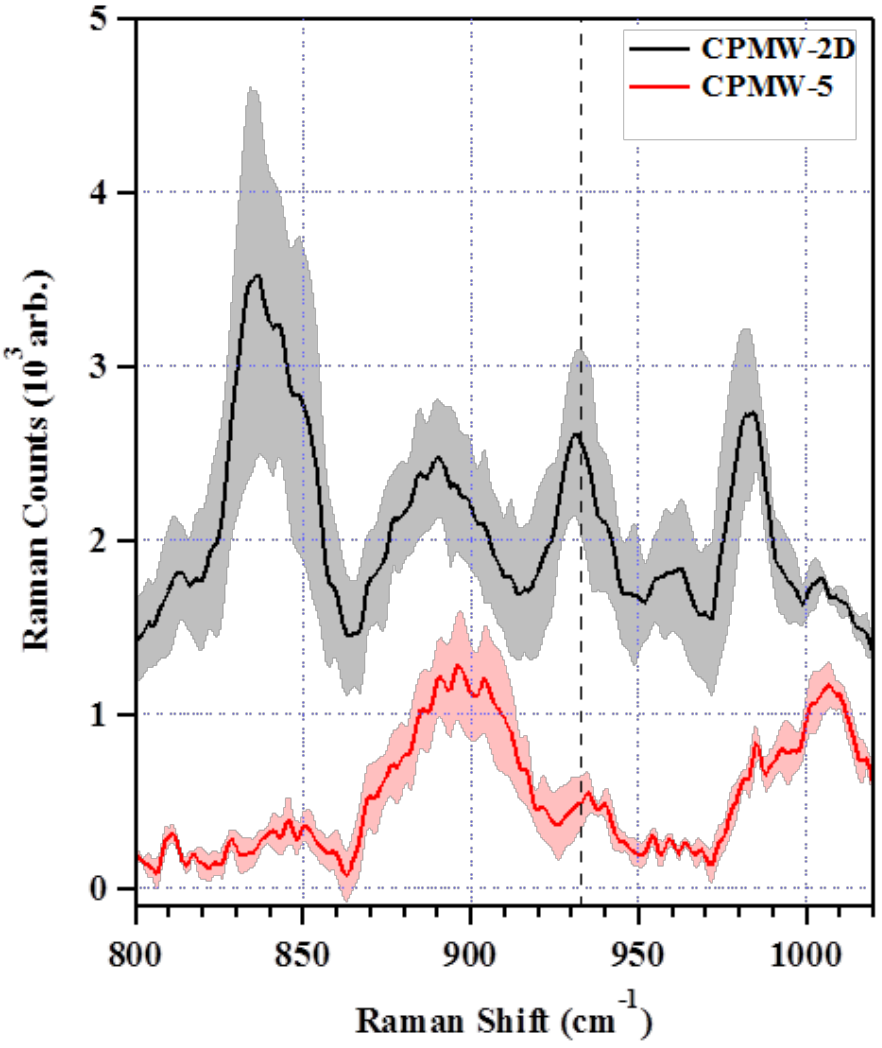

Figure 6.29. SERS Spectra of Two Groundwater Samples, CPMW-2D (*black trace*) and CPMW-5 (*red trace*), Collected from IHDIV.

Shaded regions represent ±1σ standard deviation. The spectra are the average of 3–4 spots and have been baseline corrected. Spectra are scaled for clarity. Vertical dashed line represents the peak center of the ν_{SS}-ClO_4^- mode.

Table 6.3. Comparison between Groundwater ClO_4^- Concentrations Determined with SERS versus EPA Method 314.0.

Groundwater ID	SERS Perchlorate[1] (mg L^{-1})	IC Perchlorate[2] (mg L^{-1})
CPMW-5	0.343 ± 0.025	0.261 ± 0.005
CPMW-2D	2.47 ± 0.16	2.19 ± 0.18

[1.] Error corresponds to the ±1σ precision uncertainty of the linear regression curve used in the standard addition analysis.

[2.] Error corresponds to the ±1σ standard deviation level of uncertainty determined from 3 measurements.

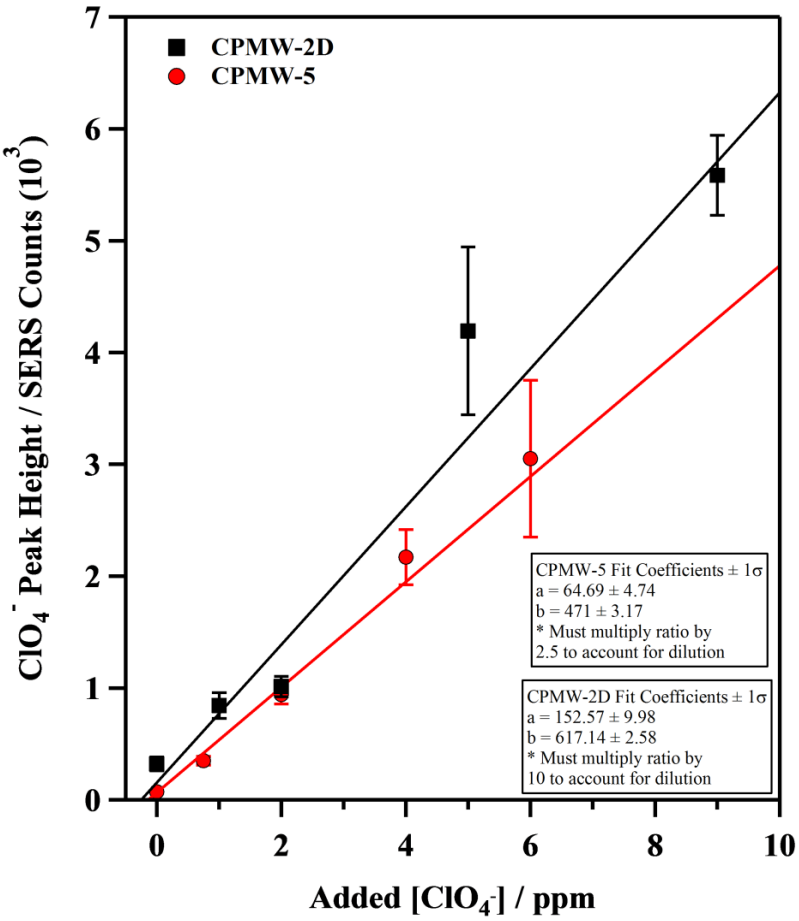

Figure 6.30. Standard Addition Curves for Groundwaters CPMW-2D (*black squares*) and CPMW-5 (*red circles*).

Solid traces are linear regression fits to the data with the respective fit coefficients given in the boxes in lower right corner along with the dilution factor used for each standard addition. Data are average of four measurements where error bars represent ± 1 standard deviation.

6.5.3 IHDIV demonstration 2

A second field demonstration of the portable Raman sensor was conducted in October 2016 at IHDIV using an improved SERS substrate. The same six groundwater wells were sampled from the ClO_4^- hog-out facility. Of the six groundwater samples collected, five were analyzed on-site with portable Raman system, including samples MW-1, CPMW-2D, MW-4, CPMW-5, and MW-11. All groundwater samples were further analyzed in the ORNL laboratory. Additionally, the ClO_4^- concentrations in all 6 samples were analyzed with IC in the laboratory for comparisons and to track concentration changes with time (Table 6.4). From the ClO_4^- concentrations detailed in Table 6.4, it is apparent that the groundwater composition is quite dynamic where both increases and decreases in ClO_4^- concentrations are observed.

Table 6.4. 2015 and 2016 ClO_4^- Concentrations from Six Groundwater Samples from Indian Head Naval Surface Warfare Center as Determined by Ion Chromatography (IC).

Standard deviations are from triplicates.

Perchlorate (µg/L)				
	October 2015		October 2016	
	Average	Standard Deviation	Average	Standard Deviation
MW-01	627	9	423	13
MW-08	375	5	1640	26
CPMW-5	261	5	6.86	0.22
CPMW-2D	2060	18	665	91
MW-4	73.0	0.7	2.38	0.42
MW-11	98.9	0.3	26.1	0.8

The SERS sensor was able to detect ClO_4^- signals in five of the six groundwaters directly (MW-01, MW-08, CPMW-2D, MW-4, and MW-11) during the in-field demonstration (Fig. 6.31), in contrast to earlier results from the October 2015 visit. This is attributed to the use of DMAET as a surface coating on the SERS substrates which can enhance the affinity of ClO_4^- ions for the SERS sensor surface (Gu et al., 2009; Jubb et al., 2017). Standard addition curves were run in the field for MW-1 and CPMW-2D; Fig. 6.32 presents a representative curve for MW-1. The SERS determined ClO_4^- concentrations from the 2016 Indian Head groundwaters are given in Table 6.5.

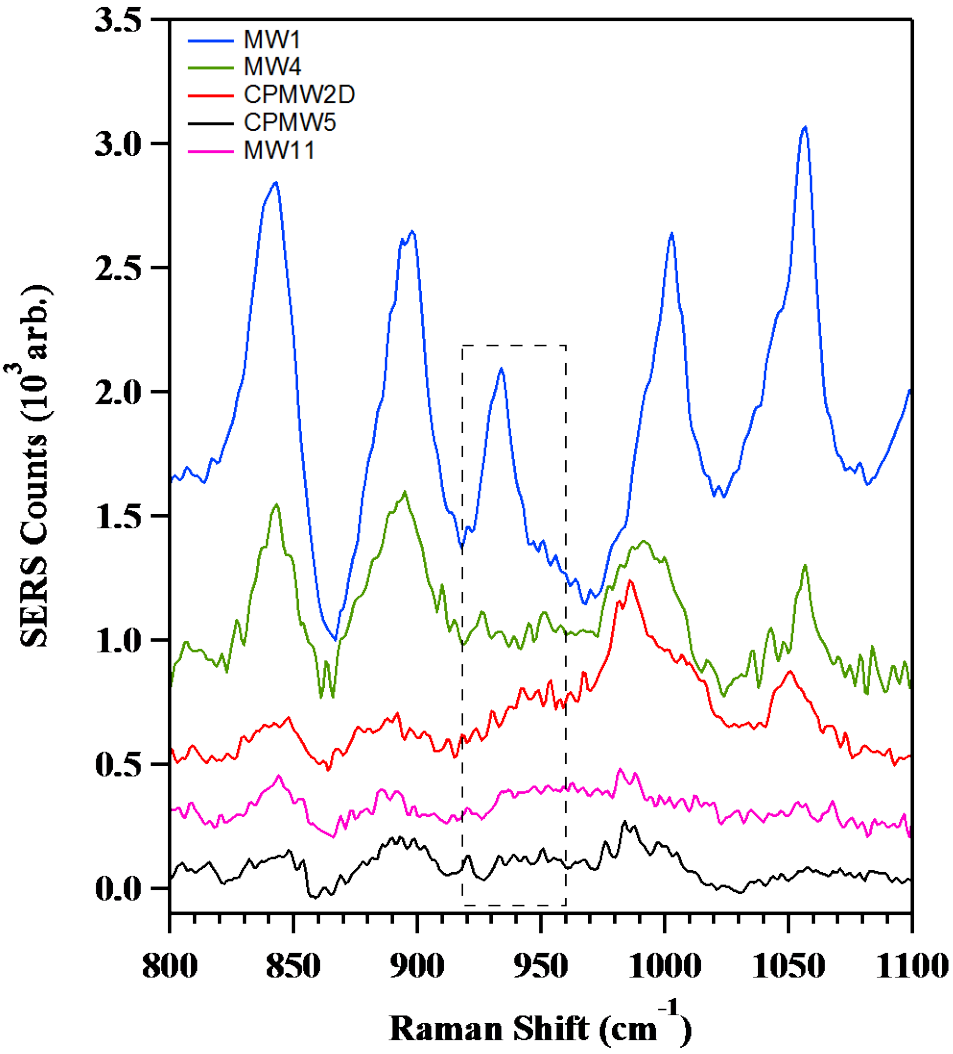

Figure 6.31. Field SERS Spectra of Undiluted Groundwater from IHDIV (October 2016).

Spectra represent the average of 3 individual spectra and have been baseline corrected and scaled for clarity. Boxed region represents ClO_4^- symmetric stretching region.

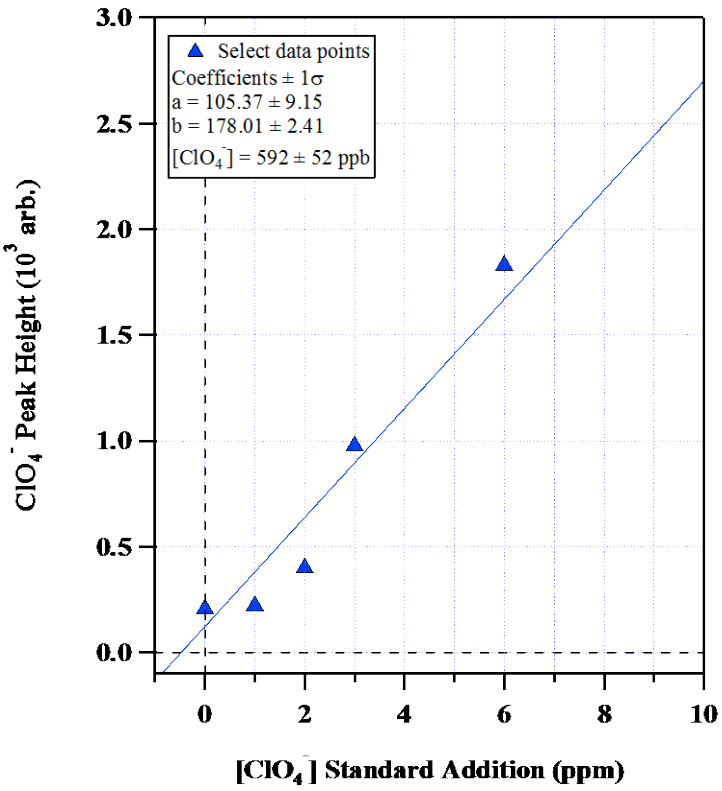

Figure 6.32. Field Collected SERS Standard Addition Determination of ClO_4^- Concentration in MW-1 Groundwater.

Data are markers. The solid trace is the linear regression fit to the data with coefficients and determined ClO_4^- concentration given in the inset box.

Table 6.5. Comparisons of ClO_4^- Concentrations Determined by Ion Chromatography (IC) and by On-site Portable Raman SERS Sensor for Indian Head Groundwaters (October 2016).

Standard deviations are from triplicate analyses.

Groundwater ID	IC ClO_4^- (mg L^{-1})	SERS ClO_4^- (mg L^{-1})
MW-1	0.423 ± 0.013	0.592 ± 0.052
CPMW-2D	0.665 ± 0.091	1.390 ± 0.215
MW-4	0.002 ± 0.001	BD
CPMW-5	0.007 ± 0.001	BD
MW-8	1.640 ± 0.026	2.00 ± 0.193
MW-11	0.026 ± 0.001	BD

BD – Concentration below the SERS detection limit.

The SERS determined ClO_4^- concentrations were observed to vary with the IC results from ±18% to ~ 50%. Note that the SERS determined ClO_4^- concentration trends in the groundwater samples between 2015 and 2016 track those determined by IC. ClO_4^- concentrations in MW-4, CPMW-5, and MW-11 were below the detection limit by the SERS approach.

6.5.4 Field demonstration at Redstone Arsenal

6.5.4.1 Field demonstration

The general site conditions at the Redstone OB/OD area are provided in Section 4.2. The field demonstration of the Raman sensor at Redstone Arsenal occurred in November 2016 (Figs 4.3 and 4.4). This enabled determination of the SERS substrate feasibility for use on samples with differing chemical compositions as the groundwater chemistry and co-contaminants at Redstone Arsenal are generally different from conditions at IHDIV. Due to site safety constraints in the OB/OD Area, all SERS data collection was done in the CB&I on-site building where the portable SERS instrument was placed on a folding table (see Fig. 6.33). All Redstone SERS data were collected with commercially produced SERS sensors.

The well water location and sample codes are given in Table 6.6 along with the ClO_4^- concentrations determined in 2015 and 2016 using EPA method 314.0 versus the concentration determined with the SERS approach. As the ClO_4^- contaminant levels for the wells sampled at Redstone were generally quite high it was possible to directly detect ClO_4^- in the undiluted well water for six of the eight wells sampled (Fig. 6.34). Two of the wells sampled had ClO_4^- concentrations below the detection limit of the SERS instrument, ~100 µg L^{-1}. The ClO_4^- concentrations determined using SERS and a standard addition approach show that the groundwater concentration for this contaminant is quite variable with time. The standard addition curves used to determine the ClO_4^- concentrations are given in Fig. 6.35. Standard deviation for the SERS measurements of the Redstone samples varied generally within ±30%, similar to those observed at the IHDIV site. Additional data comparisons between ClO_4^-concentrations measured by the SERS and IC methods were discussed below.

Figure 6.33. Photos of Sampling Facility and SERS Spectra Collection at Redstone Arsenal, Alabama, USA.

Table 6.6. Comparisons of ClO_4^- Concentrations Determined by Ion Chromatography (IC) and by On-site Portable Raman SERS Sensor from Redstone Arsenal Demonstration (November 2016).

IC data from 2016 field demonstration represent an average of all measurements performed at ORNL and CB&I.

Groundwater Location Code	Sample Code	$[ClO_4^-]$ – (mg L^{-1}) IC – 2015	$[ClO_4^-]$ – (mg L^{-1}) IC – 2016	$[ClO_4^-]$ – (mg L^{-1}) SERS – 2016
P133-RS107	3149	0.530	0.669 ± 0.134	4.530 ± 2.300
P12-RS187	3150	2.220	2.217 ± 0.207	1.700 ± 0.343
P13-RS476	3151	0.006	0.989 ± 0.162	0.669 ± 0.069
P131-RS210	3152	7.580	26.24 ± 5.151	18.00 ± 8.200
P14-RS253	3154	0.003	BD	BD
P12-RS240	3155	1.640	2.346 ± 0.334	1.250 ± 0.190
P12-RS241	3156	4.740	4.627 ± 0.717	5.300 ± 2.600
P131-RS337	3157	0.007	BD	BD

BD – Concentrations below SERS detection limit.

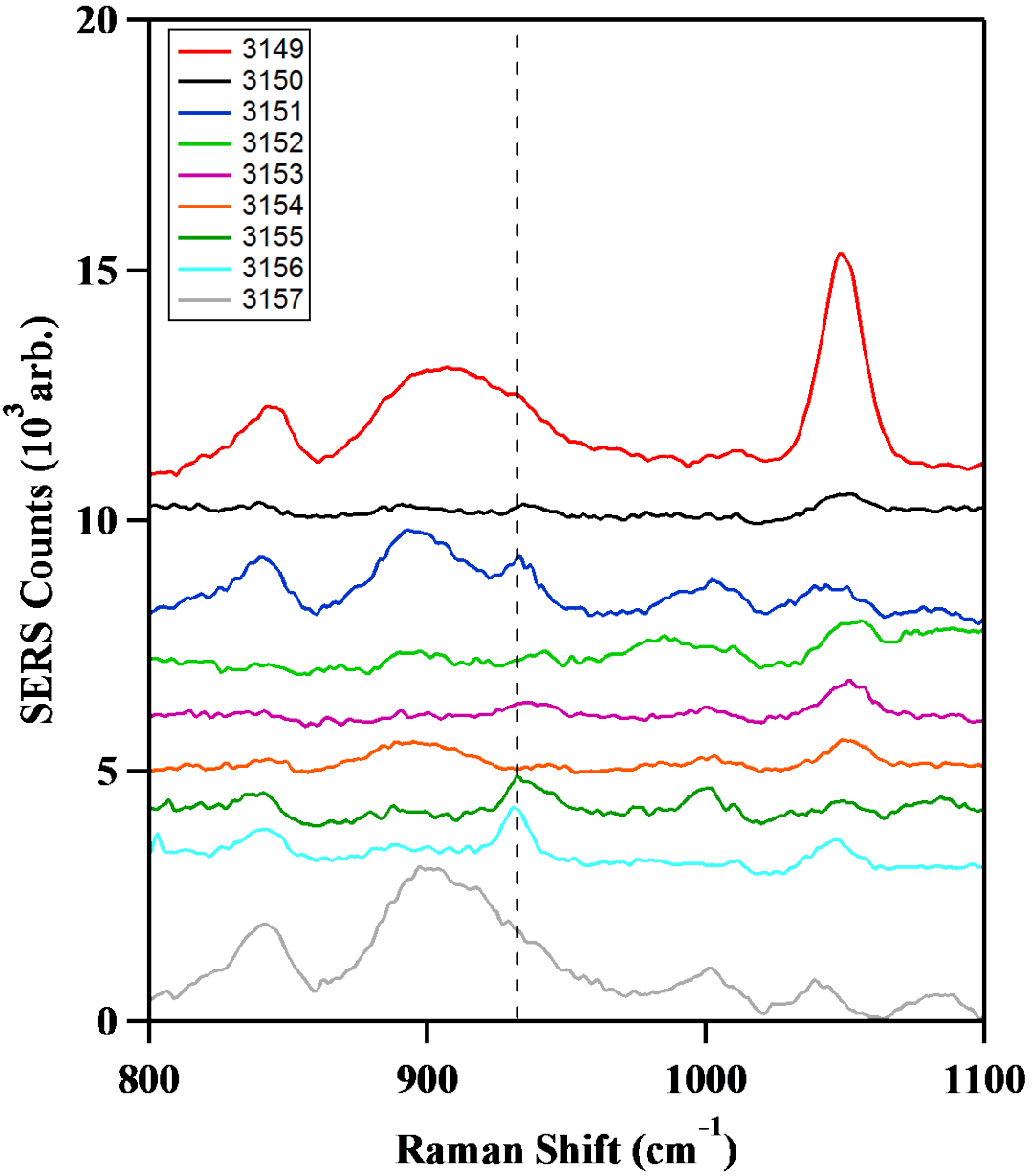

Figure 6.34. SERS Spectra of the Nine Undiluted Redstone Arsenal Groundwater Samples.

Spectra were acquired with one 60 s scan using ~75 mW of laser incident 785 nm light. Spectra have been baseline corrected and offset (Y-axis) for clarity. Dashed vertical line represents ν_{SS}-ClO_4^- peak center. Legend indicates corresponding sample code given in Table 6.6.

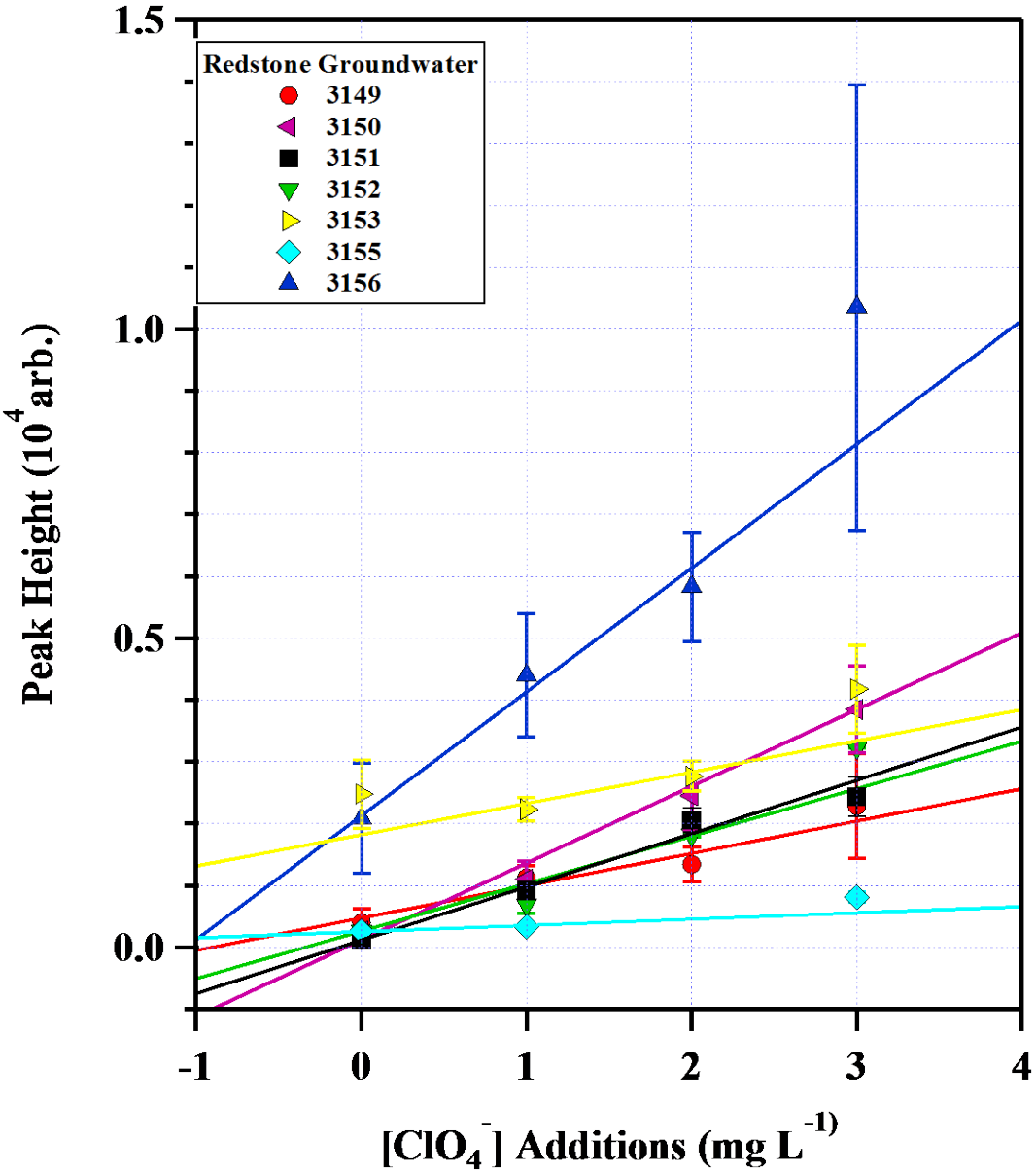

Figure 6.35. Standard Addition Curves for Six Groundwater Samples from Redstone Arsenal, Alabama.

Data are markers while solid traces represent linear regression fits to the data.

6.5.5 Statistical analyses and SERS/IC data comparisons

Based on three field demonstrations of the portable Raman sensor (with elevated Au ellipses as SERS substrates) carried out in 2015 and 2016 at IHDIV and Redstone arsenal (RS) sites, we conclude that these sensors were able to rapidly determine the ClO_4^- concentrations for groundwater samples with concentrations above ~0.1 mg L^{-1}. Comparisons of all measurable SERS data with those determined by IC (Table 6.7) (from Tables 6.3, 6.5 and 6.6) showed a general agreement between measured ClO_4^- concentrations by SERS and by IC (Fig. 6.36). However, significant variations (>30%) were observed with three of the samples (RS 3149, RS 3155, and IH CPMW-2D, 2016). Most samples had an estimated error within ±30%, although this value exceeded our performance objective of ±20%. This large variation is again attributed to the sensitivity of SERS to environmental variables, as discussed earlier, since SERS technology is prone to interferences (such as other organic and inorganic ionic species present in groundwater), which can mask the SERS signal of the target molecule. One data outlier from Redstone arsenal site (Sample ID: RS 3149) had an error >100% (Fig. 6.36 and Tables 6.6 and 6.7); SERS analysis substantially over-estimated its concentration. We don't know the exact cause of this high variation but suspect that the presence of relatively high concentrations of several organic solvents in this groundwater may be responsible. These organic co-contaminants include: methanol at 40 ppm, 1,4-benzenediamine at 1.9 ppm, and a,a-dimethylphenethyl-amine at 1.9 ppm. The presence of relatively high concentrations of these co-contaminants could result in background spectral peaks, which may overlap with the ClO_4^- peak, thereby leading to a substantially over-estimated ClO_4^- concentration. The presence of >200 µM interfering inorganic ions such as sulfate ($SO_4^=$) and nitrate (NO_3^-) could also decrease the ClO_4^- signal. As described earlier, these inorganic anions (or as salt deposits when dried) can occupy SERS active sites within the nanogap regions of the substrates and/or completely mask the SERS activity, thereby reducing or wiping out the SERS signal. Unlike the IC method, these inorganic anions are usually separated from ClO_4^- during chromatography, which allows quantitative detection. Nevertheless, results presented in Table 6.7 and Fig. 6.36 demonstrate the feasibility of implementing SERS as a tool for rapid in-field detection of ClO_4^- within impacted waters. We suggest that additional studies and optimization are needed to bring the technology to the market, and further work in this direction is warranted (see Section 8.0).

Table 6.7. Statistical Analyses and Comparisons of all Field SERS-sensor Measurable ClO_4^- Concentrations with those Determined by Ion Chromatography (IC).

(Combined data from Tables 6.3, 6.5 and 6.6).

Groundwater sample name	[ClO_4^-] (mg L^{-1}) IC	[ClO_4^-] (mg L^{-1}) SERS	[ClO_4^-] (mg L^{-1}) Average	Error (%)
IH-CPMW-5	0.261±0.005	0.343±0.025	0.302±0.058	19.20
IH CPMW-2D (2015)	2.190±0.180	2.470±0.160	2.330±0.198	8.50
IH MW-01	0.423±0.013	0.592±0.050	0.508±0.120	23.55
IH MW-08	1.640±0.026	2.000±0.193	1.820±0.255	13.99
IH CPMW-2D (2016)	0.665±0.091	1.390±0.215	1.028±0.513	49.89
RS 3149	0.669±0.134	4.530±2.300	2.599±2.730	105.05
RS 3150	2.217±0.207	1.700±0.343	1.958±0.365	18.65
RS 3151	0.989±0.162	0.669±0.069	0.829±0.226	27.26
RS 3155	2.346±0.334	1.250±0.190	1.798±0.775	43.10
RS 3156	4.627±0.717	5.300±2.600	4.964±0.476	9.59
RS 3152	26.24±5.15	18.00±8.20	22.12±5.83	26.35

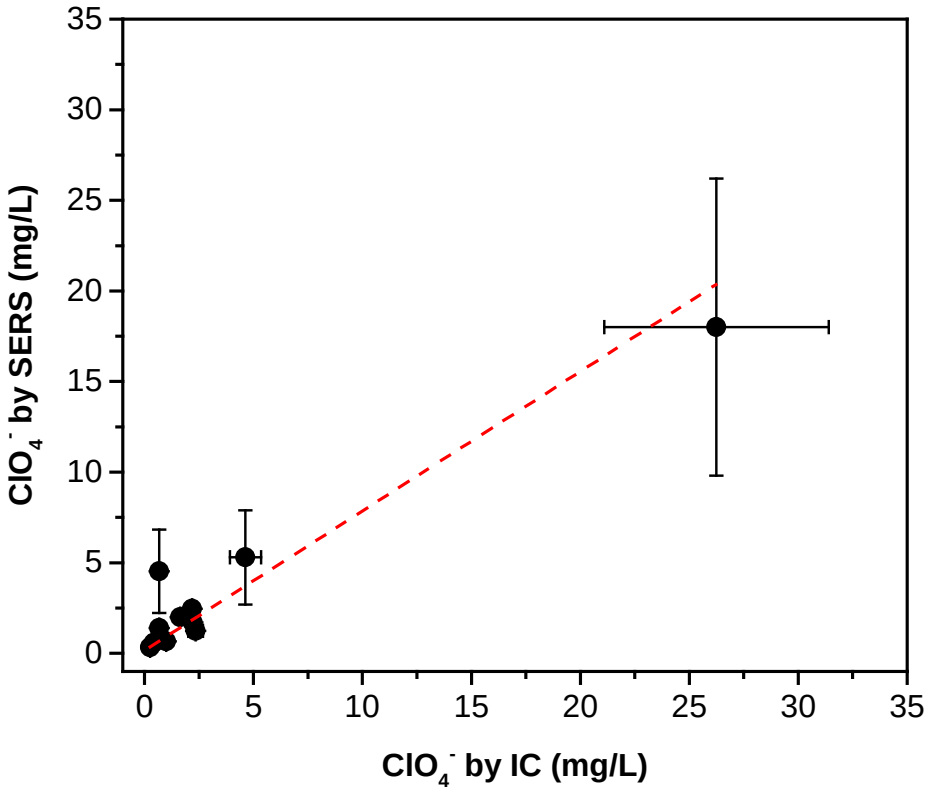

Figure 6.36. Comparisons between ClO_4^- Concentrations Measured by the SERS Sensor and Standard IC Methods (Data from Tables 6.3, 6.5 and 6.6).

Results show a general agreement between the SERS and IC methods for ClO_4^- determination, although significant variations were observed with a few selected groundwater samples.

6.6 RAMAN SENSOR FIELD OPERATION PROCEDURES AND PROTOCOLS

While additional development work is warranted to further reduce the variability and sensitivity of detection, the portable Raman sensor was successfully demonstrated for rapid, in-field analysis of ClO_4^- in groundwater at multiple DoD sites. The method is particularly suited for rapid field screening of ClO_4^- concentrations in water to aid timely decision making processes. The sensor is designed to be easy to use, and a field technician should be able to perform in-field analysis within a few hours of initial training. Listed below are step-by-step operating procedures for in-field use of the portable TZI Raman spectrometer for ClO_4^- analysis.

Sample preparation

1. Groundwater or surface water is analyzed directly without any pre-treatment, other than appropriate dilutions if needed. If the ClO_4^- concentration is greater than the standard calibration curve, appropriate dilutions can be made with purified deionized water (18.3 MΩ cm^{-1}).

2. Using a micro-pipette, transfer 1–2 µL of the water sample onto an active SERS substrate mounted on a standard glass slide, and let it air-dry or place it on a hot plate (at ~50 °C).

Standard preparation

1. All standards are prepared from solid $NaClO_4$ salt (anhydrous ACS grade).

2. $NaClO_4$ salt is baked at ~200 °C for at least 12 h and then stored in a desiccator prior to use to ensure anhydrous state.

3. Prepare ~200 mg L^{-1} stock solution with deionized water. All other standard ClO_4^- solutions are prepared from this stock through serial dilutions with deionized water.

Sensor operation procedures (may vary slightly with different Raman analyzers)

1. Power on instrument by turning power-lock key clockwise.

2. Let instrument warm up at least 20 minutes and then turn on computer.

3. Turn on fiber optic light for the stage camera (optional, if equipped), and start video acquisition mode to see the laser spot.

4. Open Raman, camera, and stage software ENWave Application Center from desktop.

5. Place glass slide with mounted SERS substrate containing sample on the SERS module and place it on the sample stage.

6. Set the Raman acquisition parameters to collect continuous 1 s spectra. Start continuous acquisition.

7. While spectrometer is acquiring continuous spectra, increase 785 nm laser power by turning the power knob clockwise until the laser spot is observed on the camera (should be blinking at 1 Hz). Only a slight increase of the power should be needed, typically <1 mW total output.

8. While observing laser spot on camera, align the SERS substrate to overlap with the laser spot by moving the glass slide around the sample stage. Overlap will be apparent as the SERS substrate will scatter the 785 nm light strongly, i.e., the laser spot will be noticeably brighten.

9. When desirable overlap has been achieved, focus laser beam. Laser spot size at focal point should be ~150 µm in diameter.

10. Stop continuous acquisition.

11. Set output 785 nm power to ~75 mW by turning the power knob to approximately ½ the maximum setting. Full power corresponds to ~350 mW.

12. Define the length of the spectral acquisition in the Raman software and collect the spectrum. Typical acquisition time is 60 s.

13. Save spectral data as both .spc and .txt file formats since the Raman software can only open .spc files while the .txt format can be loaded into a third-party software (e.g. Excel, Origin, etc.).

Standard addition and data analysis

1. To minimize or correct the matrix interference effects of unknown groundwater compositions, it is highly recommended that the standard addition technique (Section 5.3.1) is used for selected samples to ensure data quality.

2. In this method, the same amount of the groundwater sample (e.g., 1 or 5 mL) is transferred to a series of small vials (usually 3–5), to which ClO_4^- standard solutions with different concentrations are added.

3. Samples are then measured, and spectral collected, as described above (See Sample preparation).

4. Fit plot of SERS ClO_4^- peak height vs the added ClO_4^- concentration with linear regression. Weight linear regression to ±1 standard deviation of peak height.

5. Determine the ClO_4^- concentration for the sample from linear regression (i.e., intercept divided by slope) multiplied by dilution factor, as appropriate.

6. Determine ClO_4^- concentration uncertainty by propagating standard deviation of the intercept and slope and then accounting for the dilution.

Page Intentionally Left Blank

7.0 COST ASSESSMENT

7.1 COST MODEL AND COST DRIVER

A goal of the project was to evaluate the overall costs of on-site ClO_4^- analysis with the portable Raman sensor. The cost of Raman sensor-based analysis on a per sample event basis is thus estimated and compared with those using standard groundwater analyses such as EPA Methods 314.2 (IC), 331.0 (HPLC-ESI-MS), and 6850 (LC-ESI-MS). Here we detail the overall costs and document potential savings to DoD of the Raman sensor approach vs traditional off-site analytical techniques.

Typical costs associated with Raman sensor analyses include: capital equipment, i.e., a typical portable Raman spectrometer ($15,000 - 25,000) versus IC and IC-MS, LC-MS or HPLC-MS used in conventional methods, labor and analytical time including sample preparation and pre-treatment both in the laboratory and in the field, materials and consumables, sampling equipment, vehicle and rental costs (e.g., pumps, generators, pump controllers, etc.), shipping, and data analysis and interpretation (Table 7.1). The capital cost of a portable Raman spectrometer is roughly equivalent to or slightly lower than that of a typical ion chromatograph (IC) system, but should be much lower than an IC-MS, LC-MS or HPLC-MS. For simplified calculations, we assume there are no capital differences based on analytical equipment. If this technique becomes standard, rental agencies would have incentive to purchase and supply the Raman field instruments on a time basis, much like PID meters or other on-site sampling and analytical equipment. For a cost comparison, we include a $400 per week rental cost for the Raman spectrometer rather than a capital expenditure.

7.2 COST ANALYSES

We performed a basic cost comparison between Raman SERS technology and that currently being used for the analysis of ClO_4^- [e.g., Methods 314.2 (IC), 331.0 (HPLC-ESI-MS), and 6850 (LC-ESI-MS)] (Table 7.1). For the test scenario, we assumed that a total of 24 groundwater wells were to be sampled by a single field technician, and that the technician could sample 6 wells per day (80 min per well) and conduct the Raman analysis on the samples during that same day (30 min per well). Packing and shipping of coolers for off-site analysis required 1.5 hrs per day. The following additional assumptions were made for the cost comparison:

1) Rental of required sampling pumps and meters (other than Raman sensor) ($400/wk);
2) Rental of Raman sensor ($400/wk);
3) Commercial SERS substrates ($20/ea)
4) Field labor (70 per hr);
5) Vehicle rental ($375/wk);
6) Hotel and per diem, Maryland default rate ($142/day).
7) Coolers ($30 ea)
8) Shipping empty coolers to site ($25 ea)
9) Shipping samples to lab ($75 ea)
10) Other miscellaneous (sample tubes at $1 ea and ice at $5 per cooler)

Analytical costs were requested from commercial laboratories for EPA Methods 314.2 ($85 per sample), 331.0 ($165 per sample), and 6850 ($90 per sample). Based on the assumptions provided, the estimated cost of a 4-day sampling (24 wells) event using the Raman sensor was $4687 (Table 7.1). By comparison, the cost for off-site analysis was $6655 by EPA Method 314.2, $8575 by EPA Method 331.0, and $6775 by EPA Method 6850. The majority of the cost saving is realized by reduced analytical costs, with the assumption of a rental Raman sensor at $400 and total labor to analyze the samples at $840 (total of $1,240 for 24 wells). This compares to from $2040 to $3960 for off-site analytical by the different techniques, excluding shipping costs of ~$135 each day which would be added on. The savings for the sampling event using the Raman technique compared to traditional sampling and off-site analysis ranged from ~ 30 to 45%. Thus, assuming that commercial instruments are available for use (and realizing that this same instrument could potentially be utilized for a variety of other DoD contaminants, including various explosives and organics) (Hatab et al., 2010a, 2011), the potential cost savings to DoD of this on-site technique is potentially significant. However, this also assumes that the precision of the technique can be improved with further work.

Finally, the ability to have real-time measurements when monitoring remediation systems is likely to result not only in cost savings, but also in more effective and timely decision making during remediation projects. In many instances, decisions made concerning the location and screening of wells during site assessment work could be vastly improved if real-time contaminant data are available. Moreover, the precision of these data is often less important than for regulatory field data.

Table 7.1. Basic Cost Analyses and Comparisons of the Raman Sensor and Standard EPA Methods for in-field Analysis of Perchlorate (ClO_4^-) in Groundwater.

The cost analysis is framed around field sampling and field analytical costs.

Cost Element	Field Elements SERS analyses ($)	SERS method Cost per unit	Cost per 24 wells sampled	Field Elements Off-Site lab	EPA method Cost per unit	Cost per 24 wells sampled EPA Method 314.2	Cost per 24 wells sampled EPA Method 331.0	Cost per 24 wells sampled EPA Method 6850
Materials, SERS substrates	SERS Chip Corning Collection tubes	$20/ea $1/ea	$480 $24	Corning Collection tubes	$20/ea $1/ea	$480 $24	$480 $24	$480 $24
Sampling	Field labor - sampling Field labor - Raman Sampling equipment rental Raman sensor rental Truck rental Room and per diem	$70/hr $70/hr $400/wk $400/wk $375/wk $142/day	$2240 $840 $400 $400 $375 $568	Field labor - sampling Cooler packing, shipping Sampling equipment rental Truck rental Room and per diem	$70/hr $70/hr $400/wk $375/wk $142/day	$2240 $420 $400 $375 $568	$2240 $420 $400 $375 $568	$2240 $420 $400 $375 $568
Analytical	Field technician, included in sampling labor	--	--	Per sample analytical cost	Variable (see following columns)	$2040 ($85 per sample)	$3960 ($165 per sample)	$2160 ($90 per sample)
Shipping	None	--	--	Cooler Ice Cooler shipping to field Cooler shipping to lab	$30 $5 $25 $75	$120 $20 $100 $300	$120 $20 $100 $300	$120 $20 $100 $300
Total			**$ 4687**			**$ 6655**	**$ 8575**	**$ 6775**

Page Intentionally Left Blank

8.0 SUMMARY AND IMPLEMENTATION ISSUES

SERS is a technique that provides enhanced Raman signal from analyte molecules that are adsorbed onto nanostructured noble metal surfaces. Such surfaces are usually made with nanostructured gold (Au) or silver (Ag) arrays, enabling the detection of analyte molecules at ultra-trace concentration levels. In comparison with conventional absorption spectroscopic techniques, SERS is more sensitive with greater molecular selectivity (or fingerprinting) due to orders of magnitude enhanced Raman signal and the molecular vibrational information provided by Raman spectroscopy. The key is the fabrication of sensitive and reproducible SERS substrates using techniques such as EBL and nanoimprint. The SERS substrate is then integrated with a portable Raman analyzer via a fiber optic sensor probe, allowing in-situ detection and analysis of contaminants in groundwater or surface water.

- In this ESTCP project, we developed and constructed an integrated, portable SERS-Raman sensor for energetics ClO_4^- detection and analysis.
- We systematically investigated the influence of SERS substrate nanogap size, ellipse aspect ratio, and substrate orientation relative to the excitation laser polarization on the SERS response for elevated Au ellipse dimers. The optimized SERS substrate conditions were found to be a gap of 10±2 nm, an aspect ratio close to 1:1, and the polarization of the 785 nm excitation beam aligned with the ellipse x-axis.
- The tunability of the ellipse geometry provided a rational basis for the design of SERS substrates based on the elevated ellipse dimer platform for matching a desired excitation wavelength. The tunability of the ellipse dimers could potentially make them an attractive for analysis of a broad range of explosive chemicals and biological agents.
- We successfully demonstrated commercial fabrication of SERS substrates via transferring topographic ellipses patterns from a mold onto a Si wafer by nanoimprinting. The integrity and gap sizes of the imprinted nanostructural arrays were verified by SEM and/or AFM analyses. This is a substantial step forward toward the commercialization of the SERS sensors due to reduced fabrication costs.
- We found that the functionalization of the SERS substrates with DMAET had the benefit of increasing the detection efficiency.
- Commercially produced SERS substrate sensors were demonstrated to detect ClO_4^- at levels above 1×10^{-6} M (100 µg/L) using a portable Raman analyzer. The effect of interference ions on the SERS detection efficiency for ClO_4^- was investigated. It was determined that for low interference concentrations ($< 2\times10^{-4}$ M) the interference strength is ion specific with SO_4^{2-} exhibiting the largest effect.
- Three field demonstrations of the portable Raman sensor were carried out in 2015 and 2016 at both IHDIV Naval Surface Warfare Center and Redstone arsenal sites with ClO_4^- contamination. These sensors could rapidly determine ClO_4^- concentrations for groundwater samples. The result indicates the feasibility of implementing SERS as a tool for rapid in-field detection of ClO_4^- within impacted waters.
- We published 2 peer-reviewed journal articles and 1 conference presentation related to the development and application of SERS technology for energetics detection.

The results presented in this work make a case for the applicability of the SERS-based portable Raman sensor for rapid field measurements of trace levels of ClO_4^- in contaminated groundwater. To our knowledge, the work is the first of its kind in developing a SERS/Raman based field sensor for environmental detection and analysis. However, as noted earlier, challenges remain to develop and implement a field deployable and reliable portable Raman sensor. The biggest challenge is to reduce its variability due to the presence of various groundwater interferences so as to increase its sensitivity or detection limit for ClO_4^-. The reported ClO_4^- detection limit (~100 µg/L) and variability (from 8–105%) (Table 6.7) are not suitable for routine quantitative analysis, particularly at low ClO_4^- concentrations, but the sensor may be used for rapid screening of wells during site assessment work and thus to aid more effective and timely decision making during remediation. Through further field validation and demonstration, a cost reduction of ~ 30–45% may be realized using the portable Raman sensor because sample shipping and typical costs associated with laboratory analysis may be eliminated (Table 7.1).

Future work should be directed to further increase the sensitivity and selectivity of the sensor and to minimize the matrix interference effect, thereby increasing the reliability for detection and quantification, especially at low ClO_4^- concentrations. First, the controlled fabrication of reproducible nanostructured SERS dimer arrays with <10 nm gap sizes is highly desirable since SERS reactivity and/or enhancement increases exponentially with decreasing nanogap sizes. However, reducing the gap size below 10 nm is a formidable challenge due to EBL limits in fabrication and difficulties in controlling Au or Ag deposits and homogeneity on nanostructured arrays. Second, even with all the fabrication issues resolved, the stability and longevity of the fabricated SERS substrates require additional investigations because the nanostructured arrays may undergo surface and morphological changes over time due to processes such as surface oxidation and atomic rearrangements at the nanoscale. Furthermore, active SERS sites may be readily contaminated because of surface adsorption of many organic and inorganic molecules present in the air, thereby decreasing SERS activity and selectivity during storage. While SERS is highly sensitive to the analyte, it is also sensitive to surface contamination and any adsorbed molecules complicating SERS signals. Third, the presence of relatively high concentrations of organic or inorganic ions, salts or TDS (e.g. > 200 µM), in water remains a major concern as they can smear the Au SERS surface upon drying, thereby suppressing the SERS signal and causing huge variability. Therefore, increasing SERS selectivity to target analyte molecules is critically important. We demonstrated that surface functionalization of the SERS substrates (e.g., with DMAET) is beneficial leading to increased selectivity and detection efficiency. Additional studies are needed however to further explore surface modification or functionalization of the SERS substrate to increase its selective sorption and concentration of the target analyte such as ClO_4^- so that the SERS substrate may be rinsed or washed with DI water following its reaction with the sample before SERS analysis. This treatment could remove most of the salts or interfering ions, provided that ClO_4^- is selectively sorbed, and can thus result in greatly increased detection sensitivity but decreased variability.

9.0 REFERENCES

Clausen, J., Cramer, R., Clough, S., Gray, M., Gwinn, P., 2009. Assessing the sensitivity of quantitative structural activity analysis models for evaluating new military compounds. Water Air Soil Poll. 202(1-4), 141-147.

D'Andrea, C., et al., 2013. Optical nanoantennas for multiband surface-enhanced infrared and raman spectroscopy. Acs Nano 7(4), 3522-3531.

Dai, S., Lee, Y.H., Young, J.P., 1996. Observation of the surface enhanced Raman scattering spectrum of uranyl ion. Appl. Spectr. 50, 536-537.

De Jesus, M.A., et al., 2005. Nanofabrication of densely packed metal-polymer arrays for surface-enhanced Raman spectrometry. Appl Spectrosc 59(12), 1501-1508.

Gu, B., Coates, J.D. (2006). *Perchlorate Environmental Occurrence, Interactions and Treatment*. New York: Springer.

Gu, B., Ruan, C., 2007. Determination of technetium and its speciation by surface enhanced Raman spectroscopy. Anal. Chem. 79, 2341-2345.

Gu, B., Ruan, C., Wang, W., 2009. Perchlorate detection at nanomolar concentrations by surface-enhanced Raman scattering. Appl. Spectr. 63, 98-102.

Gu, B., Tio, J., Wang, W., Ku, Y., Dai, S., 2004. Raman spectroscopic detection for perchlorate at low concentrations. Appl. Spectr. 58, 741-744.

Hao, J.M., Han, M.J., Meng, X.G., Weimer, W., Wang, Q.W.K., 2015. Surface-enhanced Raman scattering of perchlorate on cationic-modified silver nanofilms - Effect of inorganic anions. Spectrochimica Acta Part a-Molecular and Biomolecular Spectroscopy 136, 1593-1599.

Hao, J.M., Xu, Z.H., Han, M.J., Xu, S.Y., Meng, X.G., 2010. Surface-enhanced Raman scattering analysis of perchlorate using silver nanofilms deposited on copper foils. Colloids and Surfaces a-Physicochemical and Engineering Aspects 366(1-3), 163-169.

Hatab, N.A., Eres, G., Hatzinger, P.B., Gu, B., 2010a. Detection and analysis of cyclotrimethylene-trinitramine (RDX) in environmental samples by surface enhanced Raman spectroscopy. J. Raman Spectr. 41, 1131-1136.

Hatab, N.A., et al., 2010b. Free-standing optical gold bowtie nanoantenna with variable gap size for enhanced Raman spectroscopy. Nano Letters 10, 4952-4955.

Hatab, N.A., et al., 2011a. An integrated portable Raman sensor with nanofabricated gold bowtie array substrates for energetics detection. Analyst 136(8), 1697-1702.

Hatab, N.A., et al., 2011b. An integrated portable Raman sensor with nanofabricated gold bowtie array substrates for energetics detection. Analyst 136, 1697-1702.

Hatzinger, P.B., Diebold, J., Yates, C.A., Cramer, R.J. (2006). Field demonstration of in situ perchlorate bioremediation in groundwater. In B. Gu, J.D. Coates (Eds.), *Perchlorate Environmental Occurrences, Interactions, and Treatment* (pp. 311-341). New York: Springer.

Homola, J., 2008. Surface Plasmon Resonance Sensors for Detection of Chemical and Biological Species. Chem. Rev. 108(2), 462-493.

Jackson, J.B., Halas, N.J., 2004. Surface-enhanced Raman scattering on tunable plasmonic nanoparticle substrates. PNAS USA 101(52), 17930-17935.

Jain, P.K., Huang, W., El-Sayed, M.A., 2007a. On the universal scaling behavior of the distance decay of plasmon coupling in metal nanoparticle pairs: A plasmon ruler equation. Nano Lett. 7(7), 2080-2088.

Jain, P.K., Huang, W.Y., El-Sayed, M.A., 2007b. On the universal scaling behavior of the distance decay of plasmon coupling in metal nanoparticle pairs: A plasmon ruler equation. Nano Letters 7(7), 2080-2088.

Jubb, A.M., Hatzinger, P., GU, B., 2017. Trace-level perchlorate analysis of impacted groundwater by elevated gold ellipse dimer nanoantenna surface-enhanced Raman scattering. J. Raman Spect., DOI: 10.1002/jrs.5070.

Jubb, A.M., Jiao, Y., Eres, G., Retterer, S.T., Gu, B., 2016. Elevated gold ellipse nanoantenna dimers as sensitive and tunable surface enhanced Raman spectroscopy substrates. Nanoscale 8, 5641-5648.

Kneipp, K., Kneipp, H., Itzkan, I., Dasari, R.R., Feld, M.S., 1999. Ultrasensitive Chemical Analysis by Raman Spectroscopy. Chem. Rev. 99(10), 2957-2975.

Kneipp, K., et al., 1997. Single molecule detection using surface-enhanced Raman scattering (SERS). Phys. Rev. Lett. 78(9), 1667-1670.

Lumerical Solutions. 2003. http://www.lumerical.com.

Mayer, K.M., Hafner, J.H., 2011. Localized Surface Plasmon Resonance Sensors. Chem. Rev. 111(6), 3828-3857.

Mosier-Boss, P.A., Lieberman, S.H., 2003. Detection of anions by normal Raman spectroscopy and surface enhanced Raman spectroscopy of cationic-coated substrates. Appl. Spectr. 57, 1129-1137.

Nie, S., Emory, S.R., 1997. Probing single molecules and single nanoparticles by surface-enhanced Raman scattering. Science 275, 1102-1106.

Polemi, A., Wells, S.M., Lavrik, N.V., Sepaniak, M.J., Shuford, K.L., 2011. Dispersion Characteristics in Disk-on-Pillar Array Nanostructures for Surface-Enhanced Raman Spectroscopy. Journal of Physical Chemistry C 115(28), 13624-13629.

Ruan, C., Wang, W., Gu, B., 2006a. Detection of alkaline phosphatase using surface-enhanced Raman spectroscopy. Analytical Chemistry 78(10), 3379-3384.

Ruan, C., Wang, W., Gu, B., 2007a. Single-molecule detection of thionine on aggregated gold nanoparticles by surface enhanced Raman scattering. Journal of Raman Spectroscopy 38(5), 568-573.

Ruan, C.M., Gu, B., Wang, W., Eres, G., Zhang, Z., 2007b. Controlled fabrication of nanopillar array substrates for surface-enhanced Raman spectroscopy. Langmuir 23, 5757-5760.

Ruan, C.M., Wang, W., Gu, B., 2006b. Surface-enhanced Raman scattering for perchlorate detection using cystamine-modified gold nanoparticles. Anal Chim Acta 567(1), 114-120.

Ruan, C.M., Wang, W., Gu, B., 2007c. Single-molecule detection of thionine on aggregated gold nanoparticles by surface enhanced Raman scattering. J. Raman Spectr. 38(5), 568-573.

Sass, J., 2004. US Department of Defense and white house working together to avoid cleanup and liability for perchlorate pollution. International Journal of Occupational and Environmental Health 10(3), 330-334.

Stewart, M.E., et al., 2008. Nanostructured Plasmonic Sensors. Chem. Rev. 108(2), 494-521.

Suidan, M.T., Atikovic, E., Maloney, S.W., 2008. Anaerobic treatment of army ammunition production wastewater containing perchlorate and RDX. Chemosphere 72(11), 1643-1648.

USEPA. 2010. Low Stress (Low Flow) Purging and Sampling Procedure for the Collection of Groundwater Samples from Monitoring Wells. EQASOP-GW 001. Rev. 3. January 19, 2010. Online: https://www.epa.gov/sites/production/files/2015-06/documents/EQASOP-GW001.pdf.

Veres, T., Cui, B., Clime, L., 2010. Fabrication of nanostar arrays by nanoimprint lithography. J. Vac. Sci. Technol. B 28(6), C6o26-C26o29.

Wang, W., Gu, B., 2005. New surface-enhanced Raman spectroscopy substrates via self-assembly of silver nanoparticles on surface functionalized glass for perchlorate detection. Appl. Spectr. 59, 1509-1515.

Weber, D., et al., 2011. Longitudinal and transverse coupling in infrared gold nanoantenna arrays: long range versus short range interaction regimes. Optics Express 19(16), 15047-15061.

Weiss, S.M., Ryckman, J.D., Liscidini, M., Sipe, J.E., 2011. Direct imprinting of porous substrates: A rapid and low-cost approach for patterning porous nanomaterials. Nano Letters 11(5), 1857-1862.

Wells, S.M., Polemi, A., Lavrik, N.V., Shuford, K.L., Sepaniak, M.J., 2011. Efficient disc on pillar substrates for surface enhanced Raman spectroscopy. Chemical Communications

47(13), 3814-3816.

Wells, S.M., Retterer, S.D., Oran, J.M., Sepaniak, M.J., 2009. Controllable nanotabrication of aggregate-like nanoparticle substrates and evaluation for surface-enhanced Raman spectroscopy. ACS Nano 3(12), 3845-3853.

Xu, H., Bjerneld, E.J., Kall, M., Borjesson, L., 1999. Spectrscopy of single hemoglobin molecules by surface enhanced Raman scattering. Phys. Rev. Let. 83, 4357-4360.

Zhao, K., Xu, H., Gu, B., Zhang, Z., 2006a. One-dimensional arrays of nanoshell dimers for single molecule spectroscopy via surface-enhanced raman scattering. J. Chem. Phys. 125(8).

Zhao, K., Xu, H., Gu, B., Zhang, Z., 2006b. One-dimensional arrays of nanoshell dimers for single molecule spectroscopy via surface-enhanced raman scattering. The Journal of chemical physics 125(8), 081102.

Zhao, L.L., Kelly, K.L., Schatz, G.C., 2003. The extinction spectra of silver nanoparticle arrays: Influence of array structure on plasmon resonance wavelength and width. J. Phys. Chem. B 107(30), 7343-7350.

Zuloaga, J., Prodan, E., Nordlander, P., 2009. Quantum description of the plasmon resonances of a nanoparticle dimer. Nano Letters 9(2), 887-891.

APPENDIX A POINTS OF CONTACT

Point of Contact Name	Organization Name Address	Phone Fax Email
Dr. Baohua Gu	Environmental Sciences Division Oak Ridge National Laboratory P. O. Box 2008, MS-6036 Oak Ridge, TN 37831	865-574-7286 (phone) 865-576-8543 (fax) gub1@ornl.gov
Dr. Paul B. Hatzinger	CB&I Federal Services, LLC. 17 Princess Road Lawrenceville, NJ 08648	609-895-5356 (phone) 609-895-1858 (fax) Paul.hatzinger@cbifederalservices.com
Dr. Andrea Leeson	SERDP/ESTCP 901 N Stuart Street, Suite 303 Arlington VA 22203	703-696-2118 (phone) 703-696-2114 (fax) Andrea.leeson@osd.mil